

Winter 2017

Expanding the applications of poly(dimethylsiloxane) in biomicrofluidics

Sawyer D. Stone

Follow this and additional works at: <https://digitalcommons.latech.edu/dissertations>

 Part of the [Biomedical Engineering and Bioengineering Commons](#)

**EXPANDING THE APPLICATIONS OF
POLY(DIMETHYLSILOXANE)
IN BIOMICROFLUIDICS**

by

Sawyer D. Stone, B.S.

A Dissertation Presented in Partial Fulfillment
of the Requirements of the Degree
Doctor of Philosophy

COLLEGE OF ENGINEERING AND SCIENCE
LOUISIANA TECH UNIVERSITY

February 2017

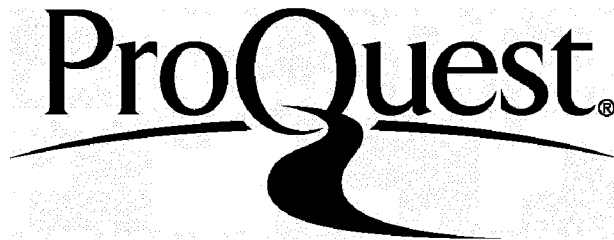
ProQuest Number: 10644141

All rights reserved

INFORMATION TO ALL USERS

The quality of this reproduction is dependent upon the quality of the copy submitted.

In the unlikely event that the author did not send a complete manuscript and there are missing pages, these will be noted. Also, if material had to be removed, a note will indicate the deletion.



ProQuest 10644141

Published by ProQuest LLC(2017). Copyright of the Dissertation is held by the Author.

All rights reserved.

This work is protected against unauthorized copying under Title 17, United States Code.
Microform Edition © ProQuest LLC.

ProQuest LLC
789 East Eisenhower Parkway
P.O. Box 1346
Ann Arbor, MI 48106-1346

LOUISIANA TECH UNIVERSITY

THE GRADUATE SCHOOL

NOVEMBER 18, 2016


Date

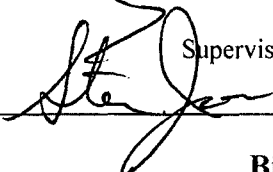
We hereby recommend that the dissertation prepared under our supervision by
Sawyer David Stone

entitled Expanding the Applications of Poly(dimethylsiloxane) in Biomicrofluidics

be accepted in partial fulfillment of the requirements for the Degree of

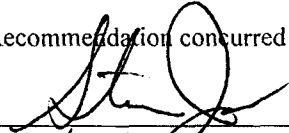
Doctor of Philosophy in Biomedical Engineering



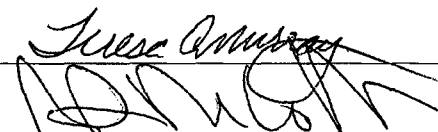
Supervisor of Dissertation Research


Head of Department
Biomedical Engineering
Department

Recommendation concurred in:



Yusef



Teresa

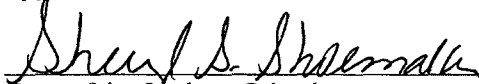
Advisory Committee

Approved:

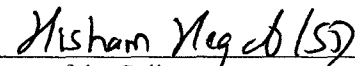


Director of Graduate Studies

Approved:



Dean of the Graduate School



Dean of the College

ABSTRACT

This work aims to create novel applications for poly(dimethylsiloxane) (PDMS) in the field of biomicrofluidics through oxidative stress detection, doping of the polymer for intentional leaching into microdevices, and the development of low-cost implements for fabricating PDMS microfluidic devices. PDMS has become the polymer of choice for research in microfluidics due to its optical clarity, ease of fabrication, flexibility in design, good mechanical properties, and the ability to chemically modify the surface.

Biomicrofluidics enables the rapid throughput and analysis of small biological samples requiring less time investment and reagent use than traditional macroscale laboratory techniques. Polymer devices are inexpensive, easily fabricated using rapid prototyping techniques, and lend themselves well to surface chemistry modifications. A new chemical surface modification has been developed that allows the selective capture of carbonylated proteins on a PDMS microchannel.

PDMS can be doped with small molecules prior to curing of the prepolymer mixture, and these small molecules can subsequently leach into cell culture media or a microfluidic flow. By quantifying the leaching amount over time, this research lays the groundwork for tunable doped microfluidic devices that can deliver a steady low concentration dose of certain molecules into a cell culture or microdevice without human interference or risk of contamination.

PDMS soft lithography traditionally relies on cleanroom techniques such as photolithography for creation of mold masters for PDMS devices. Such methods require significant investment into specialized equipment and environments to develop molds that may not be suitable for the desired applications. This research employs computational fluid dynamics (CFD) and rapid prototyping techniques in the development of novel microfluidic designs. CFD provides verification of the flow rate and pressure drop in a microfluidic channel, ensuring that the resulting flow speeds allow the captured proteins or attached cells in culture to remain attached to the microchannel. A 3D printer and an Arduino microcontroller were used to create a spin table for coating silicon wafers in photoresist, and a UV LED light source was designed for exposing the photoresist. This approach reduces the equipment cost involved in creating microfluidic molds and allows the creation of a variety of new microfluidic devices.

APPROVAL FOR SCHOLARLY DISSEMINATION

The author grants to the Prescott Memorial Library of Louisiana Tech University the right to reproduce, by appropriate methods, upon request, any or all portions of this Dissertation. It is understood that "proper request" consists of the agreement, on the part of the requesting party, that said reproduction is for his personal use and that subsequent reproduction will not occur without written approval of the author of this Dissertation. Further, any portions of the Dissertation used in books, papers, and other works must be appropriately referenced to this Dissertation.

Finally, the author of this Dissertation reserves the right to publish freely, in the literature, at any time, any or all portions of this Dissertation.

Author



Date

2/6/17

DEDICATION

This dissertation is dedicated to my family. Without their support, motivation, and the desire to learn that they instilled in me, I would not be here today.

TABLE OF CONTENTS

ABSTRACT.....	iii
DEDICATION.....	vi
LIST OF TABLES.....	xii
LIST OF FIGURES.....	xiii
ACKNOWLEDGMENTS.....	xvii
CHAPTER 1 INTRODUCTION.....	1
1.1 Background.....	1
1.1.1 Microfluidics.....	1
1.1.2 Poly(dimethylsiloxane).....	2
1.2 Project Overview.....	3
1.2.1 Hypothesis.....	4
1.2.2 Specific Aims.....	4
1.3 Significance.....	5
1.4 Dissertation Overview.....	6
CHAPTER 2 BACKGROUND.....	7
2.1 Microfluidics.....	7
2.2 Background of Poly(dimethylsiloxane).....	10
2.3 PDMS Surface Modifications.....	12
2.4 Background of PDMS Leaching and Absorption.....	17
2.5 Laboratory Techniques for Manufacturing PDMS Devices.....	18
2.5.1 Replica Molding.....	18

2.5.2	Soft Lithography	20
2.5.2.1	Microcontact printing	21
2.5.2.2	Micromolding	22
2.5.3	Three-Dimensional PDMS Microchannel Fabrication	23
2.5.4	Microfluidic Device Fabrication in PDMS	25
2.6	Oxidative Stress	27
CHAPTER 3 OXIDATIVE STRESS BIOMOLECULE DETECTION		30
3.1	Surface Modifications	30
3.1.1	Previously Reported Surface Modifications	30
3.2	Methods	32
3.2.1	PDMS Channel Fabrication	32
3.2.2	PDMS Surface Modifications	32
3.2.2.1	Aqueous acrylic acid UV grafting	32
3.2.2.2	Acetone and benzophenone acrylic acid UV grafting	33
3.2.2.3	Flow-through functionalization of PDMS	33
3.2.2.4	Attachment of oxalyldihydrazide crosslinker	33
3.2.2.5	Verification of aldehyde functional groups on PDMS	34
3.2.2.6	Protein oxidation	34
3.2.2.7	Protein labeling	35
3.2.2.8	Protein capture	35
3.2.2.9	Protein elution	36
3.3	Surface Modification Results	36
3.3.1	Aqueous Acrylic Acid UV Grafting	36
3.3.2	Acetone, Benzophenone, and Acrylic Acid Grafting	41
3.3.3	Flow-Through Functionalization of PDMS	43

3.3.4	Protein Capture	46
3.3.5	Elution of Bound Proteins.....	48
3.4	Discussion of Results.....	49
CHAPTER 4 DOPING OF PDMS FOR INTENTIONAL LEACHING INTO MICRODEVICES.....		53
4.1	Introduction.....	53
4.2	Methods	54
4.2.1	PDMS Doping.....	54
4.2.2	Concentration Measurement.....	55
4.2.3	Bulk PDMS Leaching Measurement	56
4.2.4	Microchannel Leaching Measurement.....	57
4.3	Results.....	57
4.3.1	Quantification of Leaching	57
4.3.2	Leaching in Microfluidic Flow Conditions.....	60
4.4	Discussion of Results.....	64
4.5	Conclusion	65
4.5.1	Future Work.....	65
CHAPTER 5 USING COMPUTATIONAL FLUID DYNAMICS IN MICROFLUIDICS		66
5.1	Introduction.....	66
5.2	Mathematical Modeling of Microfluidic Flow	68
5.2.1	Navier-Stokes Equations.....	68
5.2.2	Pressure Drop.....	70
5.3	Modeling Microfluidic Flows using COMSOL Multiphysics.....	71
5.3.1	COMSOL Multiphysics Background	71
5.3.2	Methods.....	72

5.3.3	PMMA Carbonylated Protein Enrichment Model	73
5.3.4	PDMS Carbonylated Protein Enrichment Model	76
5.3.5	Modeling of Microfluidics for Cell Culture Design	79
5.3.5.1	Device design	79
5.3.5.2	Velocity modeling result	80
5.3.5.3	Shear modeling result	82
5.4	Conclusion	84
CHAPTER 6 LOW COST MICROFLUIDICS IMPLEMENTATIONS		86
6.1	Introduction.....	86
6.1.1	Current Photolithography Mold Fabrication Method	86
6.2	Methods	88
6.2.1	3D Printed Spin Table.....	88
6.2.2	UV LED Light Source	89
6.2.3	Arduino Controller.....	89
6.2.4	Photolithography Procedure.....	90
6.3	Implementation of Low Cost Photolithography	91
6.3.1	Spin Table	91
6.3.2	Electrical Design of Spin Table Motor Circuit	94
6.3.3	Arduino Motor Speed Controller	95
6.4	UV Photoresist Curing.....	96
6.4.1	Light Emitting Diode Array for SU-8 Curing.....	97
6.5	Design Improvements	98
CHAPTER 7 CONCLUSIONS AND FUTURE WORK		102
7.1	Conclusions.....	102
7.1.1	Project Specific Aims	102

7.2	Future Work and Directions	105
7.2.1	Oxidative Stress Biomolecule Detection	105
7.2.2	Doping of PDMS for Intentional Leaching into Microdevices	107
7.2.3	Low Cost Biomicrofluidics Implementations	108
Appendix A	ARDUINO CONTROLLED SPIN TABLE CODE	110
A.1	Arduino Code for Spin Table Controller	110
BIBLIOGRAPHY	112

LIST OF TABLES

Table 2-1: A comparison of PMMA and PDMS as substrates for microfluidic platforms.....	11
Table 3-1: Water contact angle measurements for each mixture of modification solution.....	44

LIST OF FIGURES

Figure 2-1: Chemical structure of PDMS.....	12
Figure 2-2: Surface modification of PDMS via RF plasma treatment resulting in hydroxyl functional groups on the polymer surface.	14
Figure 2-3: UV graft polymerization of acrylic acid monomers to PDMS surface.....	15
Figure 2-4: A replica molded 2.5 cm long PDMS microchannel. Scale is in mm.	20
Figure 2-5: A 2.5 cm long microfluidic channel with drilled inlet and outlet holes seen at the top and bottom. Scale is in mm.....	25
Figure 2-6: A PDMS microchannel with drilled inlet and outlet holes bound to a flat coversheet to create a microfluidic device. The microchannel is 2.5 cm long and is seen at the center of the PDMS. The diagonal lines are on the coversheet and a result of the 3D printed mold used to cast the flat sheet of PDMS. Scale is in mm.	26
Figure 2-7: Fully assembled 2.5 cm long PDMS microdevice with PEEK tubing inserted to inlet hole for flow-through from syringe.	27
Figure 3-1: Flow through functionalization of PDMS with oxidized dextran. Dextran is further oxidized to express aldehyde functional groups.....	31
Figure 3-2: Mild fluorescence shown on the right side after UV acrylic acid grafting and binding of Alexa 488 hydrazide, compared to unmodified PDMS on the left.	37
Figure 3-3: Fluorescence image of attempted surface modification with the PDMS surface face down in the acrylic acid solution. No significant fluorescence indicating successful surface modification is seen.	38
Figure 3-4: UV grafted acrylic acid modified PDMS surface on the right showing binding of Alexa 488 hydrazide after 4 hours of exposure at 45 °C compared to the unmodified surface on the left.	39
Figure 3-5: Visible hydrophilicity change in the modified PDMS on the left compared to the unmodified surface on the right. The water in the PDMS-covered dish remains on the modified hydrophilic left side without wetting the unmodified hydrophobic side.....	40

- Figure 3-6:** PDMS modified with UV grafting of acrylic acid in benzophenone and acetone on the bottom of the image compared to the unmodified surface at the top. Fluorescence at the top is a result of tape residue stuck to the PDMS. 42
- Figure 3-7:** Permanent marker clearly writing on the modified surface surrounding the Alexa 488 hydrazide mixture on the left, compared to the thin line that was left on the unmodified surface on the right. 42
- Figure 3-8:** Alexa 488 hydrazide binding seen in a PDMS microchannel following acrylic acid/acetone UV grafting. 43
- Figure 3-9:** Comparison of water contact angle after surface oxidation. From left to right: H₂O; HCl; H₂O₂; equal parts HCl and H₂O₂; and 5:1:1 H₂O, HCl, and H₂O₂. The mixture of the three chemicals provided the largest change in water contact angle from 103° to 85°. 45
- Figure 3-10:** Dextran-modified PDMS on left side with attached Alexa 488 hydrazide compared to unmodified PDMS on the right. 45
- Figure 3-11:** Cumulative protein capture of cytochrome-C in a microfluidic channel calculated from the fluorescence of samples taken each minute from the microdevice outlet. 48
- Figure 4-1:** PDMS with varying concentrations of fluorescein. From left to right: pure PDMS, 0.1 mg fluorescein per 1 g PDMS, 0.5 mg fluorescein per 1 g PDMS, and 1 mg fluorescein per 1 g PDMS. 54
- Figure 4-2:** Concentration standards used in the fluorescein leaching experiments. 55
- Figure 4-3:** Experimental setup of 1g doped PDMS in liquid inside a 15 mL centrifuge tube. 56
- Figure 4-4:** Concentration of fluorescein leached into 5 mL of liquid after 4 days. Differences between the means of varying PDMS mass ratios for each liquid are significant at 99% confidence intervals except for that of water. 58
- Figure 4-5:** Mass of fluorescein that leached into the media (outlined bars), and the percentage of fluorescein that was leached out of the PDMS (solid bars). A lower percentage of leaching is seen from the higher starting concentrations. Samples are named according to the liquid media and the amount of fluorescein in mg per gram of PDMS. 59
- Figure 4-6:** Cumulative leached mass of fluorescein from a 2.5 cm long microfluidic channel containing 0.5 mg fluorescein per 1g of PDMS into McCoy's 5A media flowing at 5 μ L/min. 61

Figure 4-7: Leaching of microchannels with varied channel length, dopant concentration, and fluid media. Figures adorning bars indicate significance in comparisons within the same liquid media at 95% confidence intervals. Microchannels with a mass ratio of 0.1 mg/g do not show significant differences in means within the same media.	63
Figure 5-1: SolidWorks models of the two microchannel designs. The 150 post design is shown on left and 462 post channel on the right. Both are 1 mm wide.	73
Figure 5-2: a) Microchannel velocity slices in the 150 post microchannel show uniform velocity in the open rectangular channel, with acceleration between the posts. b) Though the maximum speed is marginally higher in the 465 post channel, the velocity between rows of posts is the same as the 150 post channel.	74
Figure 5-3: Streamlines showing the effect of the microposts in the channels on the laminar flow.	75
Figure 5-4: The flow velocity profile between microposts showing the region of maximum flow velocity in the 462 post microchannel. The spaces between microposts show similar flow profiles as an independent rectangular channel the size of the space between posts.	76
Figure 5-5: Dimensionless parameter a vs the aspect ratio of a rectangular microfluidic channel. The value of a is directly proportional to the pressure drop in a rectangular channel. The aspect ratio is limited to 1, at $w/h > 1$ the width and height are interchanged.	77
Figure 5-6: Flow velocity profiles in the PDMS carbonylated protein capture enrichment channel at different flow rates.	78
Figure 5-7: The three designs chosen as cell culture microchannels to model shear.	80
Figure 5-8: Velocity profiles and maximum flow velocities in mm/s for the three channel designs.	81
Figure 5-9: Velocity profile of the triangle channel in the vertical y direction, at 0.05 mm intervals from channel center to channel edge. From top to bottom, the profiles start at the center and move to the lateral edge.	82
Figure 5-10: Shear rate and shear profiles in s^{-1} of the three microfluidic cell culture channel designs.	83
Figure 6-1: Visual outline of the photolithography process for creating microfluidic molds.	87
Figure 6-2: The base of the spin table, showing the supports and the ring for holding the electric motor. All dimensions are in mm.	92

Figure 6-3: Base of the 3D printed spin table with Hall effect sensor attached via epoxy.....	92
Figure 6-4: The top of the spin table designed to securely hold the silicon wafer centered over the motor during spin coating. The design is optimized for minimal vibration and rapid printing times. All dimensions in mm.	93
Figure 6-5: Spin table top, with magnet attached to top right arm via epoxy.	93
Figure 6-6: Assembled spin table with motor and Hall effect sensor affixed.	94
Figure 6-7: Low-side transistor switch for controlling the spin table motor speed. The low-side scheme of this switch maintains a higher voltage across the motor to aid in maintaining the proper speed of the spin table.	95
Figure 6-8: The selective laser sintering-created second design of the spin table, attached to power source and the Arduino Uno microcontroller. The Hall effect sensor is on the vertical pillar protruding from one of the support arms, and the transistor is seen in front of the base of the spin table.	99
Figure 6-9: Cross section of a sealed PDMS microdevice created with the mold from the 3D printed the spin table and UV LED board.....	100

ACKNOWLEDGMENTS

I'd like to thank Dr. Bryant Hollins for providing the direction for this project and clarity when the path seemed unclear. You gave me the freedom and ability to take ideas and turn them into the work presented here, and made this research fun. I thank Dr. Steven Jones for the insightful edits and help with the leaching paper, and asking the hard questions to provide a different perspective. I thank Dr. Teresa Murray for always providing valuable and interesting discussions and for being a great motivator. I thank Dr. Mark DeCoster for his instruction and teaching in the field of fluorescence, that knowledge has been invaluable to this research. I thank Dr. Yuri Lvov for becoming a part of my advisory committee in the last year. I thank Dr. Patrick O'Neal for expanding my knowledge past my research and for the experience with the Animal Physiology Lab. I thank Dr. Eric Guilbeau for introducing me to the Biomedical Engineering department at Louisiana Tech. I thank Dr. Jim Spaulding, Emily Born, and Arlene Hill, for helping when I needed to find people, equipment, supplies, or anything else, and for letting me in when I locked myself out. I thank Francois Decuir and Hunter Montgomery for always being ready to discuss ideas and problems. Many new directions and experiment ideas were born from these conversations. I thank the American Indian Graduate Center for providing funding for tuition and conference travel and reducing financial stress. I thank my family, who has always been interested, loving, and supportive when I needed it most. Without them, I wouldn't be the person I am today. Finally, thank you to Paul and

Johnnie Hogan for being instrumental in bringing me to Louisiana Tech, and for putting a roof over my head when my apartment burned. To everybody that has had a part in making this achievement happen, thank you.

CHAPTER 1

INTRODUCTION

1.1 Background

1.1.1 Microfluidics

Microfluidics is the manipulation of liquids and gases on the sub-millimeter scale, most often with one dimension in the 10-100 μm range [1]. Since their rapid growth of popularity in the 1990's as micro-total-analysis-systems (μTAS) and lab-on-chip (LOC) devices, microfluidic platforms have been developed for a wide range of applications in biology and engineering, using a variety of materials such as glass, silicon, thermoplastics, and elastomers [2]. Microfluidic devices found their first applications in analytical chemistry as a miniaturized version of techniques like electrophoresis [2]. Recent work shows the feasibility of microfluidic devices for biomedical applications such as cell capture, stem cell culture, DNA hybridization, and implantable devices [3–7]. Polymer-based microfluidic devices lend themselves especially well to surface modification [8–17]. Microfluidics offers many advantages over macroscale techniques such as small sample sizes, minimal reagent use and waste, and reduced assay times [1], [18], [19]. Additionally, microfluidic devices provide features such as strictly laminar flow, short diffusion lengths, precise control over microenvironments, and the ability to closely mimic *in vivo* microenvironments, making them promising platforms for cell culture applications and creating and studying cellular microenvironments [5], [20].

Microfluidics is further aided by the use of rapid prototyping techniques for fabrication of new device designs, allowing faster concept-to-device times.

Since 2000, there have been 24,324 papers published on the topic of microfluidics. Since the first microfluidic devices in the 1970s emerged from the microelectronics industry, new applications have been discovered, adapted, and created for these small-scale devices in biology, engineering, chemistry, and medicine. Though microfluidics remains rooted largely in academia, some highly successful commercial products are a result of microfluidic developments, including inkjet printers and home pregnancy tests. Microfluidics provides an opportunity to perform laboratory tests and experiments with minimal reagent use, short time requirements, low limits of detection, and minimal equipment investment.

1.1.2 Poly(dimethylsiloxane)

Poly(dimethylsiloxane), or PDMS, is a flexible silicone-based polymer with rubber-like qualities, and it has emerged as a material of choice in academic research [21]. It is inexpensive, highly reproducible, strongly biocompatible, optically clear, permeable to gases, and has good elasticity and mechanical properties [14], [21], [22]. Its elastomeric properties facilitate simple device fabrication at low costs, and the methyl groups on the surface lend themselves well to chemical surface modification for creating application-specific devices. Due to these properties and the ability to make many different device designs quickly and easily, PDMS provides an excellent platform for microfluidics research. Since its introduction to microfluidics in 1997 by Effenhauser *et al.* [23], the use of PDMS has been widespread, finding applications in research ranging from cell culture and analysis, microenvironment creation, chemotaxis, vascular function,

capillary electrophoresis, drug research, bioreactors, and various other lab-on-chip applications [19], [24].

1.2 Project Overview

This research expands the use of PDMS in the field of biomicrofluidics in three novel ways: a new surface modification that allows PDMS to be used for oxidative stress biomolecule capture, a doping technique that takes advantage of the bulk diffusion properties of PDMS, and the use of modeling and rapid prototyping techniques to simplify the design and fabrication of silicon mold masters for creating PDMS microdevices. This research consisted of the following goals. First a carbonylated protein capture system was created on a PDMS microchip to provide greater flexibility, chip availability, and less cost than a comparable poly(methyl methacrylate) (PMMA) or other protein enrichment system. By attaching hydrazide functional groups to the surface of PDMS via an oxalyldihydrazide crosslinker, the carbonylated protein capture methodology demonstrated selective capture to such oxidized proteins. This surface modification and enrichment has not previously been reported on PDMS. Secondly, the doping of PDMS with small molecules for intentional diffusion and leaching out of the polymer into fluid and microchannel flow was tested and shown to be viable. The leaching was characterized and quantified, showing possible benefits to a property of PDMS that was thought to be a shortcoming. Third, Computational Fluid Dynamic (CFD) modeling was used to characterize the flow rate, shear rate, diffusion and mixing properties in microdevices and validated the design of new PDMS microchannels for microfluidic molecule capture and molecular separations. Finally, a system for generating microfluidic molds for soft lithography was designed that eliminates the need for

expensive photolithography equipment and cleanroom environments, advancing the feasibility of microfluidics as a truly portable point-of-care system.

1.2.1 Hypothesis

The overall hypothesis for this research is that the material properties of PDMS can be manipulated to create novel and improved bioanalytical solutions. In particular, PDMS-based microfluidics can provide a better platform than PMMA or other common microfluidic substrates by way of lower cost, ease of device fabrication, higher effectiveness in biomolecule capture, ability to be doped with small molecules for intentional leaching into microdevices, and be designed and created using low cost methods from concept to prototype.

1.2.2 Specific Aims

The hypothesis was tested through the following aims:

1. Design a surface modification protocol for immobilizing hydrazide onto the surface of a PDMS microchannel to enrich carbonylated proteins in a PDMS microdevice
2. Demonstrate the doping of PDMS microdevices for intentional leaching into microfluidic flow or cell culture with predictability and control over the leaching parameters
3. Apply computational fluid dynamics methods to create, test, and characterize existing and novel microfluidic channel designs by observing flow rate, shear, diffusion and mixing properties of PDMS microdevices
4. Design and implement a low-cost, rapid prototyped system for creating new microfluidic mold masters for the fabrication of PDMS microdevices without the

need for a cleanroom environment or significant investment in specialized equipment.

1.3 Significance

This research advances the field of biomicrofluidics research using PDMS in several areas. First, biomolecule detection and capture is achieved at increased efficiency and decreased costs over current methods in the field. By designing a protocol for carbonyl enrichment, biomarkers for early detection of diseases and effects of substances present in the environment can be detected using small sample sizes. PDMS enables point-of-care functionality by providing a platform for device creation in resource-limited applications.

Doping of PDMS advances assays and cell culture devices, by enabling the controlled delivery of small amounts of drugs, signal molecules, nutrients, and other factors without human interference and minimizing the risk of contamination. The doping of PDMS for intentional leaching of small molecules has not been studied, and provides yet another way to tailor PDMS for a specific application.

CFD in microfluidics allows the optimization of novel microfluidic designs before any investment is made in creating a mold or device. The verification of a cell culture device design and insight into the behavior of fluid, particles, and molecule concentration around a modeled cell layer is a possibility with this technology. CFD allows the continued optimization of a novel design, ensuring more resources are put towards the goal of the device rather than into the device itself.

Rapid prototyping techniques and commonly used microcontrollers are used in this work to create a photolithography system at a much lower cost than traditional

cleanroom techniques. This system is portable and powered by 9 Volt batteries, enabling any lab or researcher to create a new microfluidic mold without incurring costs associated with cleanroom access.

These advancements in microfluidics and applications of PDMS are made possible through the research presented in this dissertation.

1.4 Dissertation Overview

This dissertation will first outline the background of microfluidics as a research area, and the history of PDMS as it has been used in microfluidics. Background information on oxidative stress, biomolecule detection, bulk leaching in PDMS, analyte sequestration, and manufacturing techniques for PDMS will follow. The next chapters will deal specifically with each facet of this project by showing the current method, the theory, the methods and materials used in this research, results, and conclusions drawn from each experiment. CFD in microfluidics will show the shear and flow profiles in numerous microfluidic devices and discuss how these results can be applied to future device design. The low cost microfluidics implementation will detail the parts and devices created, show the building process and the coding, and discuss the rapid prototyping capabilities used to create such implementations. The dissertation will conclude by discussing the conclusions drawn from the project as a whole and how they will direct future work in this area. Improvements and optimizations will be presented as well as other possibilities for paths this project could take.

CHAPTER 2

BACKGROUND

2.1 Microfluidics

The origins of microfluidic devices can be traced to the 1970's when micro-scale techniques for a range of applications were introduced. Microscale and capillary techniques were developed for gas chromatography, high-pressure liquid chromatography, and capillary electrophoresis revolutionizing the field of chemical analysis [1], [25]. Other applications for microscale manipulation of liquids developed around the same time include inkjet printing and integrated circuit components [18]. Though inkjet printing became a major commercial success, the field of microfluidics in research saw little further development until 1990, when the concept of microfabricated total analysis systems (μ TAS) was published [26]. Many of the uses focused on expanding the low reagent volume chemical analysis abilities, and reducing the necessity of large laboratory equipment. Because microfluidics originated in microelectronics, many of these early devices were made on silicon and glass, with some attempts using thermoplastics. From here, applications in miniaturizing molecular biology coincided with the rise of genomics and DNA sequencing.

The rapid expansion of academic microfluidic studies goes hand in hand with the emergence of poly(dimethylsiloxane) (PDMS) as a microfluidic substrate. With the development of soft lithography [27] and micromolding using photolithography, the low

cost and ease of use of PDMS has made it a favorite in academic laboratories worldwide. The rapid curing times and low material cost for PDMS enables rapid prototyping techniques to be used in the development of complex microfluidic designs. A number of novel applications of this polymer have been reported in fields all across the biological and physical sciences, and many exploit the unique nature of PDMS as a microfluidic substrate, which will be covered later. Other new developments in microfluidics are related to improvements in materials science, with a variety of new elastomers, plastics, and polymers seeing utilization in new devices.

Microfluidic devices have traditionally been created for sample analysis and separations. The first microfluidic system was a gas chromatograph on a single silicon wafer, followed much later by a smaller high pressure liquid chromatography device on silicon [28]. Many microfluidic technologies seek to improve upon chromatography methods or bring them down to a small scale to reduce reagent use and simplify extraction of the target molecule. However, microfluidics has branched into sample preparation, separation, detection, reaction, cell culture, immunoassays, and diagnostics [29]. DNA analysis, polymerase chain reaction, and DNA sizing on a microfluidic chip have been developed as well [30]. Within each of these categories, the specific analyte, molecule, cell type, or protein a device can target is dependent on the surface modification, device structure, and chemistry that each researcher develops for the device. With a wide variety of materials available with modifiable surfaces, the versatility of microfluidic devices may help them maintain their prominence in academic research for some time, while also expanding their presence into clinical settings.

Microfluidic analysis offers many advantages over macroscale techniques such as small sample sizes, minimal reagent use and waste, and reduced assay times [1], [18], [19]. Additionally, microfluidic devices provide features such as strictly laminar flow, short diffusion lengths, precise control over microenvironments, and the ability to closely mimic *in vivo* microenvironments, making them promising platforms for cell culture applications and creating and studying cellular microenvironments [5], [20]. Their small sizes allow for portability and mass manufacturing, reducing the cost per test or device. The microscale dimensions minimize dead volume in the system which aids in minimizing reagent use and time to result. Microfluidics is further aided by the use of rapid prototyping techniques for fabrication of new device designs, allowing faster concept-to-device times. New designs can be created that use modular sections, by 3D printing molds, machining, or by hand. Some materials used in microfluidics are also amenable to mass production methods, enabling a proven design to be made cheaply and efficiently [2].

Microfluidic devices traditionally were fabricated in glass or oxidized silicon using micromachining, etching and photolithography [31]. Because these methods were already well established in the microelectronics and semiconductor industry, they were readily adapted to microfluidics. However, these methods often required cleanroom environments, dangerous chemicals, high temperatures, and significant time investment. Soon after the introduction of the first microfluidic devices, new materials began to surface, especially polymer-based substrates. Polymers are preferable materials to glass and silicon because they can be inexpensive, disposable, gas permeable, and optically transparent, while the surfaces can be readily modified [32]. Different polymers may be

chosen based on the desired chemical and mechanical properties of the device, the materials or solvents it may be exposed to, or the modification to be performed on the polymer. Polymers also tend to be easier to use with rapid prototyping techniques such as photolithography and 3D printing. The advent of polymer microfluidics rapidly accelerated the growth of the field, giving it the flexibility for individual researchers to create unique chip designs and tailor the geometry and chemistry to their specific needs.

2.2 Background of Poly(dimethylsiloxane)

Poly(dimethylsiloxane) has become the most popular material choice for microfluidic platforms [21]. Since its introduction to microfluidics in 1997 by Effenhauser *et al.* [23], the use of PDMS has been widespread, finding applications in research ranging from cell culture and analysis, microenvironment creation, chemotaxis, vascular function, capillary electrophoresis, drug research, bioreactors, and various other lab-on-chip applications [19], [24]. PDMS is one of the most common microfluidic substrates in academic laboratory settings [2] due to its numerous advantages over materials such as glass, silicon, or other polymers such as poly(methyl methacrylate) (PMMA). **Table 2-1** shows a detailed comparison between PMMA and PDMS, two very popular microfluidic substrates.

PDMS is inexpensive, highly reproducible, biocompatible, and optically clear. It has good elasticity and mechanical properties, and is highly permeable to gases [14], [21], [22]. Its low cost enables the production of large numbers of identical devices or a small number of experimental devices in an academic setting [33]. Small features can be replicated accurately and with high aspect ratio through soft lithography and replica

molding [27]. These features make it especially well-suited for microfluidic applications in academic and resource-limited settings.

Table 2-1: A comparison of PMMA and PDMS as substrates for microfluidic platforms.

	PDMS	PMMA
Cost	Low cost for polymer; very little polymer used to create chip (~20 g for 9 chip mold); little specialized equipment needed for fabrication	Moderate; high equipment investment including hydraulic press, vacuum chamber, micromilling machine for mold master
Chip Fabrication	Poured over silicon mold at 80 °C, cure 1 h; sealed to PDMS flat sheet using uncured PDMS as a glue or plasma oxidized and pressed together, possibility of filling microchannel with uncured PDMS	Hot embossing using high temperature and pressure in vacuum, UV surface modification, thermally bound to coverslip, possibility of melting microchannel
Flexibility of Chip Design	Multiple chip designs can be placed on one mold; multiple molds can be made using soft lithography; highly reproducible; can produce varying chip thicknesses by varying volume of uncured polymer used	Mold master must be micromilled in metal plate; mold master may wear down; Must purchase multiple thicknesses of PMMA sheet for different chip thickness
Wetting Properties	Extremely hydrophobic; water contact angle 110° [22]; requires surface modification for hydrophilicity	Hydrophilic; water contact angle 72° unmodified, lower after surface modification [34]

PDMS consists of a silicon-oxygen repeating backbone with two methyl groups attached to the silicon atom. The polymer is hydrophobic, with a water contact angle of 110°. PDMS is gas permeable, allowing for ease of transport of oxygen and carbon dioxide in cellular studies [2]. It is transparent to light, making it viable for microscopy,

fluorescence, and visual studies. The molecular structure of PDMS is shown in **Figure 2-1**.

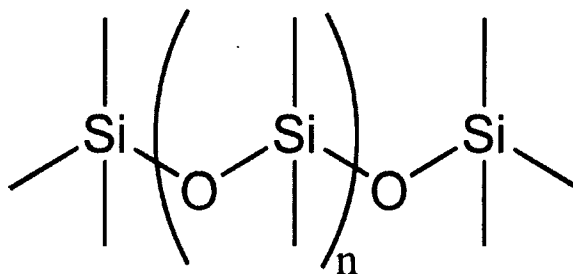


Figure 2-1: Chemical structure of PDMS.

However, some properties of PDMS can negatively impact bioassays. For example, the hydrophobic nature of the polymer allows small hydrophobic molecules to leach into the polymer, potentially affecting assay results. In addition, small uncured oligomers can leach out of the polymer bulk and into solution, also interfering with studies or assays. Some of these negative consequences can be mitigated through surface modification protocols prior to experiments.

2.3 PDMS Surface Modifications

Numerous surface modification and treatment techniques have been developed that counteract this problem of high hydrophobicity, analyte sequestration and oligomer leaching, and that allow the surface of the polymer to be tailored for a specific microfluidic application. Modifications have been reported to place monolayers of various chemicals, oxidize the surface, lay gold tracks onto a PDMS substrate, create primary amine groups, or to create small cracks to allow hydrogel-like swelling in bulk polymer [6], [15], [35–39]. Surfaces have been targeted for applications such as DNA hybridization [6], micropatterning of cells and biological materials [11], selective binding

of tagged peptides [40], immobilization of fibronectin [41], detection of cardiac biomarkers [42], to prevent protein adhesion or adsorption [43], [44], or to perform a microfluidic ELISA [45]. Because of this flexibility and ability to take advantage of the chemistry of PDMS, the polymer provides a versatile platform to run many conventional laboratory tests on a small scale, and to create new devices for cell culture, biomarker detection, or sample separation.

Native PDMS is highly hydrophobic because the surface consists of non-polar methyl groups. This property deters cellular attachment, restricts microchannel filling, and can result in non-specific adsorption of proteins and other molecules to the surface [11], [17], [24], [46]. A majority of modifications that have been developed for PDMS are designed to increase the wettability of the surface. One of the most common methods for achieving this is oxidation of the surface layer through RF plasma treatment using oxygen or air [47]. This has the additional benefit of increasing the adhesion of PDMS to another layer of PDMS or to a glass coverslip to seal the microdevice or channel [48]. The oxidation of PDMS turns the surface methyl groups into hydroxyl groups, increasing the hydrophilicity and the reactivity of the surface. From that step, further modifications can be made as the hydroxyl groups on the surface are much more reactive. The exact mechanism of reaction is unknown, but the process from Chen and Lindner (2007) is outlined in **Figure 2-2** [49]. Modifications based on plasma treatment include the grafting of acrylonitrile to the surface [50], or attachment of layers of acrylic acid and fluorocarbons [51]. From these surface functionalizations, numerous reactions could be used to attach molecules or proteins to the surface of PDMS.

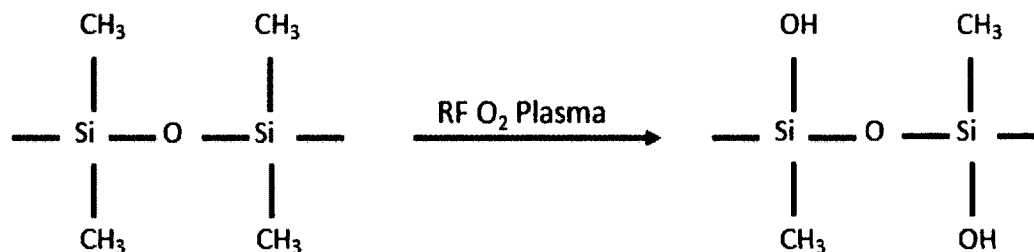


Figure 2-2: Surface modification of PDMS via RF plasma treatment resulting in hydroxyl functional groups on the polymer surface.

Other surface modification schemes seek to attach functional groups to the PDMS surface via covalent bonding, often using ultraviolet light as an energy source. Graft polymerization using UV and wet chemical immersion are popular methods of modification because they provide high specificity [17]. Because the polymer surface has no chemically reactive groups, UV irradiation is necessary to generate free radicals to create sites for graft polymerization [16]. The UV irradiation is often combined with a photoinitiator to handle electron chain transfer during polymerization, often benzyl alcohol or benzophenone [39], [52]. Hu *et al.* (2002) showed that this method could be used to attach acrylic acid, acrylamide, dimethyl acrylamide, and other monomers to confer a variety of functionalities to the surface of PDMS [22]. This technique has an advantage for microfluidics in that it allows the modification of enclosed channels filled with the monomer solution, employing the optical clarity of PDMS to allow the UV light to modify the inner surface of the microchannel [52]. The mechanism of UV radical generation and graft polymerization is shown in **Figure 2-3**.

PDMS surfaces can be functionalized without exposing the polymer to high energy sources, relying solely on chemical solutions for modification. The most common method of solution-phase modification relies on hydrochloric acid and hydrogen peroxide

in water to oxidize the PDMS surface, resulting in hydroxyl functional groups [44], [45]. From here, a variety of silane molecules can be used to bind the –OH groups on the surface and impart amine, isothiocyanate, PEG, or other groups via reactions with the silanol groups created on the surface. Using the groups bound to the surface as building blocks, an immunoassay or DNA strands for hybridization could be integrated into a microfluidic device. Oxidation is often followed by 3-aminopropyltriethoxysilane (APTES) to impart amine functionality to the surface of PDMS. Advantages of this method include the lack of need for a high energy source, and ensured modification for deeply embedded PDMS microchannels.

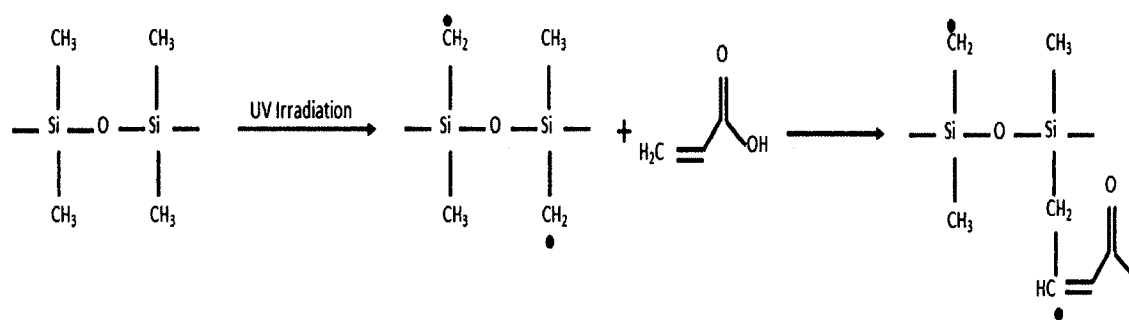


Figure 2-3: UV graft polymerization of acrylic acid monomers to PDMS surface.

PDMS surface modifications are not permanent. For plasma modified oxidized surfaces, the water contact angle reverts to that of native PDMS within 30 minutes when exposed to air in ambient conditions [31]. Similar hydrophobic recovery phenomenon have been reported with grafting modification schemes as well. Several mechanisms have been proposed to explain this phenomenon, such as condensation of surface silanol groups, reorientation of the polar groups back into the PDMS bulk, or the diffusion of low molecular weight (LMW) entities such as uncured oligomers to the surface from the PDMS bulk [12], [49]. Bulk diffusion of LMW groups is the dominant mechanism of

hydrophobic recovery [53]. The LMW PDMS oligomers migrate to the polymer surface and reduce the surface free energy [54]. Hydrophobic recovery is slowed or prevented when modified PDMS is stored in a polar solvent such as water, but this is not always practical in microfluidic channels. Additionally, these uncured and LMW oligomers can diffuse into solvents and may contaminate products of reactions in PDMS microdevices, and hydrophobic PDMS surface may also sequester small hydrophobic molecules [2], [20].

Several methods have been developed to minimize the effect of hydrophobic recovery in PDMS microdevices. As previously mentioned, storage of modified PDMS in polar solvents has extended the longevity of the surface modification to the scale of months. Thermal aging or treatment with solvents through Soxhlet extraction works to remove the uncured oligomers from the polymer [55], but can also cause swelling and distortion in the PDMS. When dealing with high aspect ratios and microscale features, this distortion is not desirable. Treatment with plasma for an extended time, or with plasmas of pure oxygen or argon, create more specific modifications as well as create a hard silanol layer on the surface of PDMS which is not easily reabsorbed into the polymer bulk. Downsides of this method include the introduction of microcracks on the PDMS surface that allows the absorption of solvents or analytes, causing swelling, distortion, or false assay results.

Covalent bonding of monomers such as acrylic acid to the surface of PDMS can minimize hydrophobic recovery if done in a way that provides sufficient cross-linking across the modified surface. When uniform “brush” grafting is performed, the monomers are small enough to be reincorporated into the polymer bulk and hydrophobic recovery

will occur. However, if the grafting is done in the presence of water, grafting can proceed in a disorganized manner causing covalent bonding of the monomer solution to both the PDMS and across itself to create a web of monomer on the polymer surface.

Hydrophobic recovery is also combated by attaching larger molecules to the surface of PDMS. The larger size prevents these molecules from being reabsorbed into the PDMS bulk, and thus creates a more stable modified surface. The stability can be provided by way of cross-linking as in the grafting modification methods, or by way of steric hindrance preventing the large molecules from being reincorporated into the polymer.

2.4 Background of PDMS Leaching and Absorption

The porous nature of PDMS, while allowing gas permeability, also allows small hydrophobic molecules to absorb into the polymer bulk. Toepke and Beebe demonstrate the absorption of Nile Red, a hydrophobic dye into PDMS from microchannels [56]. Regehr *et al.* (2009) demonstrate the absorption of estrogen into PDMS, decreasing the cellular response [20]. Absorption can cause issues in microfluidic cell culture or microfluidic assays, particularly if a molecule of interest is absorbed. Diffusion into the polymer may also cause significant measurement errors in microfluidic assays [57]. The absorption of a molecule into PDMS depends on the hydrophobic properties of the molecule [38]. Rhodamine red, a hydrophobic fluorescent dye, is readily absorbed into PDMS; the amount of absorption has been quantified and studied under different conditions [58]. Larger hydrophobic molecules such as paraffin wax have been shown to prevent absorption of small hydrophobic molecules when absorbed into PDMS [59].

2.5 Laboratory Techniques for Manufacturing PDMS Devices

PDMS is classified as an elastomer: a polymer with a uniform surface and soft, flexible mechanical properties that allow it to conform to other surfaces and bind reversibly and irreversibly [60]. To prepare PDMS, the prepolymer is mixed with its curing agent in a 10:1 wt/wt ratio and the mixture is cured for 48 hours at room temperature, overnight at 60 °C, or for 1 hour at 80 °C. Sylgard 184 from Dow Corning was used in this work, and is a commonly available elastomer kit for fabricating PDMS devices. It contains vinyl terminated siloxanes and a curing agent containing silane groups which react with a platinum catalyst through a hydrosilylation mechanism [18], [61]. The liquid mix of polymer and curing agent can be poured into any shape or over a mold and peeled off when cured, retaining very sharp and accurate features of the mold. Several methods have been developed to fabricate PDMS devices for stamping, microfluidics, three-dimensional devices, active components in flow systems, and several others. The processes for PDMS fabrication can be broken down into replica molding, soft lithography, or microcontact printing.

2.5.1 Replica Molding

Replica molding can be accomplished by any thermopolymer that is heated above its glass transition temperature and made to fill a mold or cover a pattern. For PDMS, the polymer is in a liquid state before curing, so it can be poured to fill a dish or cover a silicon mold. For the small features and high aspect ratios commonly used in microfabrication, casting PDMS over a SU-8 photoresist on silicon wafer mold is the most commonly used method.

The silicon mold is produced by spinning SU-8 100 photoresist, a photocurable epoxy, onto the surface of a clean silicon wafer. SU-8 is a negative photoresist, meaning that the portions of the epoxy exposed to UV light harden and allow the unexposed portions to wash away in the developer. The thickness of the photoresist coating is determined by the spin speed and the time that the photoresist is spun.

The PDMS is poured into a petri dish or other dish containing the silicon wafer, and cured at 80 °C for 1 hour, or any combination of temperature and time depending on the desired hardness and completeness of the cure. Following curing, the PDMS device is gently peeled from the mold master, taking advantage of the soft elastomeric properties of the PDMS [35]. The silicon wafer mold can be used for many cycles of device fabrication, and modes of failure are typically too much force from the user or separation of the photoresist from the wafer [31]. PDMS can faithfully replicate small raised features from a silicon mold, and is released easily. Its flexibility allows the created device to make conformal contact with an imperfect or curved surface, and shrinking is minimal upon curing, so microchannels remain dimensionally accurate [27]. To ensure the functionality of the device and to prevent collapsing or bending of small features because of the flexibility of PDMS, the aspect ratio of features created in replica molding must be between 0.2 and 2 [62]. The features of the PDMS microchannels studied in this work are 100 μm by 100 μm , for an aspect ratio of 1. Replica molding can be used for resolutions down to 10 nm, or paired with rapid prototyping techniques for low turnaround times on new device testing. Molds for PDMS devices can be created with a 3D printer, allowing the time from concept to device to be only a few hours. A replica molded PDMS microchannel used in this research is shown in **Figure 2-4**.

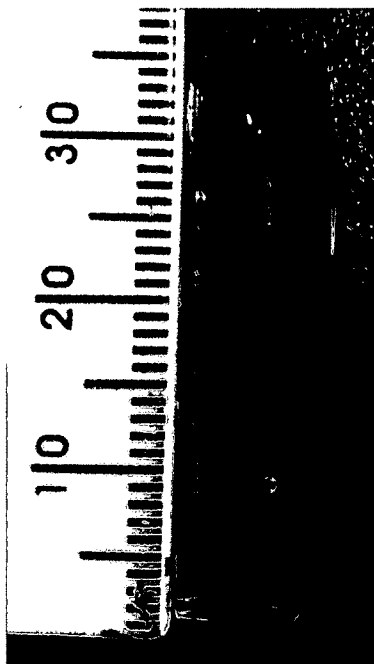


Figure 2-4: A replica molded 2.5 cm long PDMS microchannel. Scale is in mm.

2.5.2 Soft Lithography

Soft lithography refers to a series of methods introduced by the Whitesides group in the late 1990's that uses a PDMS stamp or mold created by the replica molding methods discussed in the previous section [31], [63], [64]. The stamp or mold created can then be used to pattern materials, monolayers, or other PDMS structures onto a substrate or microfluidic device [65]. Soft lithographic methods have applications in creating structures on a substrate surface, modifying the surface of a substrate to become part of a microfluidic channel, creating three-dimensional polymeric structures that could not be created photolithographically, patterning surface characteristics with self-assembling monolayers, or for patterning microchannels on a substrate to be enclosed. The common feature to all the techniques of soft lithography is the use of a PDMS mold or stamp, taking advantage of the flexibility, conformal contact capabilities, and “softness” of the

PDMS used. Though the main method for creating PDMS devices in this work is replica molding, soft lithography is the technique that provided simple microfabrication techniques to academic laboratories and resulted in the boom of PDMS in biomedical research, so the techniques will be discussed.

2.5.2.1 *Microcontact printing*

Microcontact printing, or μ CP, uses the relief pattern on a PDMS stamp created through replica molding to form patterns of self-assembled monolayers (SAMs) onto a substrate surface by contact [65]. Self-assembly refers to the spontaneous organization of subunits or molecules into a stable structure via molecular interactions dependent on the properties of the subunits [27]. The formation of these layers occurs near thermodynamic equilibrium which allows the spontaneous formation and the rejection of defects from the formed structure.

Self-assembled monolayers are created on a PDMS stamp by covering a replica molded stamp in the solution of the desired monolayer material, commonly poly-ethylene glycol or other alkyl chains, depending on the substrate to which the SAM will be transferred. The PDMS stamp containing the SAM is then pressed against the desired substrate to be patterned, often a silicon, gold, glass, or polymer. These SAMs can be used in patterning microfluidic devices, as resists in wet etching, templates for selective deposition, or for cellular immobilization [18], [27], [65]. PDMS provides a perfect platform for this transfer due to its high fidelity replication and the ability to conform to curved substrates, or for a PDMS roller to provide continuous transfer of a repeating pattern across longer distances [66].

2.5.2.2 Micromolding

Soft lithographic techniques can also be used to mold polymers and other materials using PDMS devices as mold masters. Micromolding in soft lithography includes replica molding, microtransfer molding, micromolding in capillaries, and solvent assisted micromolding [27], [64], [65]. Each method involves the use of a PDMS mold master to form and construct polymer structures onto a glass or silicon substrate. Extensions of these methods can be used to create multilayer or three-dimensional structures by repeating the process on top of the previously constructed features.

Replica molding in soft lithography is identical to the replica molding procedure discussed previously, except that the mold master is made of PDMS. The PDMS mold is filled, covered with, or placed on top of a UV or thermally cured polymer. The polymer is then cured and the flexibility of the PDMS allows easy removal of fine or fragile features on the newly cured polymer. Xia and Whitesides report replication of features down to 10 nm size with this method [27].

Microtransfer molding uses the same method as replica molding, but affixes the formed structures to a substrate. Once the PDMS mold is filled, the excess prepolymer is scraped off and the mold and prepolymer are placed on the surface of a substrate such as a silicon wafer. The prepolymer is then cured and the PDMS mold peeled away, leaving the relief pattern affixed to the surface of the substrate. The flexibility of the mold allows microstructures to be patterned on nonplanar surfaces. Additionally, repeated applications of this method onto the features already created enables the production of multilayer and three-dimensional features [67].

Micromolding in capillaries is another extension of replica molding in soft lithography. The PDMS mold master is placed onto the substrate, with open channels on the sides of the mold cast so that they do not contact the substrate. A low-viscosity prepolymer is placed at the end of the capillaries on the substrate and the features in the mold fill via capillary action. The polymer is then cured and the PDMS mold master peeled away, leaving the features on the desired substrate. The advantage of this method is the patterning of a wider variety of materials than in photolithography, and the variety of polymer materials that can be used. Polymers that are soluble can be mixed with a solvent to fill the capillaries, then the solvent evaporated away leaving only the polymer. If the features are small, closed capillaries can be filled with the gas escaping through the permeable PDMS mold [27]. Non-polymeric molecules and biomolecules can also be patterned with this method.

2.5.3 Three-Dimensional PDMS Microchannel Fabrication

Apart from microtransfer molding, all of the previously described methods are useful for patterning one layer of polymer or molecules onto a substrate. The result is a 2-dimensional, flat device or a single microchannel if enclosed into a microfluidic flow device. Because of the labor and cost-intensive methods necessary to create three-dimensional features in silicon, as well as the lack of transparency, dry etching three-dimensional channel paths in silicon is unsuitable for most biological studies [68]. Other methods for creating three-dimensional PDMS devices involve creating complex molds through stereolithography. Depending on the desired features in the microfluidic device, stereolithographic molding is limited by the necessity of peeling the PDMS from the mold.

Two common methods are used to create three-dimensional microfluidic devices in PDMS. The first is sandwich molding individual layers of two-dimensional PDMS devices on a photolithograph silicon mold, where the PDMS is placed on the mold and a glass slide is placed over the top of the mold to apply pressure, minimizing the thickness of the device. The desired features would protrude through the entire thickness of the cured PDMS. Coupled with traditional 2-dimensional devices, these components can be stacked together, or connected to the through-features to create complex, modular, three-dimensional microfluidics.

Another method involves creating embedded microchannels in PDMS by molding the PDMS around a copper wire suspended in the middle of the prepolymer mixture [69]. A copper wire is stretched across a plastic box and held in tension, while another copper wire is formed into a coil and placed around the central wire. The helical wire is held in place via attachments on either side of the plastic box. Prepolymer is poured over these wires and cured. To release the wires, the PDMS is soaked in toluene to swell the device, and the wires removed. The helical channel around the central channel created by Singh *et al.* was filled with compressed air to control the flow of liquid through the central channel [69]. This technique can be used to create channels in any arbitrary shape desired.

Three-dimensional microchannels are especially useful for mixing in microfluidic devices. The highly laminar flow schemes at the flow rates seen in most microfluidic devices ensures little mixing of fluids through a device. Hard turns in multiple directions can aid in the mixing of samples. Three-dimensional devices can also lead to the creation

of more complex analysis systems with multiple inlets and outlets for a variety of tests to be done on one microchip.

2.5.4 Microfluidic Device Fabrication in PDMS

A microfluidic device consists of an inlet, and outlet, and the microchannel in whatever design is desired between the inlet and outlet. If a microfluidic feature is cast into PDMS from a silicon mold created via photolithography, all features in the PDMS have the same thickness. Thus, the holes for fluid inlet and outlet must be drilled through the thickness of the PDMS or cast into the polymer as it is curing. Drilling with small bits at high speeds provides proper inlet and outlet size holes for the experiments performed in this work. **Figure 2-5** shows a microfluidic channel with inlet and outlet holes drilled prior to sealing.



Figure 2-5: A 2.5 cm long microfluidic channel with drilled inlet and outlet holes seen at the top and bottom. Scale is in mm.

After drilling the holes, the microchannel must be sealed against a flat PDMS sheet. Often this step is performed using RF plasma with oxygen or air, oxidizing the surfaces and then placing them in conformal contact with each other, where an irreversible bond is formed. However, the plasma can interfere with any existing surface modifications. Another method of sealing the microchannels is to use uncured PDMS mixture as a glue, bring the channels and cover sheets together, and cure the glue mixture with heat overnight. **Figure 2-6** is a fully sealed PDMS microchannel prepared for microfluidic experiments.

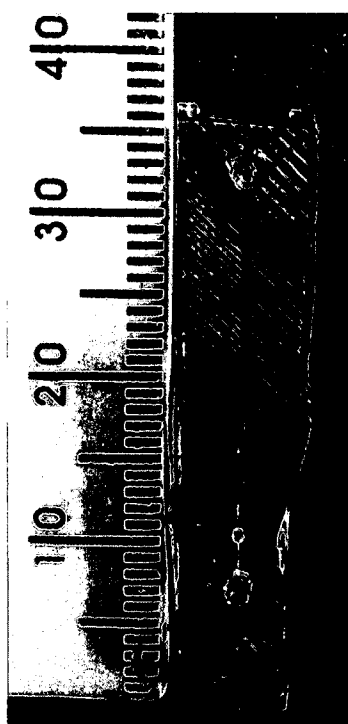


Figure 2-6: A PDMS microchannel with drilled inlet and outlet holes bound to a flat coversheet to create a microfluidic device. The microchannel is 2.5 cm long and is seen at the center of the PDMS. The diagonal lines are on the coversheet and a result of the 3D printed mold used to cast the flat sheet of PDMS. Scale is in mm.

Following the casting, drilling, and bonding of microchannels, the fully assembled microdevices are ready for surface modification and flow-through of samples. PEEK tubing is attached to a syringe, and is inserted into the hole chosen to be the microchannel inlet as shown in **Figure 2-7**. The holes are drilled slightly small so that the flexibility of the PDMS provides a self-seal around the tubing, preventing leaks. Additional tubing can be placed into the outlet hole for connection to a collection vessel or for further analysis, or samples can be taken directly from the channel outlet at specified intervals for measurement and analysis.



Figure 2-7: Fully assembled 2.5 cm long PDMS microdevice with PEEK tubing inserted to inlet hole for flow-through from syringe.

2.6 Oxidative Stress

Proteins are primary functional components in cells [70]. Proteins have numerous functions, including acting as signals, receptors, or enzymes. RNA is transcribed from DNA in the nucleus, and proteins are translated from RNA. Proteins often undergo post-translational modifications (PTMs) in the endoplasmic reticulum. These PTMs can regulate transcriptional activity [71], regulate gene expression [72], or identify proteins

for proteolysis [73]. They may also modify the protein's conformation or folding structure to impart a specific functionality to the new protein.

Oxidation is a naturally occurring process in cell development and is used in many cellular processes [74]. Oxidation is often a result of free radicals containing an unpaired electron or reactive oxygen species (ROS) [75]. Reactive oxygen species can be part of ongoing metabolic processes within an organism during respiration, or produced as a defense mechanism to a foreign invader. Organelles within the cell, such as peroxisomes, contain oxidizing agents, and mitochondria are the major source of free radicals in an organism [76–78]. These free radicals provide protection against foreign molecules by playing a role in cell signaling and oxidizing foreign macromolecules during inflammation, marking them for degradation by the immune system [79]. Free radicals can also be generated by harmful environmental factors such as UV exposure or pollutants.

Though ROS and free radicals are useful and necessary in cellular processes, they are only needed for short times. If left alone after completing their roles, they can begin to attack native macromolecules causing damage to proteins, DNA, and organelles. The effects of these on native macromolecules is termed oxidative damage, and can trigger oncogenes and lead to apoptosis, atherosclerosis, inflammation, neurodegenerative disease, and diabetes. Oxidation of proteins results in inactivation and tagging for degradation by proteasomes [80]. Proteasomes break down oxidized or ubiquitinated proteins within the cell for recycling and removal of old or broken proteins. Oxidized proteins can also trigger the apoptotic cascade, leading to cell death. The cumulative effects of oxidative damage are termed oxidative stress.

In healthy cells, free radicals and ROS are inactivated by the enzymes of the anti-oxidant system [81]. An anti-oxidant can delay or prevent the oxidation of other oxidizable substrates in the cell, and cellular antioxidants can be enzymes or other biomolecules. In a healthy cell, ROS production is balanced by ROS neutralization via anti-oxidant production. However, under physiological conditions such as infection, inflammation, attack from the immune system, or impairment of the anti-oxidant system, this balance favors the oxidants and oxidative damage can occur [82].

Oxidative stress occurs over time due to an organism's exposure to its own internal stores of oxidizing agents as well as those in its external environment [80]. Oxidation's physiological results include molecular switch action, enzyme inactivation, and triggering of the apoptotic cascade [83], [84]. As the organism ages and anti-oxidant efficiency decreases due to oxidation of anti-oxidant enzymes, these effects become more pronounced [85].

Oxidative stress can play a role in many human diseases [82]. It has been implicated in neurodegenerative diseases, atherosclerosis, and autoimmune diseases [82], [86], [87]. The most stable downstream marker of oxidative stress *in vivo* is low abundance carbonylated proteins [88]. Carbonylation is an irreversible PTM that attaches an aldehyde functional group to an amino acid residue [89], [90]. These modified proteins are formed through metal-catalyzed oxidation reactions [91], and levels of oxidative stress can be reflected by *in vivo* carbonylation levels [89]. The ability to detect oxidative stress levels with minimal amounts of sample tissue or blood in a microfluidic system can provide new insight to the protein profile of oxidative stress-related diseases and may possibly enable earlier detection of the onset of these diseases.

CHAPTER 3

OXIDATIVE STRESS BIOMOLECULE DETECTION

3.1 Surface Modifications

The highly hydrophobic surface of native PDMS tends to adsorb biological molecules [15]. To counteract the problem of high hydrophobicity and analyte sequestration, a wide variety of surface modifications have been created to confer hydrophilic properties to PDMS, and to tailor the PDMS surface to specific applications [16]. To take advantage of oxalyldihydrazide as a crosslinker, carboxylic acid functional groups must be created on the surface of PDMS. A method of linking oxalyldihydrazide to PDMS has not been reported previously.

3.1.1 Previously Reported Surface Modifications

Oxidation is the most common method of modifying PDMS, most often with RF plasma. However, this method produces only non-specific oxidation products. Ferreira *et al.* report a plasma modification that confers carboxylic acid groups to the surface using acrylic acid (AA) [7]. The surface is activated with argon plasma followed by grafting of AA with AA gas plasma. Hu *et al.* also report using AA grafted to PDMS for the expression of carboxylic acid groups onto the PDMS surface [22]. The energy for this modification is provided by UV light irradiating PDMS immersed in an aqueous AA solution containing sodium periodate and benzyl alcohol. The chemical process for this

modification is diagrammed in **Figure 2-3**. Another UV grafting technique, reported by Yang and Hou, uses acetone as a solvent for the AA and benzophenone [39], [92]. The reaction mechanism is the same, except benzophenone serves as the electron transfer agent. Water in the monomer solution can affect the structure of the grafted layer. These grafting methods integrate the monomers to the PDMS structure and can cross-link within the grafted layer, delaying hydrophobic recovery. Finally, Yu *et al.* reported a flow-through functionalization system for immobilizing the polysaccharide dextran onto the PDMS surface [45]. The surface is first oxidized with a hydrochloric acid and hydrogen peroxide mixture, functionalized with amine groups using 3-aminopropyl triethoxysilane (APTES). Dextran partially oxidized with sodium periodate is then attached to the channel and subsequently fully oxidized with additional sodium periodate. This method allows the modification of a fully embedded microchannel after device fabrication without concern for diminishing UV radiation through the surrounding PDMS. Additionally, the large dextran molecules bound to the surface may prevent hydrophobic recovery via re-inclusion of these molecules back to the bulk of the polymer. The chemical process is outlined in **Figure 3-1**.

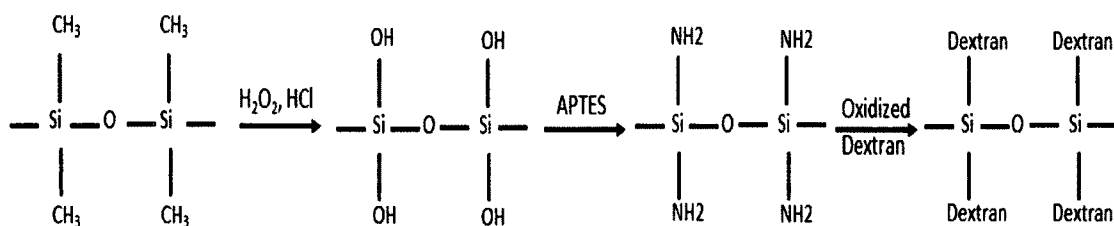


Figure 3-1: Flow through functionalization of PDMS with oxidized dextran. Dextran is further oxidized to express aldehyde functional groups.

3.2 Methods

3.2.1 PDMS Channel Fabrication

SU-8 on a silicon wafer is used to create a mold via photolithography. The pattern for the microchannels is 100 μm by 100 μm by 2.5 cm in length. Initial tests used a mold with 100 μm deep by 160 μm wide features, but the protein capture experiment microchannels used were 100 μm by 400 μm by 2.5 cm, due to the limitations of the low cost photolithography setup used in Chapter 6. Sylgard 184 (Dow Corning) is mixed in a 10:1 ratio of prepolymer to curing agent, and poured over the silicon mold and into a dish to create a flat coversheet. After curing at 80 °C for 1 hour, the microchannels are removed from the mold and inlet and outlet holes are drilled using a drill press. The drilled microchannels and the coversheet are bound using uncured PDMS mixture as a glue. The two sides are pressed together and cured overnight at 80 °C. A scalpel is used to separate the individual microchannels from each other after binding.

3.2.2 PDMS Surface Modifications

3.2.2.1 *Aqueous acrylic acid UV grafting*

PDMS microchannels or flat PDMS film is immersed in an aqueous solution containing 0.5 mM NaIO_4 , 0.5 wt % benzyl alcohol, and 10 wt % AA. The sample immersed in the modification solution is placed directly under a mercury UV lamp for 2.5 hours. Following irradiation, the sample is removed from solution and rinsed with DI water at 70 °C to remove any adsorbed AA and polymerized AA that is not grafted to the surface. Benzyl alcohol serves as an electron chain transfer agent in this reaction, while the NaIO_4 scavenges oxygen that may compete with the AA monomers for the free radicals generated on the polymer surface.

3.2.2.2 Acetone and benzophenone acrylic acid UV grafting

Acetone, AA, and benzophenone used for these experiments are mixed at a ratio of 47 mL acetone, 3 mL AA, and 250 mg benzophenone for 50 mL of reaction solution. The PDMS film or microchannels are immersed in this solution, and brought to 45 °C for 30 minutes to allow the benzophenone photoinitiator to adsorb onto the PDMS. The reaction solution containing the PDMS samples are placed directly below a UV lamp and irradiated at 45 °C for 2 hours. Following irradiation, the modified PDMS is rinsed with acetone three times to remove the benzophenone retained in the polymer.

3.2.2.3 Flow-through functionalization of PDMS

The surface of the microchannels is modified using a flow-through scheme as seen in Yu *et al.* All reagents are flowed through at 2 $\mu\text{L}/\text{min}$. Water containing 1 M HCl and 30% H_2O_2 in a 5:1:1 ratio is pushed through the channel for 35 minutes to oxidize the surface, followed by DI water and ethanol for 5 minutes each. APTES and ethanol in a 50% v/v solution is pumped through for 2 hours to functionalize the oxidized surface, resulting in primary amine groups on the surface. Prior to flow through, 0.475 g dextran and 0.232 g sodium periodate (NaIO_4) in 10 mL DI water are stirred overnight to produce aldehyde groups for binding to the primary amine groups. This solution is pumped through the channel for 2 hours, followed by 0.1 M NaIO_4 for 1 hour to further oxidize the dextran to produce aldehyde groups.

3.2.2.4 Attachment of oxalyldihydrazide crosslinker

Once carboxylic acid groups are expressed on the surface of PDMS, they must be activated to bind to the oxalyldihydrazide crosslinker via carbonyl-hydrazide affinity. A syringe pump connected to a fully enclosed and modified PDMS microchannel is used to

push MES buffer containing 200 mM N-(3-dimethylaminopropyl)-N'-ethylcarbodiimide (EDC) and 50 mM N-hydroxysuccinimide (NHS) through the channel at 2 $\mu\text{L}/\text{min}$ for 30 minutes. MES buffer containing 25 mM oxalyldihydrazide is then pumped into the channel at 2 $\mu\text{L}/\text{min}$ for a minimum of 2 hours. The oxalyldihydrazide can be incubated overnight as well.

3.2.2.5 Verification of aldehyde functional groups on PDMS

To verify the expression of aldehyde functional groups following each type of modification experiment, Alexa 488 hydrazide is used as a fluorescent tag to verify the presence of the desired functionality. Following the steps for attachment of oxalyldihydrazide, the functional groups are activated using EDC and NHS. In place of oxalyldihydrazide crosslinker, Alexa 488 hydrazide is pushed through the channel or placed on the surface of flat PDMS at a concentration of 75 mM. The solution is kept in the channel for 2 hours, then rinsed with water. The PDMS sample or microchannel is then examined under a fluorescence microscope. Alexa 488 has an excitation max at 490 nm and emission maximum of 525 nm, so the filter set for FITC is used. When blue light strikes the tag, it should fluoresce bright green in the microscope. Control experiments are conducted by covering half of a flat PDMS sample with tape then proceeding with the modification. After the modification procedure, the tape is removed and the entire sample is covered with Alexa dye. The modified side shows fluorescence while the unmodified section will not have any binding of Alexa 488 hydrazide.

3.2.2.6 Protein oxidation

Before any protein capture tests are run, proteins were oxidized using *in vitro* metal catalyzed oxidation, similar to the process of carbonylation *in vivo* [91].

Cytochrome-C was dissolved at 5 mg/mL in HEPES buffer (50 mM HEPES, pH 7.4, 100 mM KCl and 10 mM MgCl₂). Ascorbic acid and FeCl₃ at 25 mM and 100 μM, respectively, were added to 30 mL of oxidation buffer containing proteins. This protein mixture was incubated at 37 °C overnight with constant shaking. Oxidation was terminated by adding EDTA to 1 mM final concentration. Successful oxidation was confirmed by the spectrophotometric DNPH assay measuring the absorbance of the hydrazone bond formed between carbonyl groups on the proteins and 2,4-Dinitrophenylhydrazine [93]. Absorbance is measured at 375 nm, and Beer's law is used to calculate concentration, with a molar absorption coefficient of 22,000 M⁻¹cm⁻¹.

3.2.2.7 *Protein labeling*

Prior to experimentation, oxidized cytochrome-C was labelled with naphthalene-2,3-dicarboxaldehyde (NDA). NDA was dissolved in pure methanol at 5 mM concentration. 100 μL of 2 mg/mL oxidized cytochrome-C was added to a tube, followed by 400 μL of 10 mM borate buffer (pH 9.4), 100 μL of 10 mM KCN in water, and 400 μL of the NDA/methanol solution. The mix was allowed to incubate for 30 min in darkness, and rinsed in a 3000 MW cutoff centrifugal filter unit. The solution was spun down to 200 μL and supplemented with 800 μL of borate buffer, giving a final concentration 0.2 mg/mL NDA-labeled cytochrome-C.

3.2.2.8 *Protein capture*

The 0.2 mg/mL NDA-labeled cytochrome-C solution was pumped through the channel for 1h at 5 μL/min. 2 μL samples were collected from the outlet of the channel each minute and the fluorescence measured in the NanoDrop 3300

fluorospectrophotometer for comparison to the original tagged solution. Protein capture was verified under a fluorescence microscope.

3.2.2.9 Protein elution

Once proteins are bound on the chip via hydrazone bonds between the hydrazide groups on oxalyldihydrazide and the carbonyl groups on the proteins, the chip is placed on a hot plate at 60 °C and formic acid at this temperature is pushed into the chip and allowed to incubate for 30 minutes. Following incubation, the now unbound proteins were removed from the chip by borate buffer pumped through at 5 $\mu\text{L}/\text{min}$, and samples measured each minute for fluorescence.

3.3 Surface Modification Results

3.3.1 Aqueous Acrylic Acid UV Grafting

Initial tests of this modification scheme were carried out on flat sheets of PDMS cast into a small petri dish. The original basis of this modification called for 10% AA, 0.5% benzyl alcohol, and 0.5 mM of NaIO_4 to scavenge oxygen that may compete for the oxidation reaction. This mix was poured over the flat sheet and exposed to UV for 2.5 hours at room temperature. Following this experiment, the PDMS was rinsed and prepared for binding with Alexa 488 hydrazide by EDC and NHS. The initial experiment produced an acrid smoke after 2.5 hours of exposure, requiring the use of eye and breathing protection. The sheet was rinsed with water to remove adsorbed AA and after binding Alexa 488 showed mild fluorescence under a microscope, indicating a slight modification of the surface (**Figure 3-2**).



Figure 3-2: Mild fluorescence shown on the right side after UV acrylic acid grafting and binding of Alexa 488 hydrazide, compared to unmodified PDMS on the left.

To test this protocol with an unbound PDMS microchannel, a small dish was filled with the AA mixture and a microchannel placed face down on top. When placed channel side up, the microchannel floats to the surface of the mixture, leaving the surface uncovered by any AA monomer mixture. By testing with the channel face down, the ability to modify a sealed microchannel by filling with the monomer solution was also tested. Following 2.5 hours of exposure to UV, no fluorescence was present, indicating no surface modification (**Figure 3-3**).

To create a microchannel modified in this method, the microdevice would have to be modified, then bound using RF plasma, but RF plasma may interfere with the existing surface modification. If no interference occurs, there would still be fewer groups on the surface resulting from RF plasma that would bind to a PDMS coversheet, resulting in a weaker seal. Using uncured polymer as glue following the modification would risk losing some modification to hydrophobic recovery, as the PDMS glue must cure for some time.



Figure 3-3: Fluorescence image of attempted surface modification with the PDMS surface face down in the acrylic acid solution. No significant fluorescence indicating successful surface modification is seen.

To attempt to maximize the effectiveness of the surface modification, multiple concentrations of AA in the monomer mixture were tested. Mixtures of 10%, 15%, 20%, 25%, 30%, 40%, and 50% AA with the same concentration of benzyl alcohol and sodium periodate were poured over PDMS flat sheets and exposed to UV for 2.5 hours. The higher concentrations developed white crystals over the PDMS and the dish, but when washed away showed a mild improvement in surface wettability. The 10% and 15% solutions ended milky and separated, and all showed little change in the PDMS surface hydrophilicity, the quickest test for successful modification.

In an attempt to increase the speed and efficiency of the reaction, the UV box was placed inside of the incubator oven at 37 °C for 2.5 hours while exposing the PDMS to UV with the same concentrations, and some modification was achieved that was verified

by Alexa 488 binding. The literature reports that 4 hours provided the highest graft density, so 4 hours at 45 °C was also tested [22].

By covering one half of the flat PDMS with tape, UV and monomer exposure was prevented, creating an integrated control experiment on the same sheet of PDMS. This variation produced the best modification of this method, shown in **Figure 3-4** with the unmodified non fluorescent side on the left, and the modified side binding Alexa 488 hydrazide on the right. The hydrophilicity was visibly changed as well (**Figure 3-5**).

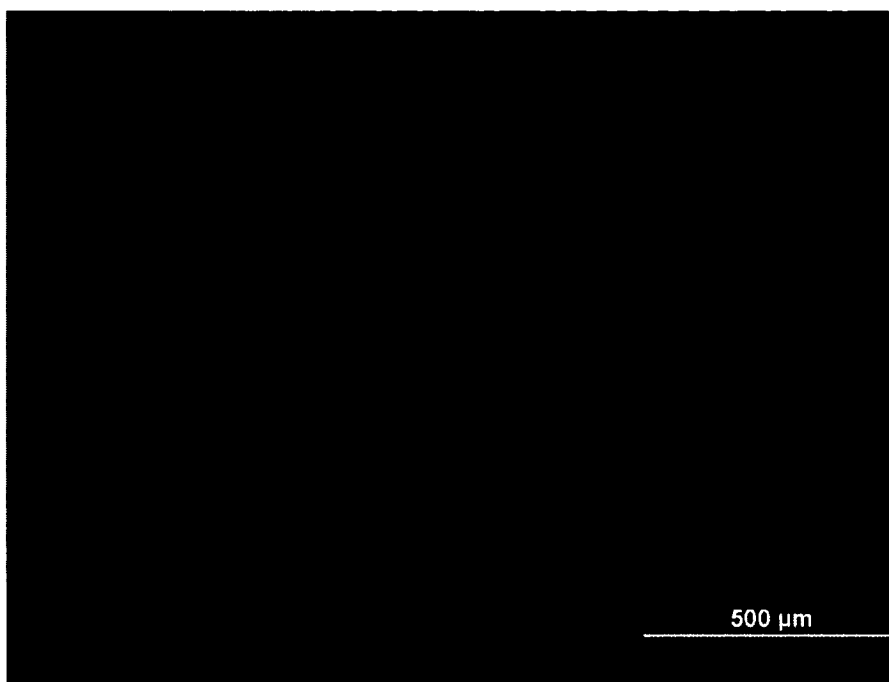


Figure 3-4: UV grafted acrylic acid modified PDMS surface on the right showing binding of Alexa 488 hydrazide after 4 hours of exposure at 45 °C compared to the unmodified surface on the left.

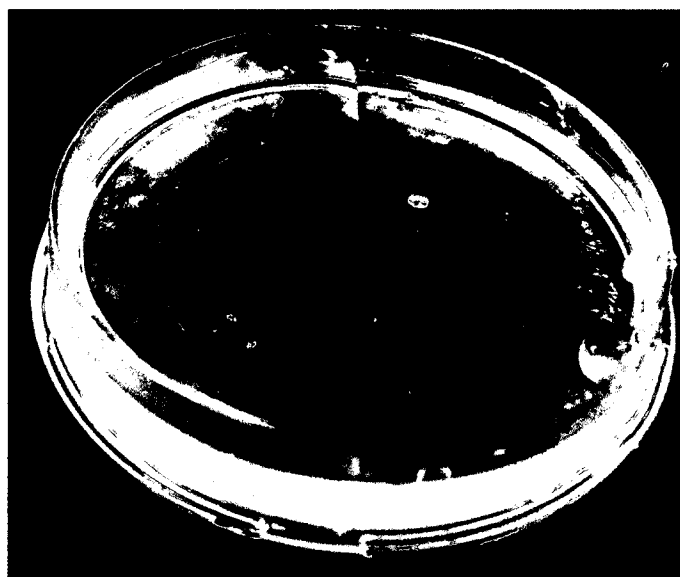


Figure 3-5: Visible hydrophilicity change in the modified PDMS on the left compared to the unmodified surface on the right. The water in the PDMS-covered dish remains on the modified hydrophilic left side without wetting the unmodified hydrophobic side.

This procedure was then followed by attempting to modify microchannels. Initially, large binding paperclips were affixed on the ends of the microchannel to hold it underneath the AA solution, but the solution flaked the paint on the clips and caused discoloration and crystallization of the solution. A clear polymer tape from 3M was placed below the PDMS chip and used to hold the microchannel under the modification solution. Modification was achieved but binding the channels to a coversheet was not possible through this modification as it is in RF plasma exposure.

An attempt was made to bind the microdevice prior to modification. The channel was filled with AA monomer solution and exposed to UV for 4 hours at 45 °C. The monomer caused a viscous blockage preventing rinsing of the channel and usage of the chip. Thus, this modification must be performed on an unbound microchannel, and the channel must be sealed following modification. These steps may interfere with the existing modification if plasma treatment is used.

3.3.2 Acetone, Benzophenone, and Acrylic Acid Grafting

Yang and Hou (2011) describe a method of grafting AA to the surface of PDMS with UV irradiation by dissolving the AA in acetone and using benzophenone as an electron chain transfer agent [92]. The initial test was with 49.243 mL of acetone, 0.757 mL AA, and 250 mg of benzophenone. This mixture was poured over PDMS sheets as in the previous experiment and irradiated for 1 h at 45 °C. The modification visibly changed the wettability of the PDMS sheet, and another test was conducted covering half of the PDMS with tape to prevent UV exposure. After 1 hour of exposure at temperature, incubation of both sides with EDC and NHS for 30 minutes, and 2 hours of 175 μ M Alexa 488 hydrazide, a clear difference between the modified and unmodified sides was seen under a fluorescence microscope (**Figure 3-6**). It is also notable that in marking the two sections of PDMS, a permanent marker easily marked on the modified side, while barely writing on the unmodified PDMS (**Figure 3-7**).

The success of this modification scheme demonstrates similar results as those seen previously, with the benefit of less time to modification and less smoke generated in the process. The solution did not form crystals or tend to discolor as in the aqueous AA solution experiments.

To verify the effectiveness of this modification scheme for PDMS microchannels, microchannels were modified first then placed on a clean silicon wafer and exposed to heat to create a seal for the microchannel (**Figure 3-8**).

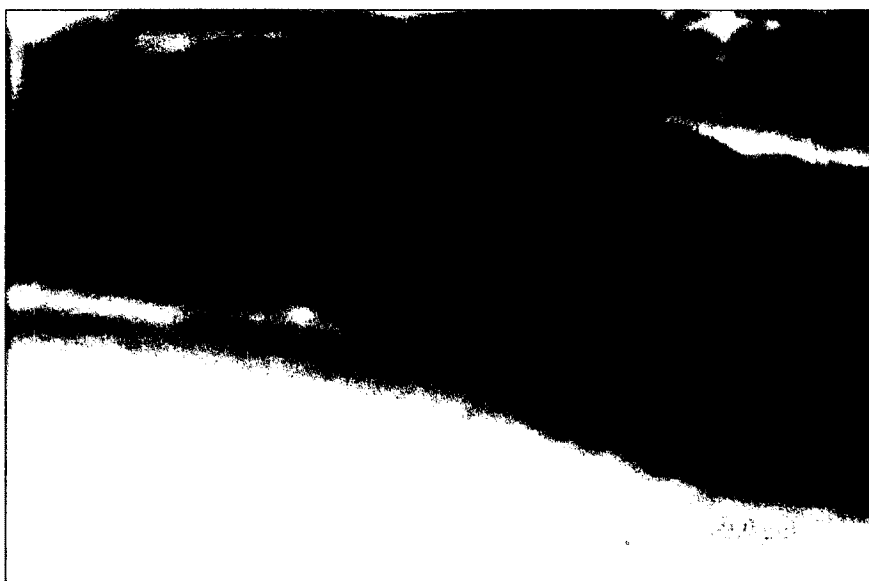


Figure 3-6: PDMS modified with UV grafting of acrylic acid in benzophenone and acetone on the bottom of the image compared to the unmodified surface at the top. Fluorescence at the top is a result of tape residue stuck to the PDMS.

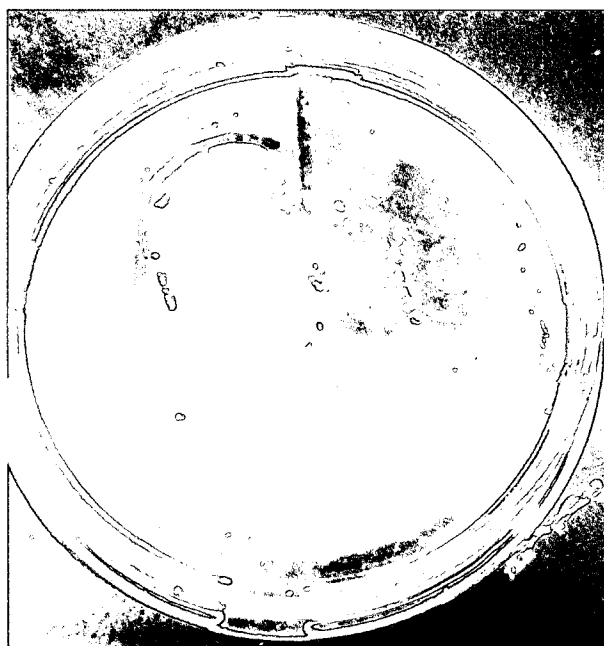


Figure 3-7: Permanent marker clearly writing on the modified surface surrounding the Alexa 488 hydrazide mixture on the left, compared to the thin line that was left on the unmodified surface on the right.

Though this process reduces possible surface area for a protein enrichment device, it allows testing of the modification scheme in a flow-through protein capture environment and creates a reversible bond that allows the inspection of the microchannel under a microscope following binding of fluorescent tags. After flowing through EDC and NHS and 175 μM Alexa 488 hydrazide, followed by flushing with water, fluorescence was seen confined to the microchannel.

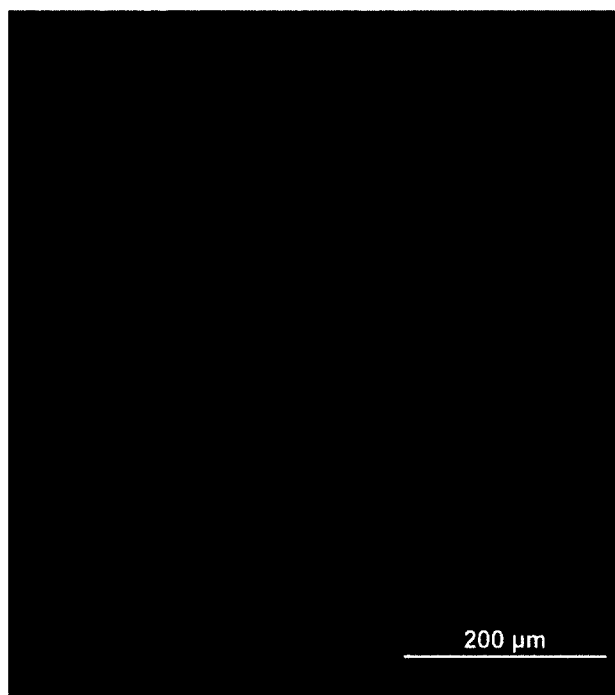


Figure 3-8: Alexa 488 hydrazide binding seen in a PDMS microchannel following acrylic acid/acetone UV grafting.

3.3.3 Flow-Through Functionalization of PDMS

Flow-through functionalization provided an attractive option for modifying PDMS microchannels, as it allowed the modification of an already-assembled microchannel without a need for a UV energy source or limitations on substrate thickness. The times and flow rates were adjusted from Yu *et al.* to adjust for the difference in microdevice dimensions and to maintain a flow rate that would facilitate

attachment of dextran to the surface of PDMS. Dextran can be partially oxidized in 4 hours of mixing at 30 °C or overnight. Successful modification depends on the resultant aldehyde groups of dextran binding to the primary amines generated by the APTES flow through. Further oxidation of dextran is required with NaIO_4 to create aldehyde groups that will bind the oxalyldihydrazide crosslinker.

To verify that PDMS is oxidized by the hydrogen peroxide and hydrochloric acid solution, a flat PDMS sheet was divided into five sections and one drop of a solution placed in each section. The drops consisted of H_2O , 1M HCl, H_2O_2 , equal parts HCl and H_2O_2 , and a 5:1:1 ratio of H_2O , HCl, and H_2O_2 . Following 1 hour of the solution on the surface of PDMS and subsequent removal and drying, one drop of pure water was placed on each of the sections of PDMS where the modification solutions were placed. A photograph was taken from the side of the PDMS section level with the polymer surface. The water contact angle observed in **Figure 3-9** was compared between each modification solution using ImageJ angle measurements, and the HCl/ H_2O_2 / H_2O solution provided the lowest water contact angle. The contact angles of the remaining sections were also reduced somewhat below that of pure water, but less than the mixture of three.

Table 3-1 outlines the angle measurements taken from **Figure 3-9**.

Table 3-1: Water contact angle measurements for each mixture of modification solution.

Sample	Angle (degrees)
$\text{H}_2\text{O}/\text{HCl}/\text{H}_2\text{O}_2$	85
HCl/ H_2O_2	91
H_2O_2	93
HCl	89
H_2O	103

To verify the successful expression of oxidized dextran aldehyde groups on the surface of PDMS, the same verification procedure was used as in the other modification schemes. Half of a flat sheet was blocked by tape from exposure to the modification chemicals. Both sides of the sheet were exposed to EDC and NHS to activate existing aldehyde groups, and then incubated with 175 μ M Alexa 488 hydrazide. **Figure 3-10** shows the successful modification of PDMS using this method.



Figure 3-9: Comparison of water contact angle after surface oxidation. From left to right: H₂O; HCl; H₂O₂; equal parts HCl and H₂O₂; and 5:1:1 H₂O, HCl, and H₂O₂. The mixture of the three chemicals provided the largest change in water contact angle from 103° to 85°.

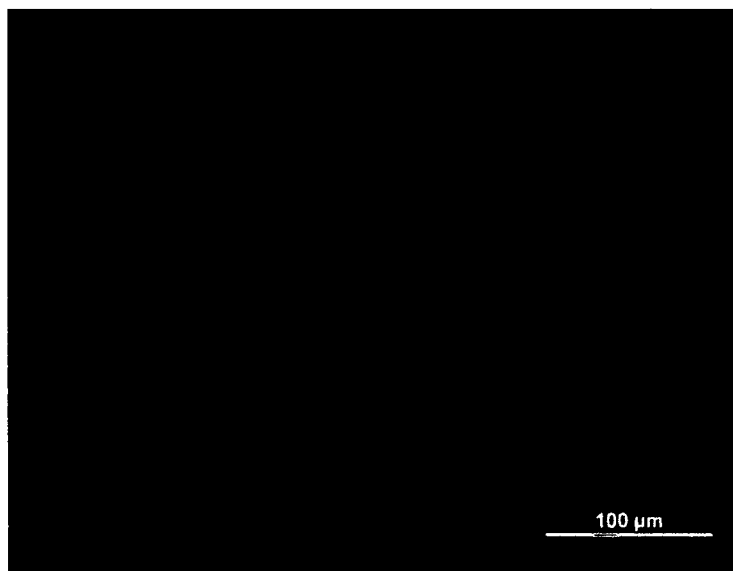


Figure 3-10: Dextran-modified PDMS on left side with attached Alexa 488 hydrazide compared to unmodified PDMS on the right.

An expected advantage of the dextran modification method is the size of dextran molecules providing many attachment points to the PDMS microchannel. The multitude of attachments provides a stronger bond holding the crosslinkers and binding sites to the PDMS microchannel, reducing the possibility of loss of bound protein from too high of flow rate or by the loss of a few bonds to PDMS. The multiple binding sites also address hydrophobic recovery problems, as the large dextran molecules are not easily reincorporated to the PDMS bulk and should remain on the surface for long periods of time. The overall size of the dextran-oxalyldihydrazide structure should also slightly diminish the maximum diffusion distance for a protein which should increase capture efficiency.

This modification procedure is the only one tested that allows for modification of the microchannel post-construction and sealing. This allows for standard PDMS binding techniques such as plasma treatment for irreversible binding without altering the surface modification. Because the oxidized surface that is not in contact with the flat PDMS coversheet will undergo hydrophobic recovery, the surface of the microchannel will be ready for modification shortly following channel binding using plasma. The numerous advantages and simplicity of this method, led to its use in the protein capture studies.

3.3.4 Protein Capture

After the PDMS surface was modified and oxidized dextran and oxalyldihydrazide crosslinker were attached, NDA-labeled carbonylated cytochrome-C at a concentration of 0.2 mg/mL was pushed through the 2.5 cm channel at 5 μ L/min. Fluorescence of the solution that was flowed through the channel was measured each minute until the outlet concentration rose to a steady fluorescence, indicating that the

available binding sites for oxidized proteins were full and protein solution was flowing through without capture. Over 70 minutes of capture time, the fluorescence of the outlet solution stabilized at around 78 RFUs, the fluorescence of the stock solution of tagged proteins.

Figure 3-11 demonstrates the protein capture profile over time of a modified PDMS microchannel. As expected, the initial capture rate is high, reflected in the steep slope of the capture line in the first 10 minutes. This high rate is attributed to the wide availability of binding sites for carbonylated proteins and little competition for binding. As the oxalyldihydrazide binding sites are taken up, the remaining available crosslinkers become encumbered by the presence of neighboring bound proteins, and steric forces may prevent binding of proteins near sites that have already captured a protein. After 70 minutes total of flow through, 4.7 μg of protein were captured on the microchannel according to fluorescence measurements. Some proteins may bind and release, and some adsorption may occur, but the majority of this fluctuation can be attributed to some inherent error in the fluorescence measuring and the amount of protein that may vary in the solution minute to minute.

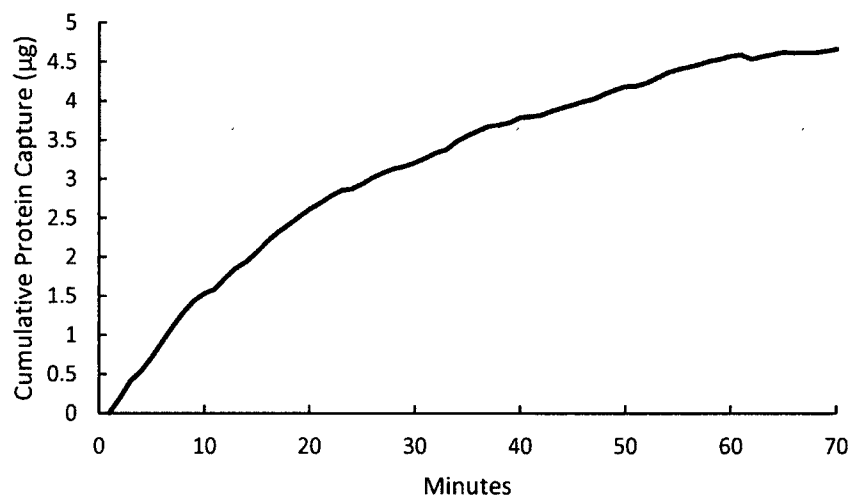


Figure 3-11: Cumulative protein capture of cytochrome-C in a microfluidic channel calculated from the fluorescence of samples taken each minute from the microdevice outlet.

3.3.5 Elution of Bound Proteins

Following the capture of carbonylated proteins, the protein solution is pushed out of the channel, and formic acid at high temperature is pushed through to break the hydrazone bonds. The solution is pushed out of the channel at 5 $\mu\text{L}/\text{min}$ and again measured each minute at the outlet for fluorescence. Because the formic acid should break all the hydrazone bonds at approximately the same rate, most of the protein should leave the microchannel in the first few minutes.

A capture experiment was run as in the previous section, yielding 12.1 μg of protein capture. After the channel was cleared with air and the bound proteins were eluted with formic acid, fluorescence was measured over 10 minutes as the formic acid broke the hydrazone bonds and pushed the oxidized proteins out of the channel. Assuming linear fluorescence of the protein solution with concentration, the elution yielded 28 μg of captured proteins. One possible explanation for this 233 percent elution

efficiency is that the formic acid breaks not only the bonds between the crosslinker and protein, but between the dextran and the PDMS as well. Excess unbound NDA dye may bind to dextran or be adsorbed into the surface modification chemicals, and show up as excess fluorescence upon elution with formic acid.

To determine the true cause of this elution anomaly, a flow through solution from elution should be collected and analyzed via capillary electrophoresis. The size of all components that may be eluted is known, and the run time for all fluorescent molecules in CE should show what contributes to the excess elution fluorescence.

3.4 Discussion of Results

A total of 4.7 μg was captured in the PDMS microchannel in 70 minutes, equivalent to a 6.7% capture efficiency at a flow rate of 5 $\mu\text{L}/\text{min}$ of flow rate. The PMMA protein capture device shows capture of 4.7 μg in 100 minutes of flow-through, for an efficiency of 4.7% [34]. The increase in efficiency from PMMA to PDMS can be attributed to a number of factors. At initial inspection, an easily attributable factor for the increase in efficiency is from the more compact dimensions of the PDMS microchannel. At 100 μm x 100 μm , the lateral diffusion distance for a protein is less than in a 1 mm x 100 μm channel, increasing the opportunity for a protein to contact a binding surface. Additionally, the PMMA microchannel had a large number of microposts in the channel, the sides of which were not easily modified by UV exposure. This low exposure led to a reduction in overall area where a protein could bind, despite the increased surface area to volume ratio. In flow through modification, all four walls of a channel can be modified, and if microposts are incorporated into the design the sides of each of them would end up

modified. Though this is more difficult to achieve in PDMS replica molding, in some applications with larger microchannels this could be beneficial.

Modification with dextran provides an additional benefit in improved attachment of the crosslinker to the polymer surface. One attachment of a dextran molecule to the PDMS surface can provide several attachments to oxalyldihydrazide molecules, and it is more likely that each dextran molecule is attached at multiple points to both the PDMS surface and other dextran molecules. These multiple attachments improves the binding strength drastically; if one attachment point of dextran becomes dislodged, the molecule is not completely unbound and the force is spread to several other binding sites. The dextran binding also extends the structure of PDMS-dextran-oxalyldihydrazide away from the polymer surface, further decreasing diffusion distances.

The more compact size of the microchannels allows faster speed of capture as well. Because there is less surface area, binding sites are filled more quickly, and the presence of an oxidized protein can be detected in much less time than in an avidin column or in PMMA microchannel capture [34], [94]. Fewer overall proteins can be caught, but this deficit is made up in increased microchannel lengths. Capture efficiency may also increase with a slightly slower flow rate, such as 2 $\mu\text{L}/\text{min}$, and a very small sample may be used to detect incredibly low concentrations of carbonylated proteins. Future work remains to determine the threshold of detection and optimal experimental parameters for this technique.

Compared to the existing microfluidic oxidized protein capture method on PMMA, the PDMS method provides a more flexible and low-cost option that can take advantage of rapid prototyping techniques. The modification requires no external energy

source and a minimum amount of reagents. The modification displays the ability to target carbonylated proteins and bind them to the microchannel surface. The flow through functionalization mechanism provides modification to the entire surface of the microchannel, unlike the PMMA method that only modifies surfaces exposed to UV light, and excludes the surfaces vertical in orientation to the light source. Microchannels can be made quickly if there is a heat source and a mold, or can be fabricated around a wire or other structure that can be extracted from the PDMS to leave a microchannel.

PDMS microfluidic protein capture encounters problems with microchannel binding to the cover sheet, as failures in binding were common with this method. Flow-through solution would break the seal in the channel and begin to flow around and outside of the limits of the microchannel, or the solution would solidify at the outlet and cause pressure to build up inside of the microchannel, breaking the seal and allowing flow through solution to leak out of the side of the microchannel. Additionally, due to the methyl groups on the surface and the stability of the PDMS surface, surface modification requires harsher chemicals and a longer process to express the necessary aldehyde groups on the polymer surface and does not always maintain the modification for long periods of time.

Overall, the work shows that PDMS can serve as a platform for targeted capture of carbonylated proteins in solution, and that it can do so in resource limited situations. Microchannels can be cast against a mold in any environment, and can cure over time without heat or within an hour at high temperatures. Microchannel designs are flexible and new designs are simple to create if needed. With some further refinement of the

method, PDMS provides a low cost and versatile substrate for creating microfluidic devices for oxidative stress detection.

CHAPTER 4

DOPING OF PDMS FOR INTENTIONAL LEACHING INTO MICRODEVICES

4.1 Introduction

The ability of microfluidic devices to closely mimic *in vivo* environments and to provide precise control over microenvironments makes them promising platforms for cell culture applications [5]. PDMS's gas permeability and compatibility with fluorescence and optical microscopy strengthen its suitability for creating and studying cellular microenvironments [20]. However, native PDMS is hydrophobic and the surface tends to adsorb biological molecules [15].

The absorption and bulk diffusion properties of PDMS have been heavily studied. Furthermore, surfactants have been added to PDMS to improve the wetting properties and impart hydrophilic properties. The surfactant decreases the water contact angle of the PDMS, and release of the wetting agent from the microdevice eliminates the need to add it to the solution or media being used [95]. Nonetheless, the bulk doping of PDMS with small molecules to deliver those molecules into liquid solvents or into a microfluidic device's fluid flow has not been directly examined. This experiment hypothesizes that PDMS can be used as a carrier for small molecule diffusion into liquid solvents and doped with small molecules for intentional, controlled leaching into microdevices. Brewer *et al.* (2012) showed that fluorescein, a small fluorescent molecule with some

water solubility, was not absorbed into PDMS like Nile Red [58]. Fluorescein comes as a powder, and as such is easily miscible with the liquid mixture of uncured PDMS and its curing agent. After fluorescein is mixed into the liquid and the polymer is cured, the cured doped PDMS retains the same texture and flexibility as pure PDMS, with the characteristic orange color of fluorescein (**Figure 4-1**). This project aims to show that diffusion of a dopant from PDMS may be applied to deliver small molecules into the flow channel of a microfluidic cell culture or assay, or into liquid media, and it seeks to establish that doped PDMS microdevices can be used as a vehicle for intentional leaching into microfluidic flow or cell culture, with a measure of predictability and control over the amount leached.

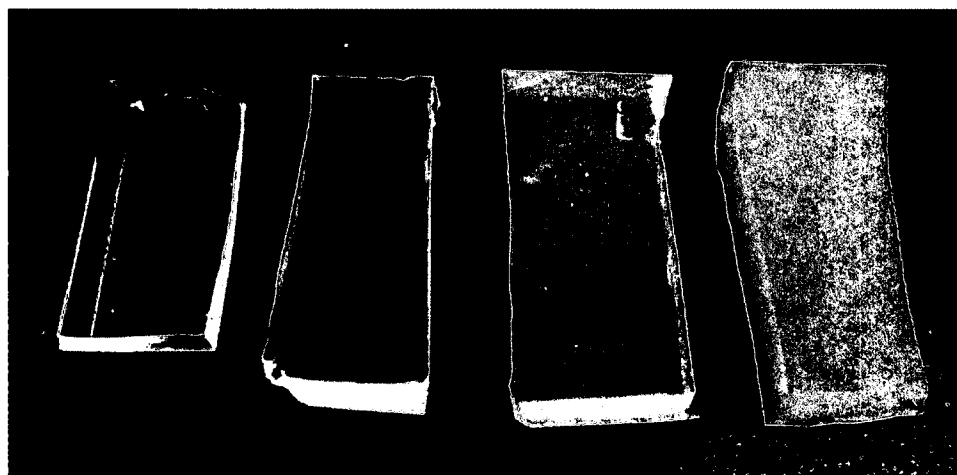


Figure 4-1: PDMS with varying concentrations of fluorescein. From left to right: pure PDMS, 0.1 mg fluorescein per 1 g PDMS, 0.5 mg fluorescein per 1 g PDMS, and 1 mg fluorescein per 1 g PDMS.

4.2 Methods

4.2.1 PDMS Doping

The PDMS prepolymer is mixed thoroughly with its curing agent in a 10:1 (w/w) ratio. Fluorescein is added in the desired concentrations (in mg fluorescein per g of

PDMS) and mixed until the uncured doped polymer mixture has a consistent color and all of the powder fluorescein is spread evenly throughout the polymer mixture. The mixture is degassed under vacuum and poured into a small polystyrene dish to generate rectangular samples or over a silicon mold master to generate microfluidic channels.

4.2.2 Concentration Measurement

Fluorescein was dissolved in the media at known concentrations from 0.5 nM to 1 mM, and the NanoDrop 3300 fluorospectrometer was used to measure fluorescence. The NanoDrop software then generated the standard concentration curve for each medium used. Linear fitting was performed on each set of standards and the resulting best fit line equation was used to calculate concentrations from measured fluorescence values. R^2 values for all standards were greater than 0.99. Concentration standards are shown for water and the cell culture media in **Figure 4-2**.

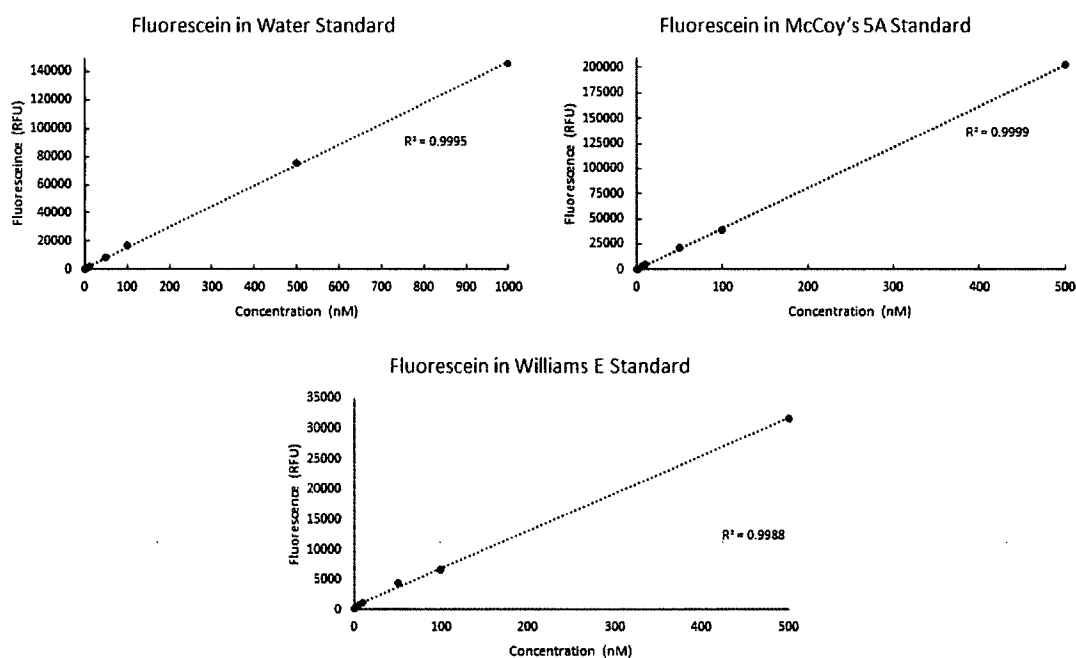


Figure 4-2: Concentration standards used in the fluorescein leaching experiments.

4.2.3 Bulk PDMS Leaching Measurement

This experimental setup for the bulk leaching experiment is shown in **Figure 4-3**. Four samples of approximately 1 g were cut from each doped sample of PDMS and immersed in 5 mL of water, formic acid, Williams E medium, or McCoy's 5A medium at room temperature. To prevent photobleaching of fluorescein, the samples were kept in a dark room under a box. The same mass of uncured PDMS was poured into each dish to ensure equal thicknesses, and the size of the samples were identical. Three solvent samples of 2 μ L each were taken daily and measured on the NanoDrop, and the average RFU value was used to calculate the concentration of fluorescein in the media.



Figure 4-3: Experimental setup of 1g doped PDMS in liquid inside a 15 mL centrifuge tube.

4.2.4 Microchannel Leaching Measurement

PDMS was cast against a mold with raised features of 100 μm to create the microchannels on the surface of a sheet of PDMS. The channels were 100 μm wide with lengths of 1 cm and 2.5 cm and made with PDMS containing 0.1 and 0.5 mg fluorescein per 1 g PDMS (four channels total). The amount of fluorescein in mg per gram of PDMS is considered the mass ratio (mg/g) of the doped polymer. Inlet and outlet holes were drilled at each end of the cast PDMS microchannels, then were bound to a flat sheet of PDMS with the same fluorescein concentration to seal the microchannel. Uncured PDMS mixture served as a glue between the two pieces. The device was cured at 80 $^{\circ}\text{C}$ overnight. This process creates a fully enclosed microchannel. Fresh water and McCoy's 5A medium at room temperature were pushed through at a flow rate of 5 $\mu\text{L}/\text{min}$ and the fluorescein concentration was measured at the channel outlet every minute for 90 minutes. After 10 minutes, the leaching became steady and the average concentration from 10-90 minutes was calculated. ANOVA was performed to determine the experimental parameters' effect during of steady state leaching. All flow experiments were performed in a dark room to prevent photobleaching of the fluorescein.

4.3 Results

4.3.1 Quantification of Leaching

The concentration (in mM) of fluorescein in the liquid media after 4 days of immersion, averaged over three measurements, is shown in **Figure 4-4**.

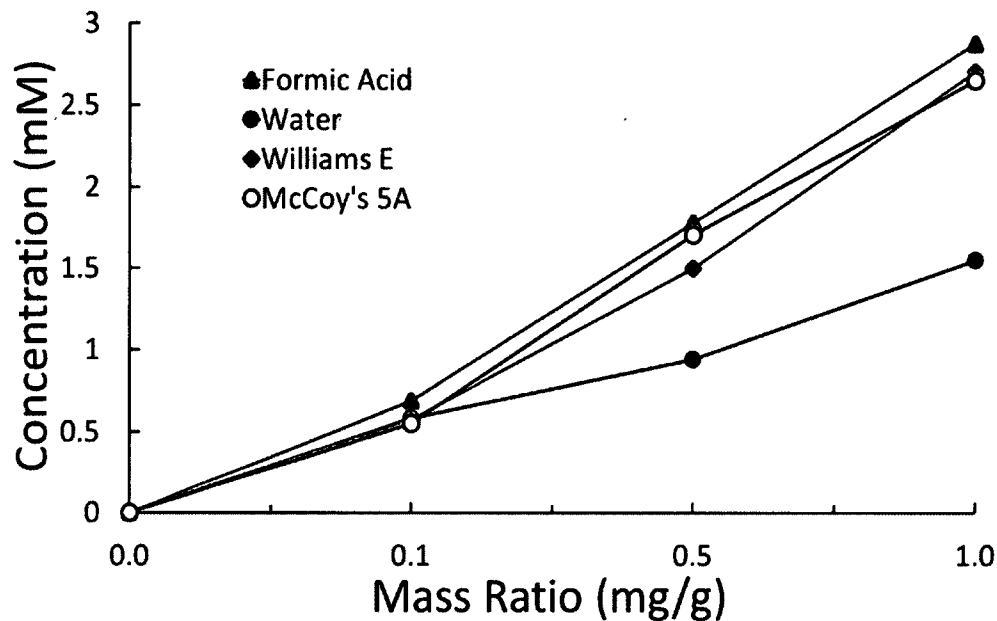


Figure 4-4: Concentration of fluorescein leached into 5 mL of liquid after 4 days. Differences between the means of varying PDMS mass ratios for each liquid are significant at 99% confidence intervals except for that of water.

Polymers with higher concentrations of dopant may leach higher amounts of dopant than low dopant polymers, and may also leach dopant for much longer as there is more dopant in the polymer bulk to diffuse into the region being depleted through leaching. Leaching may be limited by the rate of diffusion of fluorescein within the polymer bulk after washing of the surface fluorescein occurs. Fluorescein polymer concentrations are represented by the mass ratio in mg fluorescein per 1 g of PDMS. The mass of fluorescein leached from the PDMS into the fluid can be calculated and compared to the initial amount present in the polymer sample. These data are shown in **Figure 4-5.**

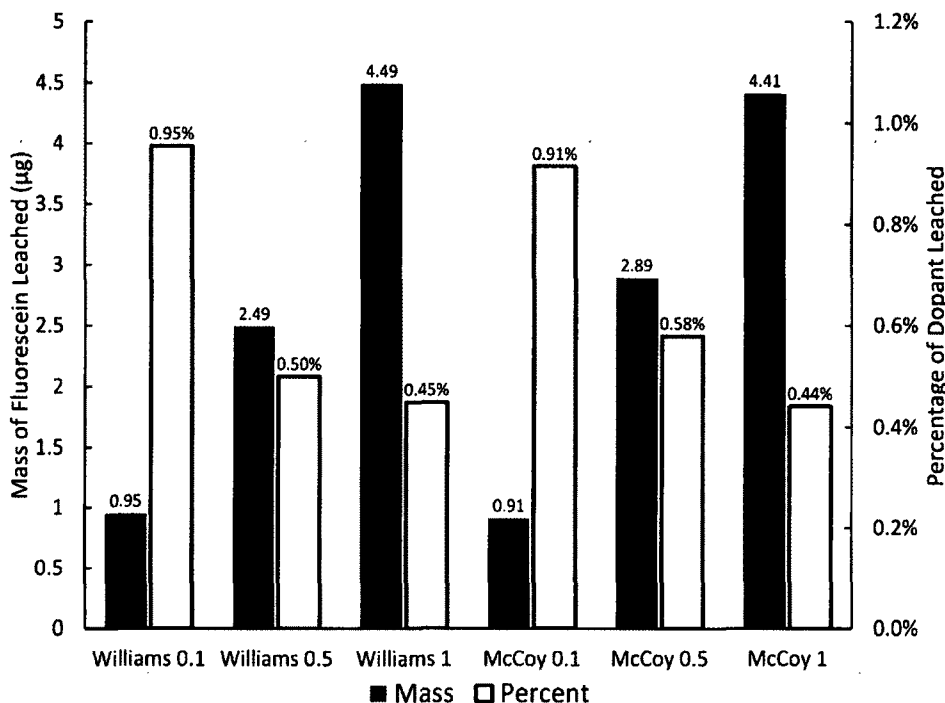


Figure 4-5: Mass of fluorescein that leached into the media (outlined bars), and the percentage of fluorescein that was leached out of the PDMS (solid bars). A lower percentage of leaching is seen from the higher starting concentrations. Samples are named according to the liquid media and the amount of fluorescein in mg per gram of PDMS.

The solid black bars for each media show a steady increase in leached dopant mass as the starting mass of dopant is increased. However, the outlined bars demonstrate an opposing trend: a decreasing percentage of dopant leached from the polymer as the starting mass of dopant is increased. These opposite trends may indicate that greater surface washing occurs at higher dopant concentrations, but leaching past the initial surface washing is in part limited by the rate of diffusion of dopant from the polymer bulk to the surface region. Over a longer period of time, the leaching percentage from PDMS with a higher concentration of dopant may become more equal with the lower dopant concentration samples. Surface washing of dopant is seen in the subsequent microfluidic flow leaching experiments.

4.3.2 Leaching in Microfluidic Flow Conditions

To study the leaching characteristics under flow conditions in a microfluidic channel, 2 μL samples of flow-through solution were collected and the concentration of fluorescein measured and calculated the mass in the sample every minute. These masses were added to a running total to determine the cumulative amount of dopant leached into the solution. **Figure 4-6** shows the cumulative mass leached over time into McCoy's 5A media in a 2.5 cm long channel with 0.5 mg of fluorescein per g of PDMS.

The instantaneous concentration of fluorescein in the media after flowing through the channel is initially ~ 100 nM, with a gradual reduction to ~ 15 -20 nM after 10 minutes of flow at 5 $\mu\text{L}/\text{min}$, remaining near this level for each minute's measurement through 90 minutes. Similar patterns were seen with all samples tested. This initial burst of leaching indicates dopant on or very near the surface of the polymer is washed away with the first liquid to flow through the channel. This burst soon gives way to lower concentrations that remain steady over time. This observation suggests leaching via diffusion from the PDMS bulk even on this small scale.

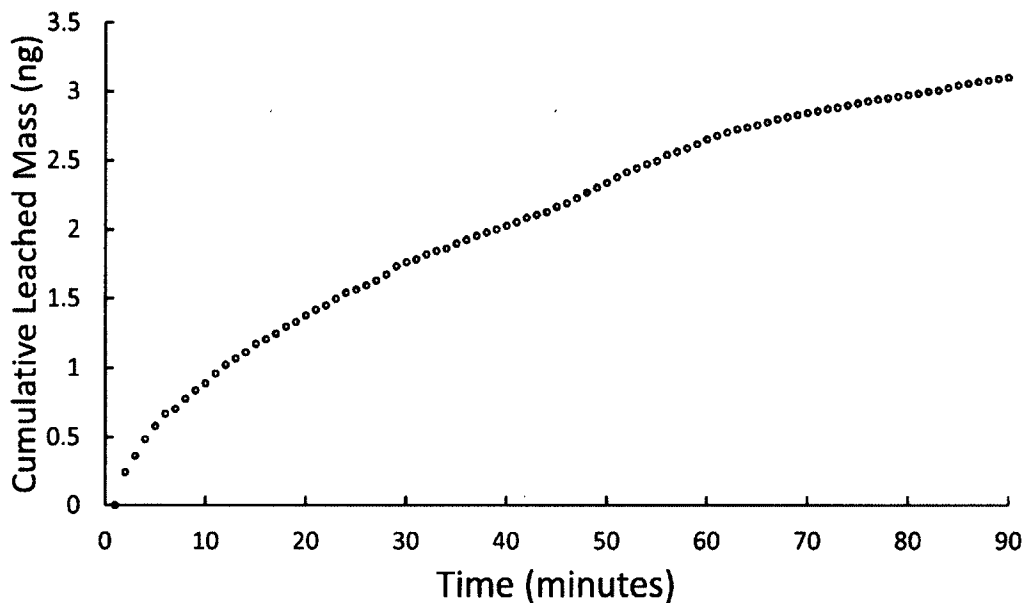


Figure 4-6: Cumulative leached mass of fluorescein from a 2.5 cm long microfluidic channel containing 0.5 mg fluorescein per 1g of PDMS into McCoy's 5A media flowing at 5 $\mu\text{L}/\text{min}$.

Leaching from PDMS bulk is confirmed by a 2.5 cm channel at a concentration of 0.5 mg fluorescein per 1 g PDMS leaching fluorescein for 3 hours before a marked decrease in leaching was observed. After clearing the channel with air and drying overnight, the microdevice continued to leach dopant into the flow at the previous concentrations under the same flow conditions. The decrease after 3 hours indicates that the region of PDMS near the channel walls has been depleted of fluorescein, creating a concentration gradient between the near-wall region and the PDMS bulk. Overnight, fluorescein diffuses into this region from the bulk and the deplete region is able to leach into the microchannel again.

To study the effect of channel length, dopant concentration, and liquid media on the amount of leaching, tests were performed with all 8 combinations of 0.1 mg/g or 0.5 mg/g fluorescein in PDMS, 1 cm or 2.5 cm channel length, and water or McCoy's 5A

media. The average concentrations for each combination are shown in **Figure 4-7**.

ANOVA shows significance between each comparison of dopant concentration, and each comparison of channel length, except in the comparison of 1 cm and 2.5 cm length channels at a fluorescein concentration of 0.1 mg per g of PDMS in both water and McCoy's 5A at a 95% confidence interval. The multiple figures above the graph's bars denote the significance difference in the means of all bars that contain the same marker. Bars have multiple markers to show that the means of the 0.1 mg fluorescein per g PDMS measurements do not differ significantly from each other, but a significant difference in means exists between those measurements and the other means. The error bars present are an indicator of the 95% confidence interval of each mean.

These data suggest the concentration of fluorescein is low enough that equilibrium is reached between the liquid and the polymer early in the channel at this flow rate. At higher concentrations, the length creates a significant difference in concentrations by allowing the fluid more time in the high concentration gradient channel to gather greater amounts of dopant. Molecule transport perpendicular to the flow direction is primarily a result of diffusion [96], as laminar flow schemes dominate the low Reynolds number flows in microfluidics [97]. Low Reynolds numbers do not allow convective mixing, backflow, or turbulence in the microfluidic device [98]. Leached dopant molecules may not completely diffuse across the microchannel flow, and dopant concentrations will be higher along the microchannel walls, decreasing the concentration gradient toward the end of the channel, decreasing the leaching in this area.

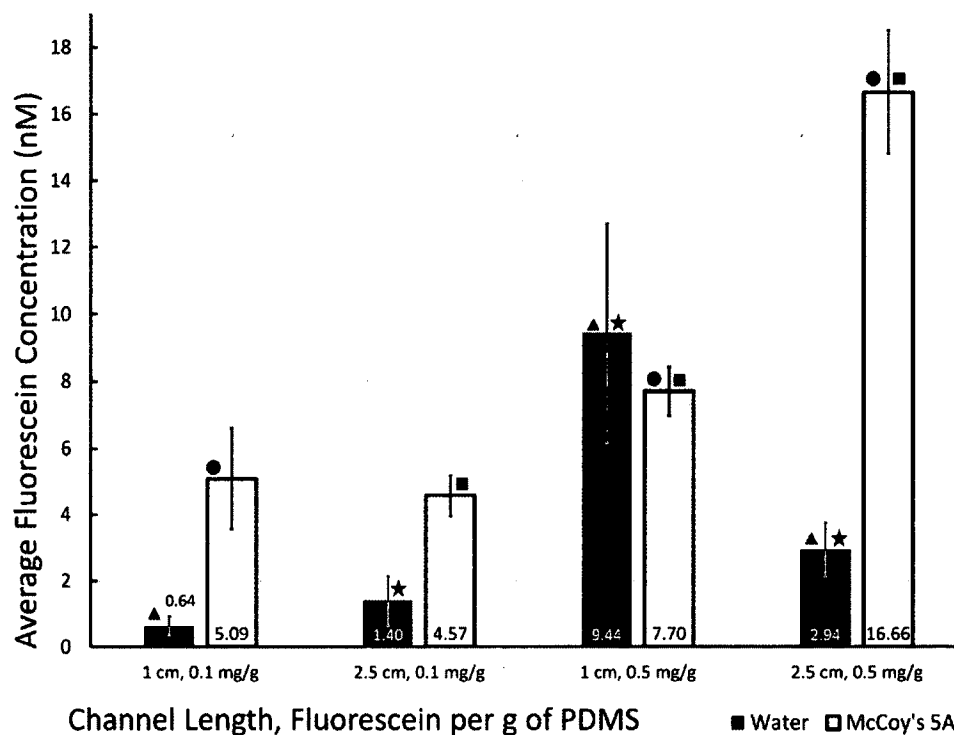


Figure 4-7: Leaching of microchannels with varied channel length, dopant concentration, and fluid media. Figures adorning bars indicate significance in comparisons within the same liquid media at 95% confidence intervals. Microchannels with a mass ratio of 0.1 mg/g do not show significant differences in means within the same media.

The differences in concentration between similar tests with different media are all statistically significant, except for the 1 cm channel containing 0.5 mg fluorescein per 1 g PDMS. Leaching into McCoy's 5A is higher in all microchannel types with a significant difference in concentration. The larger concentrations in the media support the hypothesis that this method can efficiently provide substances to microfluidic cell culture. One or more of the many substances in cell culture media may interact with fluorescein, allowing more dissolution than pure water. Similar results are expected for the Williams E media, based on the immersion leaching data.

Water in a 1 cm channel containing 0.5 mg fluorescein per gram of PDMS produces an unexpectedly high concentration of leached dopant. The reason for this increased leaching is currently unknown and warrants further investigation to determine if it is a property of PDMS microchannel leaching under those conditions.

4.4 Discussion of Results

This method is most clearly suited for administering small hydrophilic molecules into cell culture in microfluidic devices. The low concentration, steady state leaching that is shown over time proves the possibility of providing a stable chemical environment for cells that more closely resembles an *in vivo* microenvironment. In macroscale cultures, such administration of molecules must either be mixed with and diluted to small volumes in the culture media, or added all at once to a plate or well. Nutrients are often required in excess and the maintenance and study of the culture may lead to contamination [24]. Providing certain nutrients, signal molecules, or drugs to the culture through the material the cells are cultured on minimizes human interference with the culture and the possibility of errors and contamination. Additionally, the study may proceed longer without disruption. The significant results seen by varying dopant concentration in the PDMS substrate lays the foundation for developing a model of prediction control over the concentration and mass of dopant being leached.

The ability to dope PDMS prior to curing is not well reported in the literature. The technique may be able to address other problems in microfluidic cell culture on PDMS, specifically the absorption of hydrophobic molecules. Regehr *et al.* (2009) demonstrate up to 90% of estrogen diffusing into PDMS over 24 hours, while Wang *et al.* (2012) demonstrate that molecules above a certain threshold of hydrophobicity will be 75%

absorbed into PDMS in 30 minutes [20], [38]. Doping the PDMS with these molecules prior to curing of the device will minimize the concentration gradient and slow or prevent the absorption of molecules of interest. Currently, surface modifications are used to curb absorption but some modifications may have adverse effects on cells. Doping the polymer prior to device fabrication could simultaneously eliminate a device preparation step and prevent sequestration problems in PDMS cell culture devices, allowing for more robust probing of biological questions at the micro-scale.

4.5 Conclusion

These results support the hypothesis that small molecules can diffuse from PDMS bulk into solution. The microfluidic flow study strengthens this hypothesis, as leaching is seen continually after the surface fluorescein is washed off. This method shows promise for administering small amounts of specific substances to a PDMS microfluidic cell culture device. A PDMS device for cell culture could be doped with small signaling molecules or drugs, and the result of the leached molecule into culture media could be studied with minimal external interference. Molecular delivery may be tuned by adjusting the starting concentrations in the polymer or altering the dimensions of the device.

4.5.1 Future Work

Future work aims to develop a method to predict the amount of dopant that can be leached from a microdevice under a certain set of conditions and the properties of molecules capable of diffusing from the PDMS polymer bulk. Development of a prediction model would allow the use of PDMS cell culture microdevices to advance the fields of drug discovery, microfluidic cell culture, and PDMS lab-on-chip devices.

CHAPTER 5

USING COMPUTATIONAL FLUID DYNAMICS IN MICROFLUIDICS

5.1 Introduction

CFD has seen widespread use in fundamental research and in engineering applications for various fluid-related design tasks [96]. Because fluid flow behavior in microfluidic devices is different from traditional macroscale flows, CFD is a natural first choice to determine flow behavior in new microdevice designs. At the micron scale, Reynolds numbers are very small and viscous effects dominate the flow regime [99]. These low Reynolds numbers also render diffusion as the primary method of molecule transport and mixing in the fluid. Additionally, CFD can provide insight and explanation into phenomena seen in laboratory work and variation of experimental parameters [100]. COMSOL Multiphysics (COMSOL) contains a microfluidics, laminar flow, and creeping flow module ideal for modeling the types of flow seen in microfluidics.

Many microfluidic devices for cell culture have been reported [24]. Microscale systems for cell biology provide an ideal and tightly controlled microenvironment for studying cellular systems [25]. Microfluidic cell culture devices provide strong models for the study of environmental factors such as cell-cell contact and cell-extracellular matrix contact, as well as behavior of adherent cells [3]. In these applications, it is important to keep shear stress to physiological limits to maintain viable cells. Shear can

also govern the phenotype and regulate behavior in certain cell types [101]. Microfluidic systems can also be used to determine the shear required for tumor metastasis.

When designing new microfluidic devices for these purposes, 3D and CFD modeling can save resources and experiment time in the lab by providing insight into the flow characteristics before any physical experiment is performed. Using this along with fluid flow rate calculations and other simple physical models, the suitability of a new device design can be verified before resources are used to create it. In protein capture, it is important that the flow rate not cause a greater force on the bound proteins than the hydrazone bond can withstand. For a cell culture device, the flow rate and design of the channel must ensure that shear rates on the cells stay within physiological levels. When dealing with different types of cells, these levels may differ. Shear stress may cause stem cells to differentiate as well. Pressure drop through the channel, diffusion time and distance, and mixing are all considerations when designing various types of microfluidic devices.

Because the flows in microfluidic devices are laminar, this allows for easier modeling of the flows in various devices. The laminar flow schemes also allow researchers to take advantage of diffusion across the flow as a method of transport, most commonly used for H-filters or T-sensors. For some applications, the usefulness is limited by diffusion distance and time, such as protein capture channels. The proteins do not tumble or move randomly as in turbulent flow, and must diffuse to a microchannel wall to bind to the surface. The size of the molecule is also a limiting factor in the distance that it can diffuse in a given time. Microfluidic devices take advantage of the

short diffusion distances, and flow rates must be chosen to allow maximum likelihood that a protein will meet a binding site in the microfluidic protein capture channel.

5.2 Mathematical Modeling of Microfluidic Flow

5.2.1 Navier-Stokes Equations

The basic equation that governs incompressible fluid flow is the Navier-Stokes equation shown in **Eq. 5-1**.

$$\rho \left(\frac{\partial \mathbf{u}}{\partial t} + \mathbf{u} \cdot \nabla \mathbf{u} \right) = -\nabla p + \mu \nabla^2 \mathbf{u} + \mathbf{f} \quad \text{Eq. 5-1}$$

The Navier-Stokes equation (**Eq. 5-1**) describes the balance of linear momentum for a Newtonian fluid. In this equation, \mathbf{u} represents the fluid velocity, p the pressure, and \mathbf{f} is a vector field describing external forces on the fluid. The left side of the equation describes the inertial components (mass times acceleration) of the fluid, while the right side describes the forces on the fluid. The Navier-Stokes equation is Newton's law applied to a fluid [99]. Fluid flows are often characterized by dimensionless numbers that yield a comparison of the influence of different effects on the fluid flow. The most commonly seen dimensionless number in microfluidics is the Reynolds number (Re) which describes the ratio between inertial and viscous forces [96]. The Reynolds number is commonly used in fluid flows to determine if a flow is laminar or turbulent and is calculated by **Eq. 5-2**.

$$Re = \rho UL / \mu \quad \text{Eq. 5-2}$$

In **Eq. 5-2**, ρ is the fluid density, U is the characteristic flow velocity, L is the characteristic length, and μ is the dynamic viscosity of the fluid. The characteristic length of a rectangular channel is given by **Eq. 5-3**.

$$L = \frac{2wh}{w + h} \quad \text{Eq. 5-3}$$

Equation 5-3 defines w and h as the width and height of the channel in the x and y axes respectively, with flow in the z direction. Flow schemes with $Re < 2000$ are generally regarded as laminar. Most microfluidic devices operate with $Re \ll 1$, meaning that viscous effects strongly dominate the flow regime and the flow is always laminar.

Laminar flows are characterized by streamlines that are parallel and steady, while turbulent flows mix and tumble as they move through their channels. For devices where inertial effects are negligible, the left side of the Navier-Stokes equation can be ignored [99], and the governing equation simplifies to the Stokes equation in **Eq. 5-4**.

$$\mu \nabla^2 \mathbf{u} = \nabla p \quad \text{Eq. 5-4}$$

The fluid flow under **Eq. 5-4** depends solely on the pressure distribution and the boundary conditions (no-slip condition at the walls). Additionally, this flow is steady in time, as the time-dependent variables have been eliminated. In pressure-driven fully developed microfluidic flow, as with a syringe pump, **Eq. 5-4** reduces to Poisson's equation, **Eq. 5-5** [102].

$$\nabla^2 \mathbf{u} = \frac{1}{\mu} \frac{dp}{dz}, \quad u = 0 \text{ on channel perimeter.} \quad \text{Eq. 5-5}$$

5.2.2 Pressure Drop

The pressure drop across a microfluidic channel can be given generally by the fluidic resistance R in ($\text{kg}/\text{m}^4\text{s}$) and the volumetric flow rate Q in (m^3/s). Specifically for rectangular channels, the pressure drop is given in **Eq. 5-6** [103].

$$\Delta P = \frac{a\mu QL}{WH^3} \quad \text{Eq. 5-6}$$

The value of a depends on the aspect ratio of the device, W/H , and is determined by **Eq. 5-7**.

$$a = 12 \left[1 - \frac{192H}{\pi^5 W} \tanh\left(\frac{\pi W}{2H}\right) \right]^{-1} \quad \text{Eq. 5-7}$$

Because of the no-slip condition, Poiseuille flow profiles are seen across microfluidic channels. This type of flow is characterized by a parabolic profile in round and square channels and maximum velocity is seen in the center of the channel. This parabolic velocity distribution across the height of the channel of length L driven by pressure drop Δp is given by **Eq. 5-8** [104].

$$u(y) = \frac{\Delta p}{2\mu L} \left[\left(\frac{h}{2}\right)^2 - y^2 \right] \quad \text{Eq. 5-8}$$

The corresponding flow rate for this channel of width w is found via **Eq. 5-9**.

$$Q = w \int_0^h u(y) dy = \frac{wh^3 \Delta p}{12\mu L} \quad \text{Eq. 5-9}$$

In most microfluidic flows driven using a syringe pump, the volumetric flow rate is known, so the pressure drop across a microfluidic channel in **Eq. 5-10** can be found by rearranging **Eq. 5-9**.

$$\Delta p = \frac{12Q\mu L}{wh^3} \quad \text{Eq. 5-10}$$

In a square microfluidic channel, the flow profile would be uniformly parabolic across the w and h dimensions; in microchannels where $w/h > 1$ the profile tends to be flat past the boundary layers across the width, and parabolic across the height.

Pressure drop is directly correlated with flow rate; a constant pressure drop along the channel results in a constant flow rate [105]. The relationship is given in the Hagen-Poiseuille law (Eq. 5-11) with a proportionality factor called the hydraulic resistance, R_H .

$$\Delta p = R_H Q \quad \text{Eq. 5-11}$$

The units for R_H are $\text{kg/m}^4\text{s}$. Eq. 5-11 corresponds to Ohm's law for electrical circuits which relates the voltage to the resistance and current in the circuit. The hydraulic resistance for a rectangular channel is given in Eq. 5-12 [105].

$$R_H = \frac{12\mu L}{1 - 0.63\left(\frac{h}{w}\right)} \frac{1}{h^3 w} \quad \text{Eq. 5-12}$$

For a square channel the hydraulic resistance calculation is simplified to Eq. 5-13.

$$R_H = 28.4\mu L \frac{1}{h^4} \quad \text{Eq. 5-13}$$

These equations can provide a quick check of the pressure drop for a desired flow rate to ensure that the microfluidic device can withstand the pressures, or that flows are within the desired specifications.

5.3 Modeling Microfluidic Flows using COMSOL Multiphysics

5.3.1 COMSOL Multiphysics Background

COMSOL Multiphysics is a software platform that uses advanced numerical methods to model and simulate physics-based phenomena. COMSOL can be used to study the effects of multiple phenomena or coupled physics effects, such as heat and fluid flow. Different modules can be applied to each model in COMSOL to solve for solutions

to problems involving electrical, structural, fluid, heat, and chemical physics. Multiple physics problems can be solved simultaneously and the interrelated effects examined.

The COMSOL CFD module is used in this work to visualize and characterize the flow through microfluidic devices currently used in this research, and in the process of creating new microfluidic designs. The module solves multiple variations of the Navier-Stokes equations based on the conditions input to the study. The laminar flow and creeping flow (Stokes) modules are used in this work. The results can be visualized using streamlines, color maps of flow rate and shear rate, pressure contours, and a variety of other two-dimensional and three-dimensional plots.

5.3.2 Methods

To model the flow of fluid in a microchannel of any design, a 3D CAD model is first made in SolidWorks. Because most modeling in COMSOL depends on a defined fluid domain, it is most efficient to model the inverse of the microchannel in SolidWorks, i.e., the shape that the fluid inside a filled microchannel would take. This file is saved as a .stl file and imported into COMSOL using a stationary, laminar flow model or creeping flow model. The inlet and outlets are defined, as are the mass flow rates, walls, boundary conditions, and outlet conditions. Once the model is built, a mesh must be created to separate the flow into finite elements for analysis. This mesh breaks down the geometry of the fluid domain into a network of thousands of polygons, each of which is a discrete region of flow that will be solved in its subdomain. The approximations obtained from these mesh elements are then combined to yield the full solution of the problem.

5.3.3 PMMA Carbonylated Protein Enrichment Model

COMSOL was first used in this work to determine the nature of the flow in the PMMA carbonylated protein capture system [34]. This device was a 100 μm tall, 1 mm wide, 12.5 mm long channel with either 150 or 462 microposts arranged in the microchannel. The 150 post channel has a post-to-post spacing of 150 μm measured edge-to-edge, and the 462 post channel has a post-to-post spacing of 100 μm edge-to-edge, resulting in 66.67 μm diameter posts. SolidWorks renderings of the 462 post channel and the 150 post channel are shown in **Figure 5-1**. The modeled volumetric flow rate was 5 $\mu\text{L}/\text{min}$, with atmospheric pressure conditions at the channel outlet. Since proteins for capture are dissolved in an aqueous buffer, the characteristics of water were used for the fluid properties.

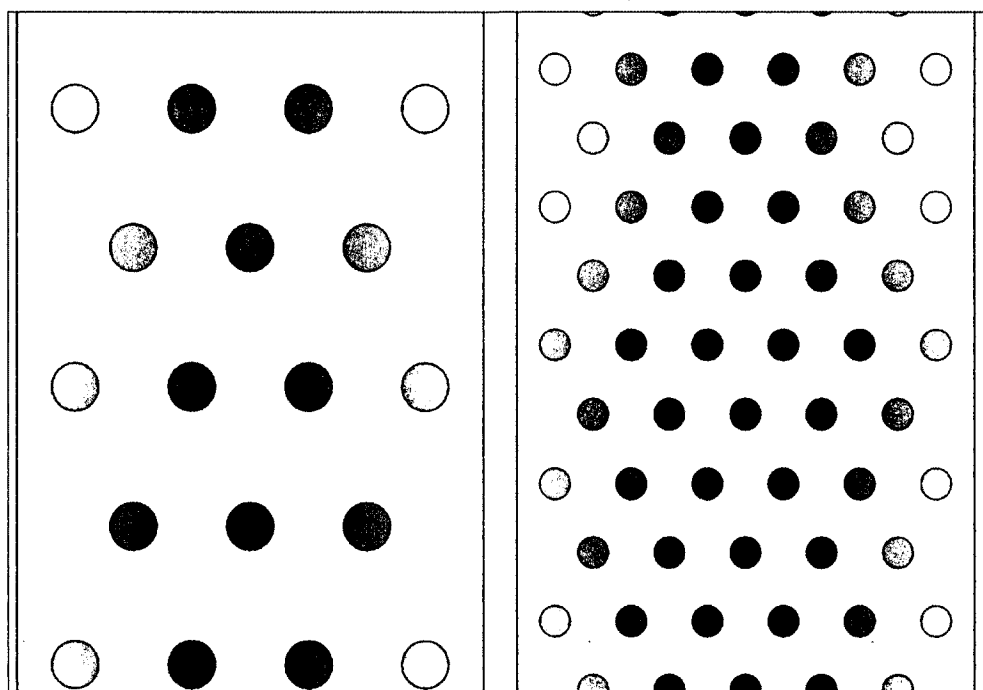


Figure 5-1: SolidWorks models of the two microchannel designs. The 150 post design is shown on left and 462 post channel on the right. Both are 1 mm wide.

The maximum velocity of the flow occurs in the region where flow intersects a row of posts, as indicated by the red colors in **Figure 5-2**. The maximum velocity for both channel designs is just above 5 mm/s. The rectangular cross-sectional area is the same for each channel between microposts and between rows of microposts (full rectangular area). A cross-sectional averaged velocity calculation for the full rectangular channel area yields an average of 0.83 mm/s. Using **Eq. 5-2** and **Eq. 5-3** and the cross-sectional averaged velocity, the Reynolds number is found to be 0.15, meaning the flow in either channel is strictly laminar.

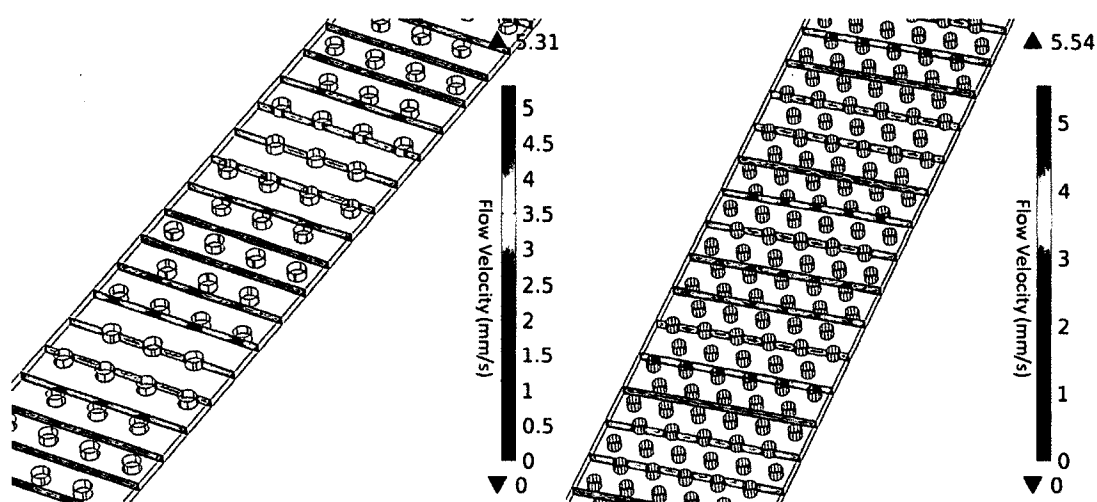


Figure 5-2: a) Microchannel velocity slices in the 150 post microchannel show uniform velocity in the open rectangular channel, with acceleration between the posts. b) Though the maximum speed is marginally higher in the 465 post channel, the velocity between rows of posts is the same as the 150 post channel.

The streamlines of each model (**Figure 5-3**) tend to show sharper lateral movement around the posts in the 462 post channel, with smoother flow in the 150 post channel. The flow layers may cover more ground and it may take longer for a protein to travel through the 462 post channel, thus increasing the chance that it will diffuse to a binding site on the channel surface. Some boundary layer effects are seen on the channel

edges, as the flow on either side of the channel is drawn further “off course” than flows in the center of the channel. The acceleration between posts does not create any turbulence in the streamlines. **Figure 5-4** shows the velocity profile through a row of posts in the channel, showing a similar flow profile between the posts as in a rectangular channel.

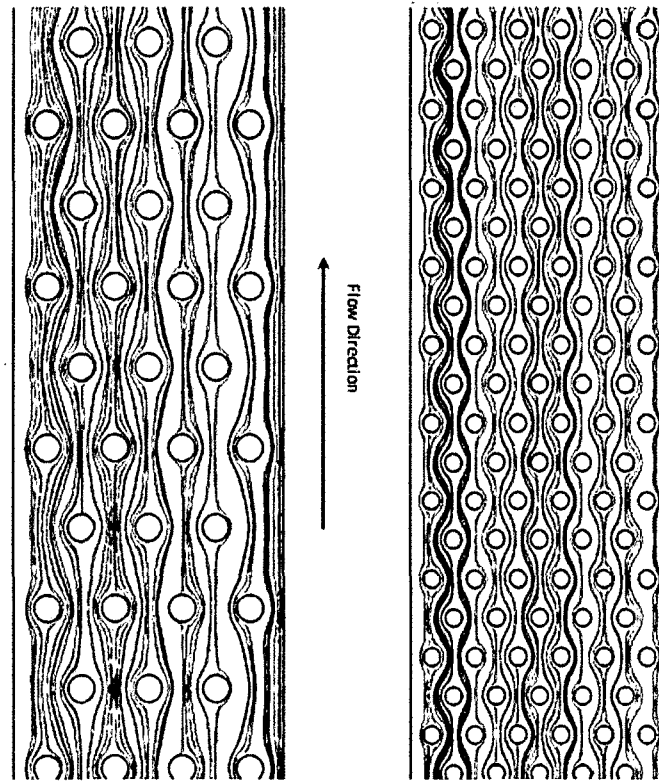


Figure 5-3: Streamlines showing the effect of the microposts in the channels on the laminar flow.

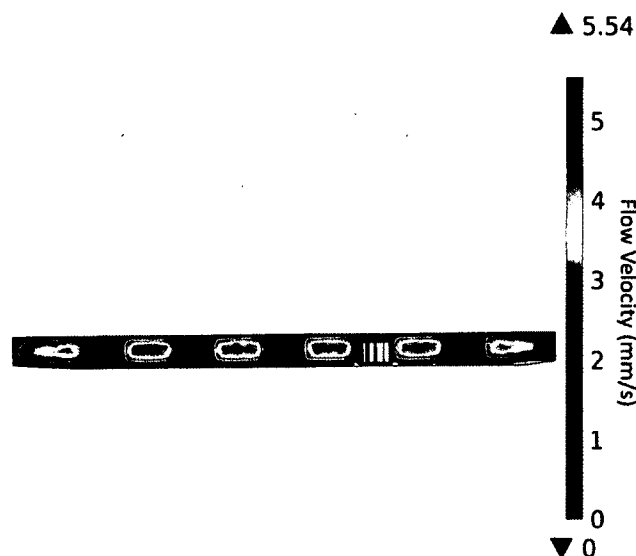


Figure 5-4: The flow velocity profile between microposts showing the region of maximum flow velocity in the 462 post microchannel. The spaces between microposts show similar flow profiles as an independent rectangular channel the size of the space between posts.

5.3.4 PDMS Carbonylated Protein Enrichment Model

COMSOL was used to verify the flow rate of the PDMS protein capture microchannel. Too high of flow rate minimizes residence time of a protein in the channel, reducing the distance that it can diffuse in the flow and the chance of reacting with an oxalyldihydrazide molecule on the microchannel surface. Additionally, an excessive flow velocity (approx. 2 m/s) can exert enough force on a cytochrome C molecule to remove it from its bonds, decreasing capture efficiency further. Hollins *et al.* found the flow rate in the PMMA microchannel, with an area of 0.1 mm^2 to be appropriate for binding and retaining cytochrome C and other proteins in the chip [34]. As shown in a previous section, the maximum flow velocity for the 150 micropost microchannel design is 5 mm/s, and for the 462 micropost design 560 mm/s.

The dimensions for the PDMS microchannel were chosen to minimize the diffusion distance in all directions for a protein in the center of the flow and to simplify device fabrication and pressure requirements. The pressure drop of a laminar flow in a rectangular channel is calculated by Eq. 5-7 from Fuerstman *et al.*, and contains a dimensionless parameter a which depends on the aspect ratio w/h [103]. The a value is directly proportional to the pressure drop, so a lower value minimizes pressure drop in the channel. Figure 5-5 shows the calculated value of a for aspect ratios from 0.05 to 1. The pressure drop in a channel is minimized in a square channel. This setup also yields equal diffusion distances and an absolute maximum of 50 μm that a protein must travel to meet a binding site. Fluid velocities for a 100 μm by 100 μm channel, as computed through CFD, are shown in Figure 5-6.

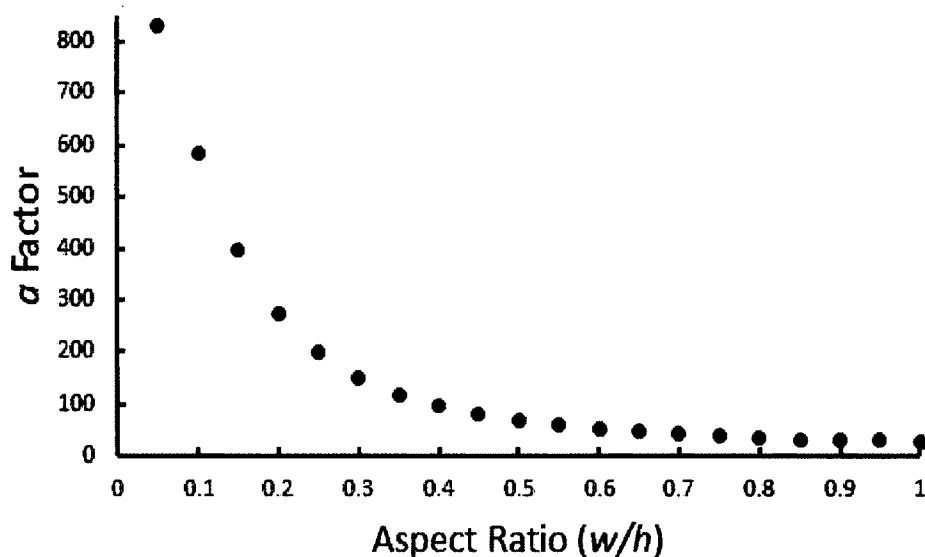


Figure 5-5: Dimensionless parameter a vs the aspect ratio of a rectangular microfluidic channel. The value of a is directly proportional to the pressure drop in a rectangular channel. The aspect ratio is limited to 1, at $w/h > 1$ the width and height are interchanged.

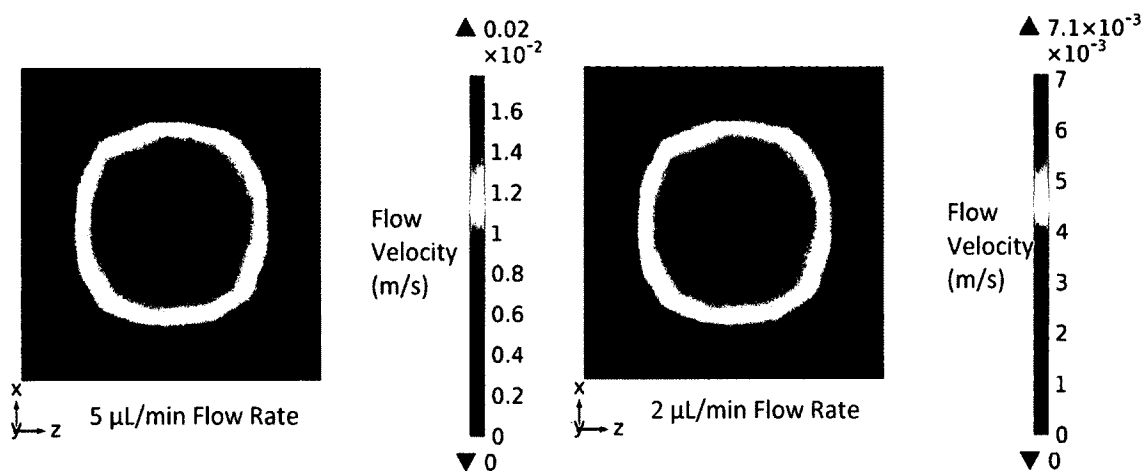


Figure 5-6: Flow velocity profiles in the PDMS carbonylated protein capture enrichment channel at different flow rates.

A simplified calculation of flow velocity in this channel based on volumetric flow rate of $5 \mu\text{L}/\text{min}$ and the channel cross-sectional area shows that the flow velocity is expected to be around $8.3 \text{ mm}/\text{s}$, ignoring the no-slip condition and assuming uniform velocity across the channel. In a 2.5 cm microchip, a protein would be in the channel for an average of 3 seconds. A COMSOL model of this channel and flow rate shows the expected flow profile and a maximum velocity of $20 \text{ mm}/\text{s}$, with the flow velocity of $8.3 \text{ mm}/\text{s}$ occurring closer to the channel wall than the center of the channel. Proteins in the center of the fluid flow would remain in the channel just over 1 second, reducing the chances of them diffusing to the binding surface. Reducing this flow rate to $2 \mu\text{L}/\text{min}$ slows the maximum flow velocity to $7.1 \text{ mm}/\text{s}$, increasing residence time of a protein in the channel. However, the decrease in flow rate may increase the time for a capture experiment to yield significant results. These results must be corroborated with physical experimental results to determine the best flow scheme for microfluidic protein enrichment.

5.3.5 Modeling of Microfluidics for Cell Culture Design

5.3.5.1 Device design

Recent work has shown the feasibility of microfluidic devices for biomedical applications such as cell capture, angiogenesis promotion, and stem cell culture.

Microfluidic devices allow for very tight control of microenvironments and can provide strong models for the study of environmental factors such as cell-cell contact and cell-extracellular matrix contact, as well as the behavior of adherent cells [3]. A

physiologically relevant concern in microfluidic cell culture is to keep shear stress under physiological maximums to maintain viable cells. Shear is also known to govern the phenotype of endothelial cells and may regulate behavior in other cell types [101]. Shear controlled microfluidic systems may be used to determine the required shear for a tumor to metastasize and could provide insight into a link between hypertension and metastasis. Thus, microfluidic designs must be created with shear in mind, and CFD can be used to determine the shear of a certain channel geometry with a given flow rate to ensure that it is within the necessary ranges before device fabrication is started.

To test possible microfluidic cell culture device designs, three geometries were modeled as possible shapes for culturing cells on a microfluidic lab-on-chip device: a rectangular channel with $w > h$, a trapezoidal channel with tapered sides at 30° from vertical, and a triangular channel, all $1000 \mu\text{m}$ wide (**Figure 5-7**). The rectangular and trapezoidal channels are each $50 \mu\text{m}$ tall, and the triangular channel is $75 \mu\text{m}$ tall. Each model was imported into COMSOL and flow of water was modeled. The flow profiles and the shear rate profiles of each were determined for a $5 \mu\text{l}/\text{min}$ flow rate. The shear stress at the wall was calculated from the shear rate and the viscosity of the fluid. The

shear stress 10 μm above the channel surface was calculated from the derivative of velocity with respect to height and multiplied by the viscosity, as seen in the Newtonian hydrodynamic shear stress calculation (Eq. 5-14).

$$\tau = \mu \left[\frac{\partial u(y)}{\partial y} \right]_{y=0,h} \quad \text{Eq. 5-14}$$

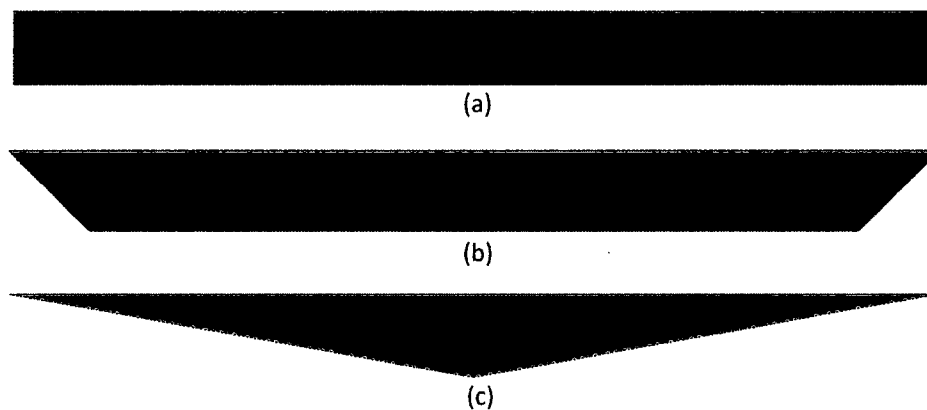


Figure 5-7: The three designs chosen as cell culture microchannels to model shear.

5.3.5.2 Velocity modeling result

The velocities for each channel are shown in **Figure 5-8**, with higher velocities being seen in the center of the devices as is expected in Poiseuille flow. The highest flow velocity is seen in the triangular channel, as its cross-sectional area is smaller than the other two designs. The rectangular channel has the lowest maximum flow velocity as it has the largest area. In the triangular channel, the flow slows lateral to the centerline, as the boundary layer effects dominate a larger proportion of the narrowing space between the upper and lower walls.

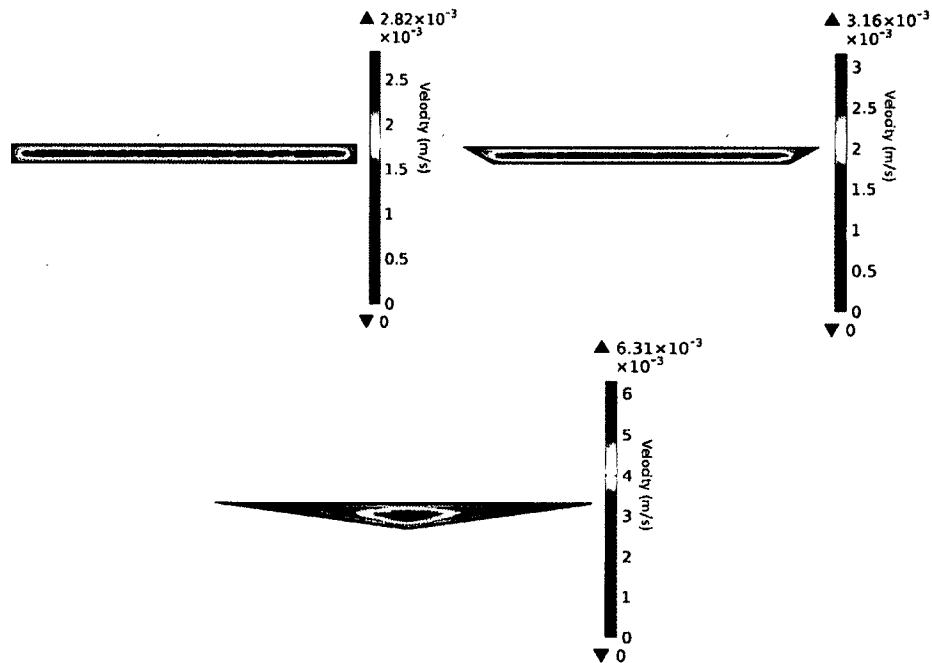


Figure 5-8: Velocity profiles and maximum flow velocities in mm/s for the three channel designs.

The flow profile in a microfluidic chip can be demonstrated through all of these velocity slices, but the triangle channel allows the visualization of the profile vertically and horizontally across the flow direction. Taking points at 0.05 mm intervals from the centerline toward the lateral edge of the channel, the velocity at points in increasing distances from the bottom of the channel can be plotted (**Figure 5-9**). The mostly parabolic flow is seen throughout the channel regardless of the height. Some roughness in the data is caused by the coarseness of the mesh used in the CFD model, as finer meshes produce more smooth results but take vastly more computing resources and time to solve.

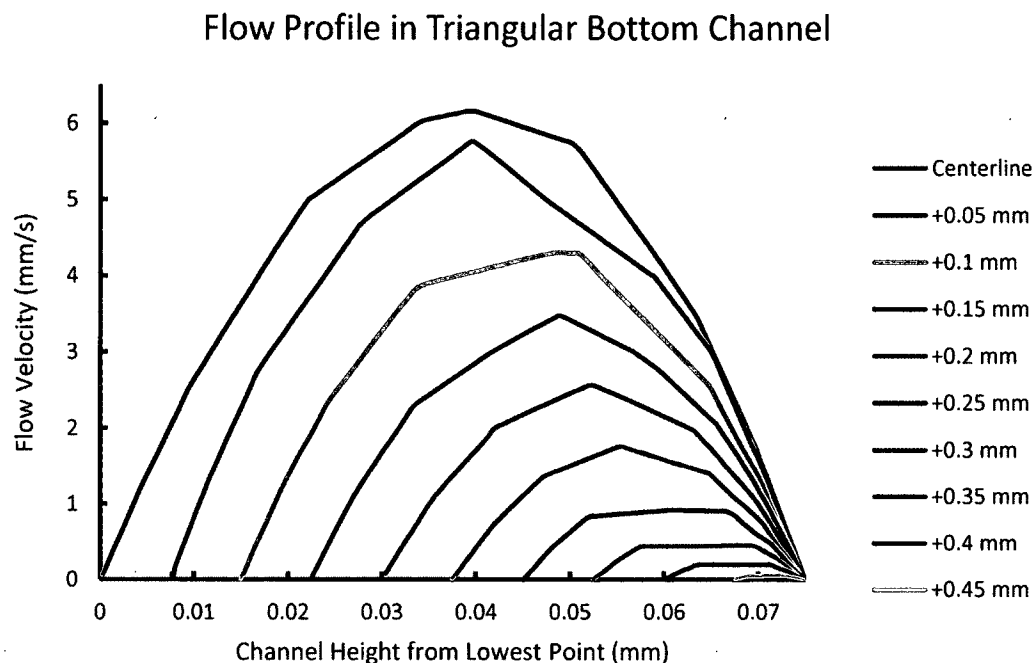


Figure 5-9: Velocity profile of the triangle channel in the vertical y direction, at 0.05 mm intervals from channel center to channel edge. From top to bottom, the profiles start at the center and move to the lateral edge.

5.3.5.3 Shear modeling result

Shear rate is a gradient of velocity in a flowing material, and is given in s^{-1} . The higher the velocity difference between the fastest flow and flow at a point the higher the shear rate will be. Viscosity is the ability of a fluid to resist being sheared, and is the proportion of shear stress to shear rate, or when the viscosity is known, it can be multiplied by the shear rate to yield shear rate. COMSOL can provide shear rate data at any desired point in a model and can generate color plots similar to those shown above for velocity. These data can be used to calculate shear stress and compare it to physiological values, or to verify that the device is suitable for the desired cells in culture. Because shear is related to the velocity gradient, the plots have some similarity to those seen for velocity, but the higher values for shear will be seen near the walls where the

velocity gradient is at its highest. The shear rate plots for the three designs are seen in

Figure 5-10.

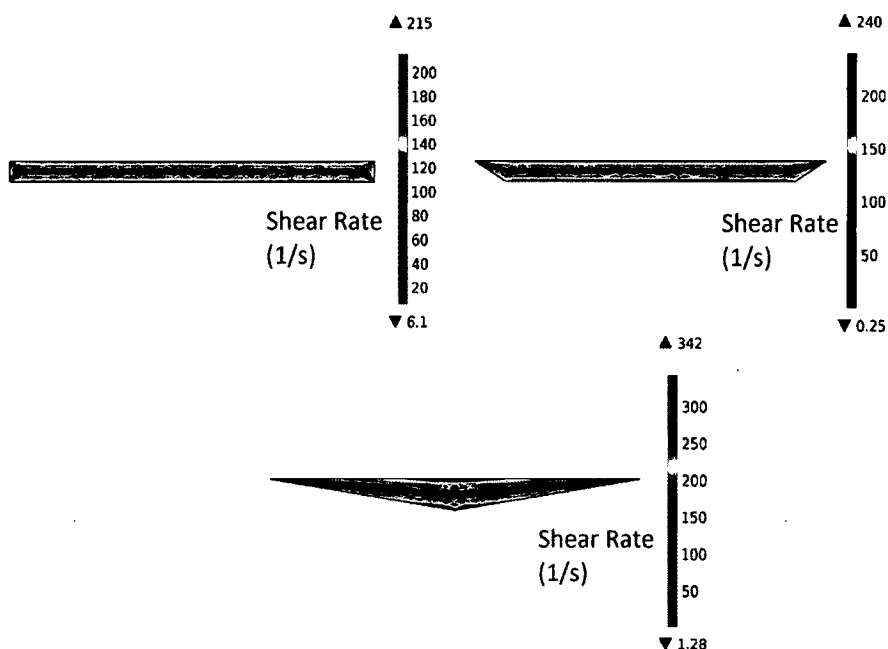


Figure 5-10: Shear rate and shear profiles in s^{-1} of the three microfluidic cell culture channel designs.

Because the triangular channel has the highest flow velocity, the shear rate is also highest in this device, and the lowest maximum shear rate is seen in the rectangular channel. The shear rates for the triangular channel drop to similar rates as the other two channels about 1/3 of the way to the side of the device from the channel center. This model yields another unique result to the triangular microchannel design in that it has a steady gradient of shear from the centerline to the edges. If the flow rate is set to keep shear stress within the physiological limits, a single culture of cells could be exposed to a range of shear stresses, allowing an all-in-one lab-on-chip device that can show the physiological effects of shear stresses on certain types of cells.

The rectangular channel provides the largest mass flow with the lowest resulting shear rate, which is best for maintaining stem cell viability with ample nutrients without risking differentiation under shear flow. Another advantage of this geometry is that it avoids the complex setups of a two-compartment lab-on-chip device or the possibility of contamination with traditional cell culture systems.

5.4 Conclusion

CFD is a powerful tool for analyzing and predicting flow in microfluidic devices. The technology can be used to pinpoint problems in a laboratory device, or to validate experimental parameters being used to more closely approximate the predicted result with the obtained result. It can also be used in the design of a new microfluidic device, to keep experimental parameters within the necessary ranges for available equipment, desired use of the device, and for the strengths of the materials to be used. Coupled with the defining equations of microfluidic flow, difficult designs and complex devices can be created, modeled, and optimized before a single mold is fabricated or a device assembled. CFD can provide immense savings in material cost, time investment, and minimize failures when creating the myriad of new devices seen constantly in the field of microfluidics.

Future work in this area will seek to incorporate the diffusion module of COMSOL to implement new designs for T-sensors, H-filters, and novel diffusion filter designs. When two microchannels merge with flow traveling in the same direction, the laminar flow schemes keep the streamlines parallel. If one flow contains a complex sample of analytes and the other flow contains a buffer or pure solution, the smaller molecules will diffuse much faster than large ones such as cells or proteins, and the

concentration of an analyte can be calculated from that found in the pure sample side outlet. A filter design with multiple outlets may be able to separate a small amount of complex sample quickly and efficiently.

CHAPTER 6

LOW COST MICROFLUIDICS

IMPLEMENTATIONS

6.1 Introduction

Microfluidics is known for its ability to provide low cost, high throughput systems for analyzing biological samples and enriching biomarkers using small samples and minimizing reagent and substrate waste. Microfluidics techniques stem from well-established processes in the semiconductor and microprocessor manufacturing industry, especially in the use of photolithography. Photolithography is the most common method for creating molds for PDMS microfluidic devices. Photoresist is cured via exposure to UV light as in a negative photoresist, or hardened where not exposed to light in the case of a positive photoresist. The substrate is often a silicon wafer which has been spin coated with a photoresist and cured in the desired pattern. The patterning of light exposure is controlled via a photomask, or digital light projection (DLP) systems.

6.1.1 Current Photolithography Mold Fabrication Method

Manufacture of many PDMS microfluidic devices depends on soft lithography (**Figure 6-1**). A negative photoresist SU-8 is spin coated onto a clean silicon wafer using a computer controlled spin table. The spin table spins the wafer at a predetermined rotational speed to evenly distribute the SU-8 on the wafer at a desired thickness. For SU-8 100, the viscosity of photoresist used in these studies, a desired feature thickness of 100

μm requires spinning at 3000 RPM for 30 seconds. The manufacturer recommends ramping to 500 rpm at 100 rpm/second, then ramping to the final spin speed at 300 rpm/second. Following coating, the coated wafer is baked at 65 °C for 10 minutes, and 95 °C for 30 minutes to help set the photoresist in place.

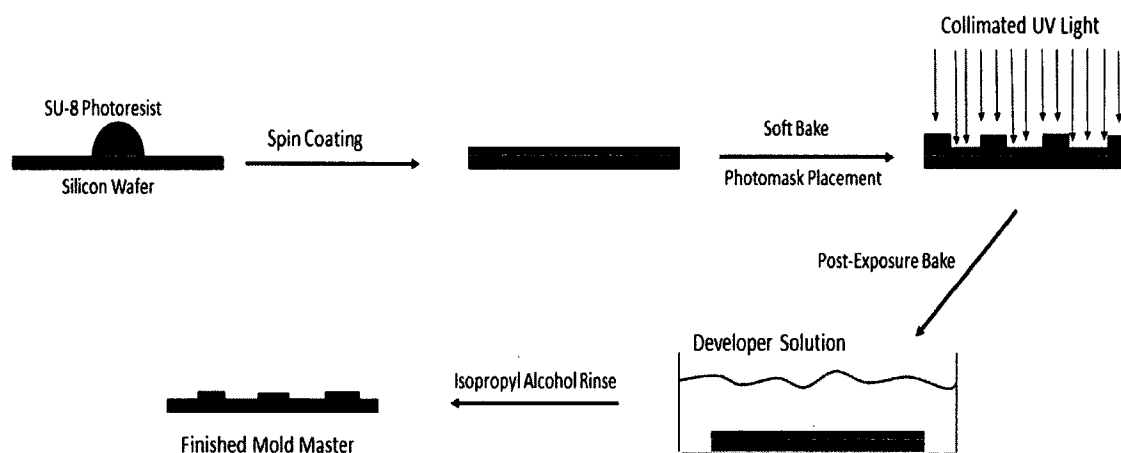


Figure 6-1: Visual outline of the photolithography process for creating microfluidic molds.

A photomask allows light to pass only in the design of the desired microchannels. The light allowed to pass through the photomask will cross-link and harden the photoresist in the desired areas to create the features of the microfluidic mold. The photomask is placed on top of the coated wafer and exposed to a highly collimated UV light source for 350-400 nm wavelength exposure. Exposure time depends on the strength of the light source; if exposure time is too short the features will come off of the mold during development, if it is too long the features will be wider than usual due to the reflected UV light crosslinking photoresist outside of the transparent areas of the photomask. Following exposure, the wafer is again baked at 65 °C for 1 minute, then ramped to 95 °C for 10 minutes and allowed to cool to room temperature slowly.

The final step in photolithographic mold creation is the development. SU-8 is provided with a developer chemical which will remove the non-cross-linked photoresist from the wafer, leaving only the exposed, cross-linked mold features. The wafer is immersed in the developer chemical and agitated for 10 minutes or until the desired features are all that remains on the wafer.

This process requires very delicate manual work with expensive and precise equipment and materials, and it is often performed in a cleanroom environment. To truly take advantage of the low cost, point-of-care opportunities that are provided by microfluidics, a simpler but equally effective method must be used to create microfluidic mold masters. This work includes the development of a technique that takes advantage of rapid prototyping techniques and widely available consumer electronics to lower the necessary equipment investment and make photolithographic techniques more widely available.

6.2 Methods

6.2.1 3D Printed Spin Table

SolidWorks (Dassault Systèmes) was used to design the spin table. The design was created around the dimensions of the motor used and the silicon wafer. To minimize rotating mass, a three post table design was created where small posts held the silicon wafer in place. The wafers have a flat edge that indicates the direction of the crystalline structure, and one of the three posts was installed closer to the center of the spin table to secure the wafer in place and provide a face to drive the rotation.

The SolidWorks 3D CAD file was saved as a .stl file and exported to the MakerBot Desktop software, which slices the design into layers and creates a G-code file

to direct the 3D printer. A MakerBot Replicator 2x filament printer (MakerBot Industries LLC, Brooklyn, NY, USA) was used to print a spin table base and wafer holder. The MakerBot Replicator can extrude ABS or PLA filament in a fused-deposition modeling process to build up the prototype parts layer-by-layer. ABS plastic was used for the spin table prototypes. For the final model of the spin table, printing was outsourced to Xometry, Inc., to provide a higher quality and more durable product out of nylon using selective laser sintering.

6.2.2 UV LED Light Source

A printed circuit board was used as a platform for mounting UV LED lights in a parallel circuit format. The LEDs have an angle of incidence of 15 degrees, the lowest that are available commercially. This angle was reduced by surrounding the sides of the LEDs with shrink tubing. The LED circuit was built for an input voltage of 9 V, so that the board could be powered by a 9 Volt battery or a bank of batteries for longer runtime. A common power and ground wire was run down one side of the PCB, with each row of LEDs forming their own parallel circuit off of this common rail. A 330 Ω resistor was placed in series before each LED to bring the voltage down to the 3V that each LED needs. A total of 104 UV LEDs were used in this design.

6.2.3 Arduino Controller

The spin table was controlled by an Arduino Uno and the pulse-width modulation capabilities of the digital output. A Hall effect sensor was affixed to the base of the spin table directly underneath a magnet attached to the wafer holder of the table. The magnet triggers a counter in the Arduino program, which calculates the time required to reach 50 rotations and calculates the RPM of the table. Based on the calculated RPM value, the

PWM duty cycle is increased or decreased to adjust the speed of the motor and hold the rotational speed within 400 RPM of the set value. Timing was manually controlled, starting when power is turned on to the Arduino and at the end of the set time, power is shut off to the motor.

6.2.4 Photolithography Procedure

The protocol described in Chapter 2 for fabricating the mold master was followed using the rapid prototyped spin table and UV LED light source. The silicon wafer is covered in Omni-coat followed by approximately 4 mL of SU-8 100. MicroChem recommends approximately 1 mL per inch of silicon wafer. The silicon wafer is spun at 3000 RPM for 30 seconds to distribute the viscous photoresist evenly onto the wafer. The spin coater is placed inside of a cardboard box to contain the excess photoresist that is spun off of the wafer. Following spin coating, the wafer is baked at 65 °C for 10 minutes and then 95 °C for 30 minutes.

A photomask printed on a plastic transparency is placed directly onto the surface of the photoresist and held in place with masking tape to ensure that there is no distance between the photoresist and photomask, and to prevent movement of the photomask over the photoresist surface. The UV LED array is placed approximately 4 cm above the wafer and supplied with 9 V of power from either a battery or power supply. The wafer is rotated under the array approximately 45 degrees every hour to prevent double features as a result of the angle of incidence of the LEDs and their spacing on the PCB. After 4 hours, the photomask is removed from the wafer and the wafer is baked at 65 °C for 1 minute and 95 °C for 10 minutes.

After exposure and baking, the wafer is immersed in SU-8 developer solution to remove the unexposed photoresist from the wafer. The wafer is immersed and constantly agitated for 10 minutes, and rinsed with isopropyl alcohol, and only the features exposed to UV under the photomask should remain on the wafer.

6.3 Implementation of Low Cost Photolithography

6.3.1 Spin Table

Solid-object printing or 3D printing has become a widely affordable and available method for rapid prototyping of designs in a variety of thermoplastic materials. The most common form of 3D printing is fused deposition modeling which uses a filament of acrylonitrile butadiene styrene (ABS) or poly-lactic acid (PLA) heated through an extruder and laid down in a thin line one layer at a time. These printers allow a CAD model to be turned into a physical prototype in a couple of hours, depending on the size of the prototype. The base was designed with a ring at the top to hold a small electric motor capable of turning the wafer holder and wafer at the desired rotational speeds. A dimensioned drawing of the base as created in SolidWorks is shown in **Figure 6-2** and the 3D printed product is shown in **Figure 6-3**. The mild angles and short distances between arms around the motor holder ring allowed the entire piece to be printed without the use of supports, minimizing material use and printing time.

The top of the spin table contains three arms on which the silicon wafer rests, and three posts at the end of the arms to hold the wafer in place without impeding the removal of excess photoresist during coating. Because the wafers contain one flat edge indicating the crystalline direction, one post is slightly closer to the center of the table, allowing the wafer to be tightly secured and reducing vibrations. A small hole in the center of the table

fits tightly onto the motor shaft. A dimensioned drawing of the spin table top is detailed in **Figure 6-4**, with the physical printed part shown in **Figure 6-5**. The fully assembled 3D printed spin table is shown in **Figure 6-6**.

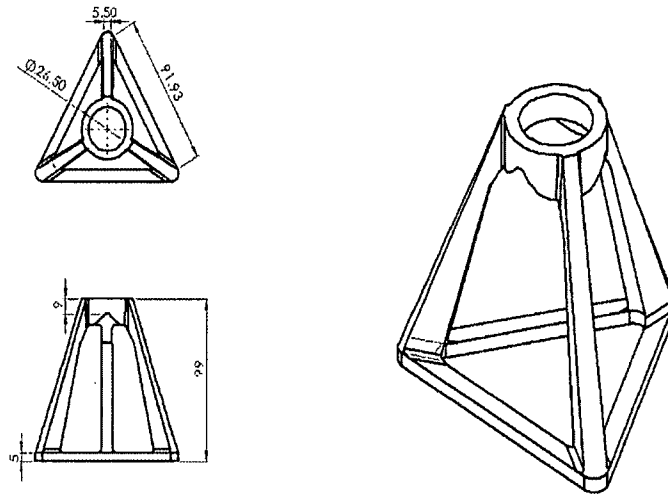


Figure 6-2: The base of the spin table, showing the supports and the ring for holding the electric motor. All dimensions are in mm.



Figure 6-3: Base of the 3D printed spin table with Hall effect sensor attached via epoxy.

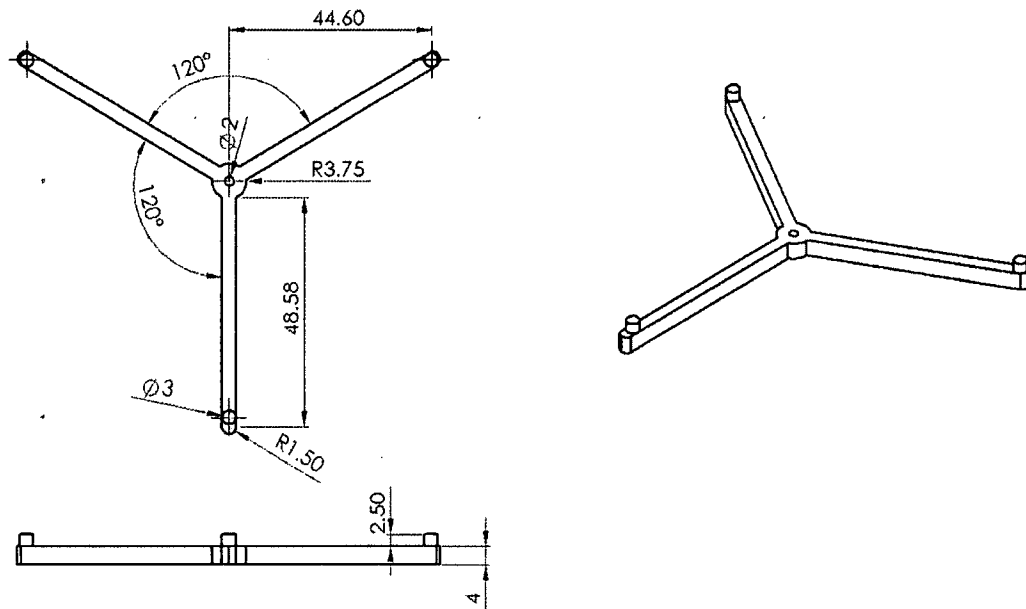


Figure 6-4: The top of the spin table designed to securely hold the silicon wafer centered over the motor during spin coating. The design is optimized for minimal vibration and rapid printing times. All dimensions in mm.



Figure 6-5: Spin table top, with magnet attached to top right arm via epoxy.



Figure 6-6: Assembled spin table with motor and Hall effect sensor affixed.

6.3.2 Electrical Design of Spin Table Motor Circuit

The motor used is a Super Speed Hobby Motor available from RadioShack (P/N 2730256). The motor is capable of operating on 9 VDC, 12 VDC, and 18 VDC inputs, and at 9 VDC has a no load specification of 11000 RPM and 150 g/cm torque. To keep the motor speed at an acceptable level for spin coating, the pulse width modulation capabilities of an Arduino Uno are used to switch a 9 V circuit via a 2N2222 NPN switching transistor. Arduino Uno provides only 5 V and very low current to its outputs, but the control of the signals duty cycle can open and close the circuit at varying duty cycles to control the speed of the motor. The circuit used is shown in **Figure 6-7**. R1 is used at the transistor's base to limit the current and protect the output of the Arduino. The resistance value is determined from the Arduino output voltage and the current draw by the motor. For the components used in this setup the resistor value should be

approximately 170Ω . Additionally, a diode is attached in parallel with the motor to provide a path for the current produced by the spinning motor when the circuit is switched off.

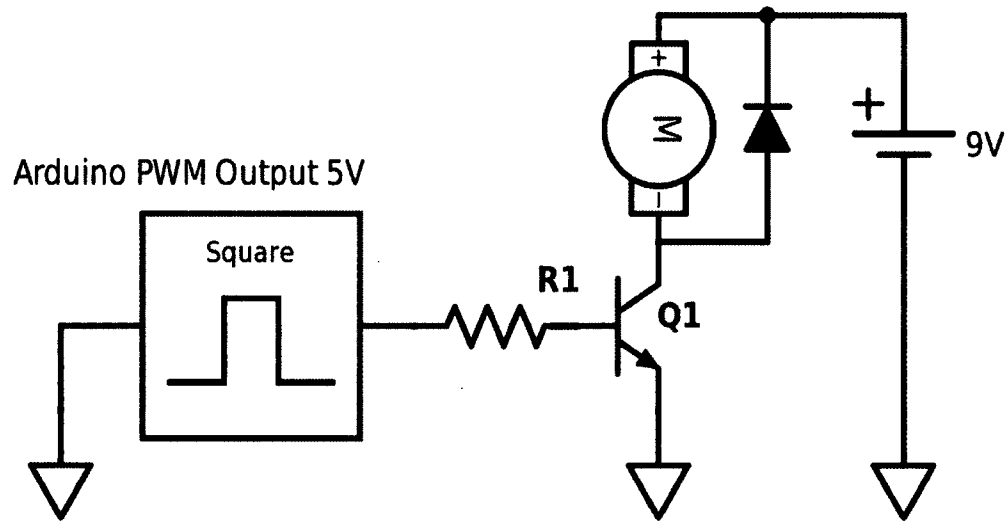


Figure 6-7: Low-side transistor switch for controlling the spin table motor speed. The low-side scheme of this switch maintains a higher voltage across the motor to aid in maintaining the proper speed of the spin table.

6.3.3 Arduino Motor Speed Controller

To determine the duty cycle of the PWM signal necessary from the Arduino, the spin table's RPM must be calculated and compared to the desired value. To achieve this goal, a Hall effect speed sensor was used. A small magnet was attached to one of the arms of the spin table, and the sensor was attached to the spin table base and positioned so that the magnet passed directly past the sensor on each revolution. The output of the Hall effect sensor was connected to the digital input of the Arduino and the number of pulses counted over a set period of time. This was used to calculate rotational speed, and increase or decrease the PWM duty cycle accordingly. Thus, the table is able to reach the

correct speed and constantly adjust the speed based on the load, which could vary due to the amount of photoresist on the wafer or voltage changes in the power supplied to the motor. The code for calculating the current rotational speed and adjusting the control signal is found in the Appendix.

The code calculates the time difference between the previous and the current calculation along with the number of rotations since the previous calculation, and it uses these two figures to calculate RPM. Based on the calculated RPM, the code either increases the PWM duty cycle by 1%, decreases by 1%, or pauses temporarily. Following the calculation of RPM, the time and RPM counters are reset and after adjustment and a pause the RPM is calculated again. This method requires manual timing of the spin cycle and power control, but a timer or loop counter could be instituted into the program to control this function. Manual control was sufficient for the times this was used in lab.

6.4 UV Photoresist Curing

Following even spin coating of the silicon wafer with photoresist and soft baking the coated wafer, a photomask must be applied over the surface. Because soft baking hardens the photoresist enough for gentle handling, the photomask can be placed directly on the surface of the coated wafer. This practice minimizes the amount of incident light that can penetrate the photomask at an angle and reduce the resolution of fine features of the mold. Incident light during curing can cause features with angled sides rather than vertical, and result in an overall reduction in aspect ratio. Maintaining sharp, fine features is critical to the operation of many microfluidic devices.

Traditionally, photoresist is cured using a high strength UV lamp and a collimator. Both require significant monetary investment in the equipment and optics

required to produce a UV beam of perfectly vertical light. However, the perfectly vertical beam reduces incidence and maintains the sharpness of microfluidic mold features. The UV lamp produces enough light energy that the curing process takes only a few minutes. However, neither of these are very portable or low cost, detracting from the appeal of microfluidics.

6.4.1 Light Emitting Diode Array for SU-8 Curing

UV light emitting diodes (LEDs) are available with low angles of incidence, less than 15° . When arranged in parallel, many of these can be powered by one or more 9 V battery for a few hours. A 9 V power source can also power these lights easily. To complete the low cost photolithography system, a printed circuit board (PCB) was used as a substrate for a UV LED array for curing photoresist. 104 UV LEDs were wired in parallel with a 330Ω resistors to bring the input voltage to the correct range for each LED. Using one positive and one ground wire, the entire board can be powered for around 2 hours on one 9 V battery, or more with multiple batteries. When placed above the photoresist coated wafer and the photomask at close range, the UV LEDs will cure the photoresist in approximately 4 hours. To produce even exposure across the entire photomask, the wafer is rotated under the UV lights 45 degrees every hour.

When the wafer is not rotated, the combination of angle of incidence and spread of the UV light sources can lead to thin double features on the silicon wafer. Light is not hitting a transparent portion of the photomask vertically, but is rather entering at an angle from either side of the transparent section. Thus, a line of photoresist is cured on one side of the feature, and another line is cured on the other, leaving the area between the two lines without cured photoresist despite the transparent section of the photomask. Rotation

solves this problem, but the continued radiation by angled light causes features to be slightly wider than the corresponding transparent section of the photomask. A future design should reduce the spacing of the LED lights and stagger the rows. The reduced spacing will minimize dead spots of less UV exposure, and the staggered rows will ensure that a dead spot won't be present along a single line so that a microchannel won't be fully missed by UV exposure. Surrounding the sides of the LEDs with shrink tubing or coating in a dark paint or epoxy will reduce the angle of incidence, resulting in features that are truer to the photomask feature size. If angle of incidence and total distance between photomask and silicon wafer are known, the expected feature size can be calculated and the photomask adjusted if desired, eliminating the need to decrease angle of incidence of the LED light sources.

6.5 Design Improvements

After the capabilities of this new system were verified, a new design iteration was created to better integrate the multiple components of the spin table. The support structure for the motor was shortened to improve stability and to lower the center of gravity. A storage box was incorporated into the lower section of the base to house the battery, circuits, and microcontroller while protecting them from the photoresist that is thrown from the wafer during spinning. Rather than epoxying the Hall effect sensor to the table and making continual adjustments to place it in the exact location below the passing magnet, a pillar was added to one of the three legs of the support structure. This pillar holds the sensor in the correct orientation and places it directly under the magnet passing overhead. Additionally, the spin table top incorporates a recessed dish to house the magnet and center it directly over the Hall effect sensor. These improvements should

result in a cleaner signal to the Arduino and allow more precise control over the motor's speed.

To ensure the longevity of the final product, 3D printing was outsourced to Xometry, Inc. and produced using selective laser sintering (SLS) and nylon (**Figure 6-8**). This process ensured tighter tolerances and more accurate printing, as well as a more complex design. The design should minimize vibration during spinning to create a more even coating of photoresist. The magnet well was incorporated onto the short arm of the spin table, which should aid in the balance of the table. With the wafer in place, vibration was minimal and the spin table did not have to be weighted for stability.



Figure 6-8: The selective laser sintering-created second design of the spin table, attached to power source and the Arduino Uno microcontroller. The Hall effect sensor is on the vertical pillar protruding from one of the support arms, and the transistor is seen in front of the base of the spin table.

The microchannels created with this new table (**Figure 6-9**) achieved a feature thickness of 107 μm , close to the target thickness of 100 μm and identical to the thickness

of microchannels created with traditional photolithography equipment. The previous design required a weight on the base to prevent shaking and movement of the table, and the improved iteration requires no such stabilization. The result of the stable motion is a smooth coating of photoresist across the surface of the wafer, aiding in uniformity of features in the finished mold. The increased angle of incidence of the UV LEDs caused the width of the channels to be approximately 400 μm , much greater than the 100 μm feature width on the photomask. The PDMS microchannels created with traditional photolithography equipment had dimensions of 107 μm depth and 160 μm width.

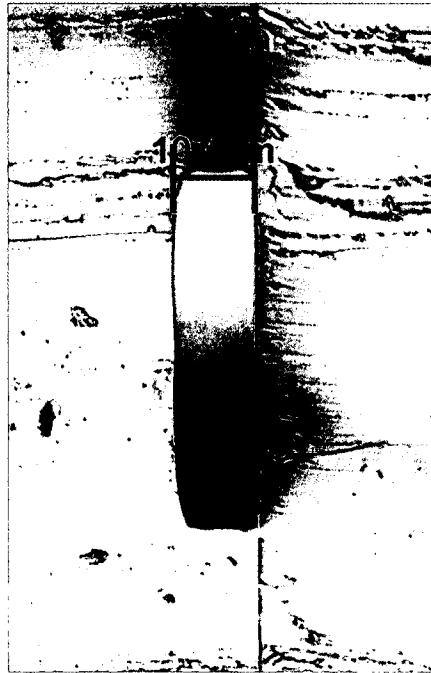


Figure 6-9: Cross section of a sealed PDMS microdevice created with the mold from the 3D printed spin table and UV LED board.

Future designs of the UV LED system or a reduction in photomask feature size can address this issue and reduce the feature size to the desired width. Covers can be added to the sides of the UVs to block the light exiting from the sides of the board,

allowing only the vertical rays to hit the photomask and photoresist. Extra light can reflect off of the silicon wafer and harden additional photoresist as well; using the low power LED lights may reduce the likelihood of this if the first incident ray problem can be solved.

CHAPTER 7

CONCLUSIONS AND FUTURE WORK

7.1 Conclusions

7.1.1 Project Specific Aims

This research aimed to demonstrate that PDMS-based microfluidics perform better than PMMA or other microfluidic substrates by providing a robust, flexible, modifiable, low cost, and highly effective platform to serve in novel microfluidics applications. The specific aims to prove this are addressed in Chapters 3-6 of this work, and each specific aim was accomplished successfully.

Several suitable surface modification protocols were found and one chosen based on its simplicity and effectiveness for modifying a fully enclosed microchannel, as well as its robust attachment of the crosslinker to the PDMS substrate. Flow through modification addressed several incidental problems associated with surface modification of PDMS devices. The larger dextran molecule attachment to the surface provides a resistance to hydrophobic recovery that is commonly seen in PDMS. The large surface molecules resist incorporation into the polymer bulk, thus stabilizing the modified surface in storage for longer periods of time, allowing modification of several devices at once to be saved for later use.

Flow-through dextran-modified PDMS demonstrated selective and efficient capture of carbonylated proteins in the microchannel. Over 60 minutes, the fluorescence

of the flow-through solution had risen to stock levels and remained there, indicating the binding of all available crosslinker to proteins.

In addressing the problem of reincorporation of modified PDMS groups into the polymer bulk and transport of LMW groups to the surface, the question of using PDMS as a carrier for small molecule delivery into cell culture or microfluidic flows was addressed. PDMS demonstrated leaching of fluorescein molecules when immersed in cell culture media, and steady leaching of fluorescein into microfluidic flows. The intentional doping of PDMS with small molecules for intentional leaching into microdevices was successfully demonstrated.

Throughout this research, new designs were considered and some implemented, but throughout the entire process CFD was used to ensure that the designs and features in these theoretical microfluidic channels produced flow rates and characteristics that were expected and desirable. CFD demonstrated the possibility of using microfluidic channels as cell culture devices to mimic physiological shear rates, or to provide a shear gradient across a single microdevice. CFD further reduces the cost of microfluidic research by producing experimental results without investing in the creation of a new photomask and mold and going through the photolithographic process.

When a new microfluidic design is verified and a mold is to be made, traditional techniques for microfluidics involve photolithography setups that are often expensive and time consuming, and that require specialized environments. To improve the suitability of PDMS microfluidic research in an academic laboratory setting, a low cost photolithography setup was successfully designed and produced using rapid prototyping techniques widely available. An Arduino Uno microcontroller was integrated to a spin

table that housed a motor and Hall effect sensor. Using pulse-width modulation to a transistor-switched circuit, the Arduino successfully controlled the rotational speed of the silicon wafer to spin the SU-8 photoresist to the correct thickness. A UV LED printed circuit board was created with low angle of incidence LEDs to provide the energy source necessary for cross-linking the photoresist in the desired pattern. Using a transparency-sheet printed photomask, the resulting features were near the scale originally intended.

All five of the specific aims outlined in this dissertation were successfully completed and demonstrated. The results obtained show novel applications of PDMS in the area of biomicrofluidics. The attachment of oxalyldihydrazide to PDMS has not been reported in the literature, and PDMS has not been used as a microfluidic substrate to selectively capture carbonylated proteins. The ease of use and flexibility of creating various PDMS designs represents an improvement over PMMA microfluidics. PDMS does not require high pressures and vacuum to hot emboss microchannel designs, and micromilling equipment is not needed to create the mold master. The low cost implementations designed in this research address the complexity of creating mold masters for microfluidics and makes photolithography more accessible.

PDMS adsorbs and absorbs hydrophobic and biological molecules, and can leach non-cross-linked oligomers from the polymer bulk. To date, the only work on doping PDMS is with surfactants to improve the surface wettability, but surface modifications seem to provide better results. However, doping of PDMS with small molecules for intentional delivery to fluids and microfluidics has not been reported. This work is foundational to developing microfluidic cell culture systems that can operate with very

low, steady state concentrations of molecules of interest with minimal human interference.

Microfluidics takes advantage of a unique flow scheme not seen in macroscale applications. The high surface area to volume ratios, short diffusion distances, strictly laminar flow, and small amounts of samples involved allow researchers to take advantage of physical phenomena that would be impossible or highly impractical in traditional laboratory procedures. Microfluidics provides incredible advantage over techniques such as affinity chromatography, static cell culture, and sample analysis. Most significant is the reduction in sample size and reagent use, with microfluidics often using much less than 1 mL. The rapid throughput capabilities and ability to tailor devices to very specific applications increases the versatility of what a laboratory can accomplish.

Overall, PDMS provides an exciting platform that has been at the center of an explosive growth in research interest. The widespread applications and the ease of fabrication and modification brings microfluidics closer to the “killer application” that the field has been in search of since its inception [106].

7.2 Future Work and Directions

This research lays the groundwork for novel applications in biomicrofluidics for PDMS and provides a number of future directions for the research to follow. Ongoing research for this work will build upon the foundations established in this dissertation, and will seek to expand the applications and effectiveness of the techniques developed.

7.2.1 Oxidative Stress Biomolecule Detection

This work demonstrated that oxalyldihydrazide can be attached to PDMS and used to selectively bind and capture carbonylated proteins. Future work in this project

will involve the implementation of an on-chip detection system and testing of the system with complex biological samples. Samples of a mix of oxidized proteins will be tested, and the eluted proteins after capture analyzed via capillary electrophoresis to verify that all oxidized protein types are present. A mix of oxidized and native proteins will be tested in the microchannel and analyzed to ensure that only the carbonylated proteins are captured in the microchannel. This set of experiments will verify the expected selectivity of the device and prepare the microchip for use in biological samples from mouse models of oxidative stress diseases. Samples of blood or tissue will be homogenized and diluted in buffer, then pushed through the microchip. The proteins that are captured will be analyzed, and proteins that are involved in the models of oxidative stress diseases will be identified. Identification of protein profiles in these diseases will provide a clearer picture of the progression of oxidative stress disease and may identify proteins involved in the disease state that are not yet known. The low abundance detection ability of this microdevice will allow the detection of rare proteins that may undergo carbonylation as part of the progression of a disease involving oxidative stress.

This device can be used for detection of any carbonyl containing compound in a sample due to the specificity of carbonyl-hydrazide affinity. The modification presented in this work can be applied to chemical detection and enrichment in a variety of biological and non-biological samples, and could be used as the basis for further surface modifications of PDMS.

On-chip quantification of bound proteins will eliminate a step in the current procedure of oxidized protein capture in microfluidics. The most likely method to achieve this capability is through amperometric detection of bound target proteins.

Several methods of creating electrodes in microdevices have been described for various assays [107]. Many of these have been created on paper or test strips; blood glucose measurement devices are a common commercial application of this technology [108]. Integrating on-chip detection and quantification of bound proteins will eliminate the need for a sensitive fluorescent tag on the oxidized proteins, and eliminate the need for a follow-up CE step in certain tests. If a test is needed to measure carbonylation levels of a certain sample where the type of protein carbonylated is unimportant, on-chip quantification of bound proteins will eliminate the tagging and elution steps of the microfluidic capture protocol, allowing point-of-care application of this microfluidic device. Over time, the device can be developed into a rapid test for the presence or likelihood of various disease states using a small sample of blood or cells from a patient.

7.2.2 Doping of PDMS for Intentional Leaching into Microdevices

Future work in the doping of PDMS with small molecules relies on the ability to predict and tune the amount of dopant that will leach out of a certain device. Quantification of the leaching in various situations and over periods of time forms a basis for discovering the limits of this technique. Ongoing research in this area will be performed with the goal of creating a model that can be used to accurately predict the amount of dopant that will be leached based on the dimensions and dopant concentration of the PDMS device.

To achieve this goal, the properties of molecules that will readily leach from doped PDMS must be discerned. Once the characteristics of a suitable dopant are identified, it will be possible to determine a diffusion and leaching rate for various molecules that will predict their behavior in doped PDMS microdevices. These rates,

coupled with the effects of dimensions of the microchannel and concentration of dopant, will allow the development of a mathematical model that will be able to predict the leaching of dopant over time in a certain microdevice. This model will allow the creation of specialized cell culture devices with integrated drug, signal molecule, or tagging molecule delivery systems.

7.2.3 Low Cost Biomicrofluidics Implementations

The main direction of future work in the low cost and rapid prototyped photolithography system involves improving the UV light source for exposing the photoresist. The current device meets all the targets for cost, ease of use, and portability, but lacks the high collimation needed for perfect feature size replication. The angle of incidence of the LED's used in the light board create features on the silicon mold wider than those expected from the photomask. Light travels through the transparent section of the photomask at an angle, hardening the photoresist underneath an opaque section and widening the feature past its expected dimension. By adding covers to the sides of the LEDs, or by sourcing LEDs with lower angles of incidence, this problem can be addressed. Another way to address this, if the printing equipment used allows, is to reduce the size of the features on the photomask to account for the incident light, but this may not be possible for smaller features.

The spin table was redesigned, and printing was outsourced to create a final product with better feature resolution and longevity than available with the rapid prototyping capabilities in the lab. Future work for the spin table will be to better integrate the components and wiring into the device; the compartment built into the bottom of the spin table can be used to house the Arduino and the power source. This

additional weight will further balance and anchor the table to create higher quality molds. A different Arduino would be more suitable as the Uno board contains more ports and connections than are necessary for this design and its size makes full integration into the printed table difficult. An Arduino Mini or Pro Micro contains all the capabilities of the Uno in a smaller package that is easier to integrate into devices. A dedicated microcontroller specifically for the spin table will be the next iteration of design.

Being able to make, modify, and use the microchips in a resource limited situation is the ultimate goal of the work. By developing that capability, a true point-of-care device that takes full advantage of the flexibility and ease of use of PDMS can become a reality. This research creates and tests novel applications of PDMS in the field and lays groundwork for reaching that goal.

APPENDIX A

ARDUINO CONTROLLED SPIN TABLE CODE

The code for controlling the speed of the spin table is an RPM counter using a Hall effect sensor reading magnetic pulses on each rotation of the wafer holder. The RPM is calculated every 250 milliseconds if the table's rotational speed is not within the set range, or every second if the previous calculation of the RPM shows that it is within the proper range. A magnet detection counter increases each time the magnet causes the non-latching Hall effect sensor to send a 5 V signal to the Arduino. Each time the RevCalc loop is called, the time from the last calculation is compared to the current time, and used along with the number of rotations in that time to calculate the revolutions per minute. Both the time tracking variable and the magnet counting variable are reset after each calculation of speed. The following code contains comments for each statement after a double slash.

A.1 Arduino Code for Spin Table Controller

```
volatile byte revs; //counter for each magnet pass
unsigned int rpm; //Stores calculated RPM value
unsigned long timeold; //Time Tracking Variable
int motorPin = 3; //PWM Output port
int speed = 100; //Starting motor speed (Range 0-255)

void setup()
{
  attachInterrupt(0, magnet_detect, RISING); //Call
  magnet_detect when Hall sensor sends signal at magnet pass
  pinMode(motorPin, OUTPUT); //Set output pin
  revs = 0; //Counter for each rotation of table
```

```
rpm = 0; //variable for calculated RPM
timeold = 0; //Initialize time-tracking variable
}

void loop()
{
  RevCalc; //Calculate RPM from pulses and elapsed time since
last calculation
  if (rpm < 2800 && speed < 255) //3000 RPM target
  {
    speed = speed * 1.01; //Increase duty cycle by 1% if under
2800 RPM
    delay(250);
  }
  else if (rpm > 3200 && speed > 0)
  {
    speed = speed * 0.99; //Decrease duty cycle by 1% if over
3200 RPM
    delay(250);
  }
  else
  {
    delay(1000); //1 second pause if speed in range, wait for
next calculation
  }

  analogWrite(motorPin, speed); //Set new motor speed
}

void magnet_detect()
{
  revs++; //Add 1 to revolution counter for each magnet pulse
}

int RevCalc(int rpm)
{
  float r;
  r = ((60*1000)/(millis() - timeold))*revs;
//RPM=revs/ms*60000ms
  rpm = (int) r; //integer value of RPM calculation
  timeold = millis(); //reset time counter
  revs = 0; //reset rev counter
}
```

BIBLIOGRAPHY

- [1] G. M. Whitesides, "The origins and the future of microfluidics.," *Nature*, vol. 442, no. 7101, pp. 368–373, 2006.
- [2] P. N. Nge, C. I. Rogers, and A. T. Woolley, "Advances in microfluidic materials, functions, integration, and applications," *Chem. Rev.*, vol. 113, no. 4, pp. 2550–2583, 2013.
- [3] K. Jang, Y. Xu, Y. Tanaka, K. Sato, K. Mawatari, T. Konno, K. Ishihara, and T. Kitamori, "Single-cell attachment and culture method using a photochemical reaction in a closed microfluidic system.," *Biomicrofluidics*, vol. 4, no. 3, p. 32208, 2010.
- [4] C. G. Sip, N. Bhattacharjee, and A. Folch, "A modular cell culture device for generating arrays of gradients using stacked microfluidic flows.," *Biomicrofluidics*, vol. 5, no. 2, p. 22210, 2011.
- [5] H.-W. Wu, C.-C. Lin, and G.-B. Lee, "Stem cells in microfluidics.," *Biomicrofluidics*, vol. 5, no. 1, p. 13401, 2011.
- [6] J. Zhou, A. V. Ellis, and N. H. Voelcker, "Poly(dimethylsiloxane) surface modification by plasma treatment for DNA hybridization applications," *J. Nanosci. Nanotechnol.*, vol. 10, no. 11, pp. 7266–7270, 2010.
- [7] A. M. Ferreira, I. Carmagnola, V. Chiono, P. Gentile, L. Fracchia, C. Ceresa, G. Georgiev, and G. Ciardelli, "Surface modification of poly(dimethylsiloxane) by two-step plasma treatment for further grafting with chitosan–Rose Bengal photosensitizer," *Surf. Coatings Technol.*, vol. 223, pp. 92–97, 2013.
- [8] U. Dharmasiri, M. A. Witek, A. A. Adams, J. K. Osiri, M. L. Hupert, T. S. Bianchi, D. L. Roelke, and S. a Soper, "Enrichment and detection of *Escherichia coli* O157:H7 from water samples using an antibody modified microfluidic chip," *Anal. Chem.*, vol. 82, no. 7, pp. 2844–2849, 2010.
- [9] Y. Bai, C. G. Koh, M. Boreman, Y.-J. Juang, I.-C. Tang, L. J. Lee, and S.-T. Yang, "Surface modification for enhancing antibody binding on polymer-based microfluidic device for enzyme-linked immunosorbent assay," *Langmuir*, vol. 22, no. 22, pp. 9458–9467, 2006.

- [10] D. B. Weibel, A. Lee, M. Mayer, S. F. Brady, D. Bruzewicz, J. Yang, W. R. Diluzio, J. Clardy, and G. M. Whitesides, "Bacterial printing press that regenerates its ink : contact-printing bacteria using hydrogel stamps," *Langmuir*, vol. 21, no. 11, pp. 6436–6442, 2005.
- [11] C. Seguin, J. M. McLachlan, P. R. Norton, and F. Lagugne-Labarthe, "Surface modification of poly(dimethylsiloxane) for microfluidic assay applications," *Appl. Surf. Sci.*, vol. 256, no. 8, pp. 2524–2531, 2010.
- [12] J. Roth, V. Albrecht, M. Nitschke, C. Bellmann, F. Simon, S. Zschoche, S. Michel, C. Luhmann, K. Grundke, and B. Voit, "Surface functionalization of silicone rubber for permanent adhesion improvement.," *Langmuir*, vol. 24, no. 21, pp. 12603–11, 2008.
- [13] J. M. Goddard and J. H. Hotchkiss, "Polymer surface modification for the attachment of bioactive compounds," *Prog. Polym. Sci.*, vol. 32, no. 7, pp. 698–725, 2007.
- [14] S. Hemmilä, J. V. Cauich-Rodríguez, J. Kreutzer, and P. Kallio, "Rapid, simple, and cost-effective treatments to achieve long-term hydrophilic PDMS surfaces," *Appl. Surf. Sci.*, vol. 258, no. 24, pp. 9864–9875, 2012.
- [15] I. Wong and C. M. Ho, "Surface molecular property modifications for poly(dimethylsiloxane) (PDMS) based microfluidic devices," *Microfluid. Nanofluidics*, vol. 7, no. 3, pp. 291–306, 2009.
- [16] H. Makamba, J. H. Kim, K. Lim, N. Park, and J. H. Hahn, "Surface modification of poly(dimethylsiloxane) microchannels.," *Electrophoresis*, vol. 24, pp. 3607–3619, 2003.
- [17] Q. Tu, J.-C. Wang, Y. Zhang, R. Liu, W. Liu, L. Ren, S. Shen, J. Xu, L. Zhao, and J. Wang, "Surface modification of poly(dimethylsiloxane) and its applications in microfluidics-based biological analysis," *Rev. Anal. Chem.*, vol. 31, no. 3–4, pp. 177–192, 2012.
- [18] A. Waldbaur, H. Rapp, K. Länge, and B. E. Rapp, "Let there be chip—towards rapid prototyping of microfluidic devices: one-step manufacturing processes," *Anal. Methods*, vol. 3, no. 12, p. 2681, 2011.
- [19] D. Mark, S. Haeberle, G. Roth, F. von Stetten, and R. Zengerle, "Microfluidic lab-on-a-chip platforms: requirements, characteristics and applications.," *Chem. Soc. Rev.*, vol. 39, no. 3, pp. 1153–82, 2010.

- [20] K. J. Regehr, M. Domenech, J. T. Koepsel, K. C. Carver, S. J. Ellison-Zelski, W. L. Murphy, L. a Schuler, E. T. Alarid, and D. J. Beebe, "Biological implications of polydimethylsiloxane-based microfluidic cell culture.," *Lab Chip*, vol. 9, no. 15, pp. 2132–2139, 2009.
- [21] K. Ren, Y. Chen, and H. Wu, "New materials for microfluidics in biology," *Curr. Opin. Biotechnol.*, vol. 25, pp. 78–85, 2014.
- [22] S. Hu, X. Ren, M. Bachman, C. E. Sims, G. P. Li, and N. Allbritton, "Surface modification of poly(dimethylsiloxane) microfluidic devices by ultraviolet polymer grafting," *Anal. Chem.*, vol. 74, no. 16, pp. 4117–4123, 2002.
- [23] C. S. Effenhauser, G. J. M. Bruin, A. Paulus, and M. Ehrat, "Integrated capillary electrophoresis on flexible silicone microdevices: analysis of DNA restriction fragments and detection of single DNA molecules on microchips," *Anal. Chem.*, vol. 69, no. 17, pp. 3451–3457, 1997.
- [24] S. Halldorsson, E. Lucumi, R. Gómez-Sjöberg, and R. M. T. Fleming, "Advantages and challenges of microfluidic cell culture in polydimethylsiloxane devices," *Biosens. Bioelectron.*, vol. 63, pp. 218–231, 2015.
- [25] E. Berthier, E. W. K. Young, and D. Beebe, "Engineers are from PDMS-land, biologists are from Polystyrenia," *Lab Chip*, vol. 12, no. 7, p. 1224, 2012.
- [26] A. Manz, H. M. Widmers, and N. Graber, "Miniaturized total chemical analysis systems: A novel concept for chemical sensing," *Sensors Actuators B Chem.*, vol. 1, no. 1–6, pp. 244–248, 1990.
- [27] Y. Xia and G. M. G. Whitesides, "Soft lithography," *Annu. Rev. Mater. Sci.*, no. 12, 1998.
- [28] D. R. Reyes, D. Iossifidis, P. A. Auroux, and A. Manz, "Micro total analysis systems. 1. Introduction, theory, and technology," *Anal. Chem.*, vol. 74, no. 12, pp. 2623–2636, 2002.
- [29] P. A. Auroux, D. Iossifidis, D. R. Reyes, and A. Manz, "Micro total analysis systems. 2. Analytical standard operations and applications," *Anal. Chem.*, vol. 74, no. 12, pp. 2637–2652, 2002.
- [30] G. S. Fiorini and D. T. Chiu, "Disposable microfluidic devices: Fabrication, function, and application," *Biotechniques*, vol. 38, no. 3, pp. 429–446, 2005.
- [31] J. C. McDonald, D. C. Duffy, J. R. Anderson, D. T. Chiu, H. Wu, O. J. Schueller, and G. M. Whitesides, "Fabrication of microfluidic systems in poly(dimethylsiloxane).," *Electrophoresis*, vol. 21, no. 1, pp. 27–40, 2000.

- [32] J. C. McDonald, M. L. Chabinyc, S. J. Metallo, J. R. Anderson, A. D. Stroock, and G. M. Whitesides, "Prototyping of microfluidic devices in poly(dimethylsiloxane) using solid-object printing," *Anal. Chem.*, vol. 74, no. 7, pp. 1537–1545, 2002.
- [33] E. K. Sackmann, A. L. Fulton, and D. J. Beebe, "The present and future role of microfluidics in biomedical research.," *Nature*, vol. 507, no. 7491, pp. 181–9, 2014.
- [34] B. C. Hollins, S. A. Soper, and J. Feng, "Enriching carbonylated proteins inside a microchip through the use of oxalyldihydrazide as a crosslinker.," *Lab Chip*, vol. 12, no. 14, pp. 2526–32, 2012.
- [35] J. L. Wilbur, A. Kumar, E. Kim, and G. M. Whitesides, "Microfabrication by microcontact printing of self-assembled monolayers," *Adv. Mater.*, vol. 6, no. 78, pp. 600–604, 1994.
- [36] G. S. Ferguson, M. K. Chaudhury, H. A. Biebuyck, and G. M. Whitesides, "Monolayers on disordered substrates: self-assembly of alkyltrichlorosilanes on surface-modified polyethylene and poly(dimethylsiloxane)," *Macromolecules*, vol. 26, no. iii, pp. 5870–5875, 1993.
- [37] S. Befahy, S. Yunus, V. Burguet, J.-S. Heine, M. Troosters, and P. Bertrand, "Stretchable gold tracks on flat polydimethylsiloxane (PDMS) rubber substrate," *J. Adhes.*, vol. 84, pp. 231–239, 2008.
- [38] J. D. Wang, N. J. Douville, S. Takayama, and M. Elsayed, "Quantitative analysis of molecular absorption into PDMS microfluidic channels," *Ann. Biomed. Eng.*, vol. 40, no. 9, pp. 1862–1873, 2012.
- [39] H. Yang and Z. Hou, "Homogenous grafted poly(acrylic acid) brushes on ultra-flat polydimethylsiloxane (PDMS) films by UV irradiation," *Nano Biomed. Eng.*, vol. 3, no. 1, pp. 42–46, 2011.
- [40] D. Wang, V. Goel, R. D. Oleschuk, and J. H. Horton, "Surface modification of poly(dimethylsiloxane) with a perfluorinated alkoxy silane for selectivity toward fluorinated tagged peptides.," *Langmuir*, vol. 24, no. 3, pp. 1080–6, 2008.
- [41] N. Volcker, D. Klee, H. Hocker, and S. Langefeld, "Functionalization of silicone rubber for the covalent immobilization of fibronectin," *J. Mater. Sci.*, vol. 12, pp. 111–119, 2001.
- [42] Y. Zhang, L. Ren, Q. Tu, X. Wang, R. Liu, L. Li, J.-C. Wang, W. Liu, J. Xu, and J. Wang, "Fabrication of reversible poly(dimethylsiloxane) surfaces via host–guest chemistry and their repeated utilization in cardiac biomarker analysis," *Anal. Chem.*, vol. 83, no. 24, pp. 9651–9659, 2011.

- [43] T. Mcpherson, A. Kidane, I. Szleifer, K. Park, and W. Lafayette, "Prevention of protein adsorption by tethered poly (ethylene oxide) layers: experiments and single-chain mean-field analysis," *Langmuir*, vol. 14, no. 12, pp. 176–186, 1998.
- [44] G. Sui, J. Wang, C.-C. Lee, W. Lu, S. P. Lee, J. V Leyton, A. M. Wu, and H. Tseng, "Solution-phase surface modification in intact poly(dimethylsiloxane) microfluidic channels," *Anal. Chem.*, vol. 78, no. 15, pp. 5543–5551, 2006.
- [45] L. Yu, C. M. Li, Y. Liu, J. Gao, W. Wang, and Y. Gan, "Flow-through functionalized PDMS microfluidic channels with dextran derivative for ELISAs," *Lab Chip*, vol. 9, no. 9, pp. 1243–1247, 2009.
- [46] J. Zhou, H. Yan, K. Ren, W. Dai, and H. Wu, "Convenient method for modifying poly(dimethylsiloxane) with poly(ethylene glycol) in microfluidics," *Anal. Chem.*, vol. 81, no. 16, pp. 6627–6632, 2009.
- [47] A. Y. N. Hui, G. Wang, B. Lin, and W.-T. Chan, "Microwave plasma treatment of polymer surface for irreversible sealing of microfluidic devices.," *Lab Chip*, vol. 5, no. 10, pp. 1173–1177, 2005.
- [48] K. Chau, B. Millare, A. Lin, S. Upadhyayula, V. Nuñez, H. Xu, and V. I. Vullev, "Dependence of the quality of adhesion between poly(dimethylsiloxane) and glass surfaces on the composition of the oxidizing plasma," *Microfluid. Nanofluidics*, vol. 10, no. 4, pp. 907–917, 2010.
- [49] I. J. Chen and E. Lindner, "The stability of radio-frequency plasma-treated polydimethylsiloxane surfaces," *Langmuir*, vol. 23, no. 6, pp. 3118–3122, 2007.
- [50] Q. He, Z. Liu, P. Xiao, R. Liang, N. He, and Z. Lu, "Preparation of hydrophilic poly (dimethylsiloxane) stamps by plasma-induced grafting," *Langmuir*, no. 15, pp. 6982–6986, 2003.
- [51] I. T. Martin, B. Dressen, M. Boggs, Y. Liu, C. S. Henry, and E. R. Fisher, "Plasma modification of PDMS microfluidic devices for control of electroosmotic flow," *Plasma Process. Polym.*, vol. 4, no. 4, pp. 414–424, 2007.
- [52] S. Hu, X. Ren, M. Bachman, C. E. Sims, G. P. Li, and N. L. Allbritton, "Surface-Directed, Graft Polymerization within Microfluidic Channels," *Anal. Chem.*, vol. 76, no. 7, pp. 1865–1870, 2004.
- [53] A. Toth, I. Bertoti, and M. Blazso, "Oxidative damage and recovery of silicone rubber surfaces . 1 . X-ray photoelectron spectroscopic study," *Appl. Polym. Sci.*, vol. 52, pp. 1293–1307, 1994.

- [54] H. Hillborg, N. Tomczak, A. Ola, H. Scho, and G. J. Vancso, "Nanoscale hydrophobic recovery: a chemical force microscopy study of UV/ozone-treated cross-linked poly(dimethylsiloxane)," *Symp. A Q. J. Mod. Foreign Lit.*, no. 3, pp. 785–794, 2004.
- [55] D. T. Eddington, J. P. Puccinelli, and D. J. Beebe, "Thermal aging and reduced hydrophobic recovery of polydimethylsiloxane," *Sensors Actuators B Chem.*, vol. 114, no. 1, pp. 170–172, 2006.
- [56] M. W. Toepke and D. J. Beebe, "PDMS absorption of small molecules and consequences in microfluidic applications.," *Lab Chip*, vol. 6, no. 12, pp. 1484–1486, 2006.
- [57] L. Gui and C. L. Ren, "Temperature measurement in microfluidic chips using photobleaching of a fluorescent thin film," *Appl. Phys. Lett.*, vol. 92, no. 2, pp. 23–25, 2008.
- [58] B. Brewer, Y. Gao, and D. Li, "A study of small molecule absorption in polydimethylsiloxane," in *Proceedings of the ASME 2012 3rd Micro/Nanoscale Heat & Mass Transfer International Conference*, 2012, pp. 15–19.
- [59] K. Ren, Y. Zhao, J. Su, D. Ryan, and H. Wu, "Convenient method for modifying poly(dimethylsiloxane) to be airtight and resistive against absorption of small molecules," *Anal. Chem.*, vol. 82, no. 14, pp. 5965–5971, Jul. 2010.
- [60] G. Maltezos, E. Garcia, G. Hanrahan, F. A. Gomez, S. Vyawahare, R. M. van Dam, Y. Chen, and A. Scherer, "Design and fabrication of chemically robust three-dimensional microfluidic valves.," *Lab Chip*, vol. 7, no. 9, pp. 1209–1211, 2007.
- [61] D. Ortiz-Acosta and C. Densmore, "Los Alamos Sylgard® cure inhibition characterization," p. LA-UR-12-25325, 2012.
- [62] E. Delamarche, H. Schmid, B. Michel, and H. Biebuyck, "Stability of molded polydimethylsiloxane microstructures," *Adv. Mater.*, vol. 9, no. 9, pp. 741–746, 1997.
- [63] G. M. Whitesides, E. Ostuni, X. Jiang, and D. E. Ingber, "Soft lithography in biology and biochemistry," *Annu. Rev. Biomed. Eng.*, vol. 3, pp. 335–373, 2001.
- [64] S. Brittain, K. Paul, X. M. Zhao, and G. Whitesides, "Soft lithography and microfabrication," *Physics World*, vol. 11, no. 5, pp. 31–36, 1998.
- [65] P. Kim, K. W. Kwon, M. C. Park, S. H. Lee, and S. M. Kim, "Soft lithography for microfluidics : a review," *Biochip J.*, vol. 2, no. 1, pp. 1–11, 2008.

- [66] J. C. Love, J. R. Anderson, and G. M. Whitesides, "Fabrication of three-dimensional microfluidic systems by soft lithography," *MRS Bull.*, pp. 523–528, 2001.
- [67] X. Zhao, Y. Xia, and G. M. Whitesides, "Fabrication of three-dimensional microstructures: microtransfer molding," *Adv. Mater.*, vol. 8, no. 10, pp. 837–840, 1996.
- [68] B. H. Jo, L. M. Van Lerberghe, K. M. Motsegood, and D. J. Beebe, "Three-dimensional micro-channel fabrication in polydimethylsiloxane (PDMS) elastomer," *J. Microelectromechanical Syst.*, vol. 9, no. 1, pp. 76–81, 2000.
- [69] R. K. Singh, A. Kumar, R. Kant, A. Gupta, E. Suresh, and S. Bhattacharya, "Design and fabrication of 3-dimensional helical structures in polydimethylsiloxane for flow control applications," *Microsyst. Technol.*, vol. 20, no. 1, pp. 101–111, 2014.
- [70] C. Vogel, "Translation's coming of age," *Mol. Syst. Biol.*, vol. 7, no. 1, pp. 498–498, 2011.
- [71] A. Duquet, A. Polesskaya, S. Cuvellier, S. Ait-Si-Ali, P. Héry, L. L. Pritchard, M. Gerard, and A. Harel-Bellan, "Acetylation is important for MyoD function in adult mice.," *EMBO Rep.*, vol. 7, no. 11, pp. 1140–1146, 2006.
- [72] J. Yang, J. Huang, M. Dasgupta, N. Sears, M. Miyagi, B. Wang, M. R. Chance, X. Chen, Y. Du, Y. Wang, L. An, Q. Wang, T. Lu, X. Zhang, Z. Wang, and G. R. Stark, "Reversible methylation of promoter-bound STAT3 by histone-modifying enzymes.," *Proc. Natl. Acad. Sci. U. S. A.*, vol. 107, no. 50, pp. 21499–21504, 2010.
- [73] N. Shigi, "Posttranslational modification of cellular proteins by a ubiquitin-like protein in bacteria," *J. Biol. Chem.*, vol. 287, no. 21, pp. 17568–17577, 2012.
- [74] Y. Zhao and O. N. Jensen, "Modification-specific proteomics: Strategies for characterization of post-translational modifications using enrichment techniques," *Proteomics*, vol. 9, no. 20, pp. 4632–4641, 2009.
- [75] A. M. Pisoschi and A. Pop, "The role of antioxidants in the chemistry of oxidative stress: A review," *Eur. J. Med. Chem.*, vol. 97, pp. 55–74, 2015.
- [76] L. Zhou, M. A. Aon, T. Almas, S. Cortassa, R. L. Winslow, and B. O'Rourke, "A reaction-diffusion model of ROS-induced ROS release in a mitochondrial network.," *PLoS Comput. Biol.*, vol. 6, no. 1, p. e1000657, 2010.
- [77] T. Finkel and N. J. Holbrook, "Oxidants, oxidative stress and the biology of ageing.," *Nature*, vol. 408, no. 6809, pp. 239–247, 2000.

- [78] R. S. Balaban, S. Nemoto, and T. Finkel, "Mitochondria, oxidants, and aging," *Cell*, vol. 120, no. 4, pp. 483–495, 2005.
- [79] P. Klatt and S. Lamas, "Regulation of protein function by S-glutathiolation in response to oxidative and nitrosative stress," *Eur. J. Biochem.*, vol. 267, no. 16, pp. 4928–4944, 2000.
- [80] T. C. Chang, W. Y. Chou, and G. G. Chang, "Protein oxidation and turnover.," *J. Biomed. Sci.*, vol. 7, no. 5, pp. 357–63, 2000.
- [81] M. C. Reed, R. L. Thomas, J. Pavisic, S. J. James, C. M. Ulrich, and H. F. Nijhout, "A mathematical model of glutathione metabolism.," *Theor. Biol. Med. Model.*, vol. 5, p. 8, 2008.
- [82] I. Dalle-Donne, D. Giustarini, R. Colombo, R. Rossi, and A. Milzani, "Protein carbonylation in human diseases," *Trends Mol. Med.*, vol. 9, no. 4, pp. 169–176, 2003.
- [83] L. Alberghina and A. M. Colangelo, "The modular systems biology approach to investigate the control of apoptosis in Alzheimer's disease neurodegeneration.," *BMC Neurosci.*, vol. 7 Suppl 1, p. S2, 2006.
- [84] D. L. Krause and N. Müller, "Neuroinflammation, microglia and implications for anti-inflammatory treatment in Alzheimer's disease.," *Int. J. Alzheimers. Dis.*, vol. 2010, pp. 1–9, 2010.
- [85] B. I. Frohnert and D. a Bernlohr, "Protein carbonylation, mitochondrial dysfunction, and insulin resistance.," *Adv. Nutr.*, vol. 4, no. 2, pp. 157–63, 2013.
- [86] A. Nunomura, R. J. Castellani, X. Zhu, P. I. Moreira, G. Perry, and M. A. Smith, "Involvement of oxidative stress in Alzheimer disease.," *J. Neuropathol. Exp. Neurol.*, vol. 65, no. 7, pp. 631–641, 2006.
- [87] C. R. White, T. A. Brock, L. Y. Chang, J. Crapo, P. Briscoe, D. Ku, W. A. Bradley, S. H. Gianturco, J. Gore, and B. A. Freeman, "Superoxide and peroxynitrite in atherosclerosis.," *Proc. Natl. Acad. Sci. U. S. A.*, vol. 91, no. 3, pp. 1044–1048, 1994.
- [88] E. Čolak, "New markers of oxidative damage to macromolecules," *J. Med. Biochem.*, vol. 27, no. 1, pp. 1–16, 2008.
- [89] A. G. Madian, A. D. Myracle, N. Diaz-Maldonado, N. S. Rochelle, E. M. Janle, and F. E. Regnier, "Differential carbonylation of proteins as a function of in vivo oxidative stress.," *J. Proteome Res.*, vol. 10, no. 9, pp. 3959–72, 2011.

- [90] Y. J. Suzuki, M. Carini, and D. A. Butterfield, "Protein carbonylation.," *Antioxid. Redox Signal.*, vol. 12, no. 3, pp. 323–5, 2010.
- [91] A. Amici, R. L. Levine, L. Tsai, and E. R. Stadtman, "Conversion of amino acid residues in proteins and amino acid homopolymers to carbonyl derivatives by metal-catalyzed oxidation reactions.," *J. Biol. Chem.*, vol. 264, no. 6, pp. 3341–3346, 1989.
- [92] H. Yang, Z. Hou, and J. Hu, "Surface modification of ultra-flat polydimethylsiloxane by UV-grafted poly(acrylic acid) brushes," *J. Appl. Polym. Sci.*, vol. 123, pp. 2266–2271, 2011.
- [93] R. L. Levine, D. Garland, C. N. Oliver, A. Amici, I. Climent, A.-G. Lenz, B.-W. Ahn, S. Shaltiel, and E. Stadtman, "Determination of carbonyl content in oxidatively modified proteins," *Methods Enzymol.*, no. 186, pp. 464–478, 1990.
- [94] D. L. Meany, H. Xie, L. V. Thompson, E. A. Arriaga, and T. J. Griffin, "Identification of carbonylated proteins from enriched rat skeletal muscle mitochondria using affinity chromatography-stable isotope labeling and tandem mass spectrometry," *Proteomics*, vol. 7, no. 7, pp. 1150–1163, 2007.
- [95] J. Seo and L. P. Lee, "Effects on wettability by surfactant accumulation/depletion in bulk polydimethylsiloxane (PDMS)," *Sensors Actuators B Chem.*, vol. 119, no. 1, pp. 192–198, 2006.
- [96] G. Hu and D. Li, "Multiscale phenomena in microfluidics and nanofluidics," *Chem. Eng. Sci.*, vol. 62, no. 13, pp. 3443–3454, 2007.
- [97] H. A. Stone and S. Kim, "Microfluidics: Basic issues, applications, and challenges," *AIChE J.*, vol. 47, no. 6, pp. 1250–1254, 2001.
- [98] K. S. Elvira, X. Casadevall i Solvas, R. C. R. Wootton, and A. J. de Mello, "The past, present and potential for microfluidic reactor technology in chemical synthesis.," *Nat. Chem.*, vol. 5, no. 11, pp. 905–15, 2013.
- [99] J. P. Brody, P. Yager, R. E. Goldstein, and R. H. Austin, "Biotechnology at low Reynolds numbers.," *Biophys. J.*, vol. 71, no. 6, pp. 3430–3441, 1996.
- [100] B. C. Hollins, S. D. Stone, and J. Feng, "Optimization of oxalyldihydrazide-immobilized carbonylated protein capture in PMMA microchips," *Am. J. Sci. Eng.*, vol. 2, no. 2, pp. 9–17, 2013.
- [101] N. K. Inamdar, L. G. Griffith, and J. T. Borenstein, "Transport and shear in a microfluidic membrane bilayer device for cell culture.," *Biomicrofluidics*, vol. 5, no. 2, p. 22213, 2011.

- [102] M. Akbari, D. Sinton, and M. Bahrami, "Pressure drop in rectangular microchannels as compared with theory based on arbitrary cross section," *J. Fluids Eng.*, vol. 131, no. 4, p. 41202, 2009.
- [103] M. J. Fuerstman, A. Lai, M. E. Thurlow, S. S. Shevkoplyas, H. A. Stone, and G. M. Whitesides, "The pressure drop along rectangular microchannels containing bubbles," *Lab Chip*, vol. 7, no. 11, pp. 1479–1489, 2007.
- [104] H. A. Stone, "Introduction to fluid dynamics for microfluidic flows," *C. Biotechnol.*, pp. 5–30, 2007.
- [105] H. Bruus, "Governing equations in microfluidics," *Microscale Acoustofluidics*, pp. 1–28, 2015.
- [106] N. Blow, "Microfluidics: in search of a killer application," *Nat. Methods*, vol. 4, no. 8, pp. 665–670, 2007.
- [107] W. K. Tomazelli Coltro, C. M. Cheng, E. Carrilho, and D. P. de Jesus, "Recent advances in low-cost microfluidic platforms for diagnostic applications," *Electrophoresis*, vol. 35, no. 16, pp. 2309–2324, 2014.
- [108] K. F. Lei, "Microfluidic systems for diagnostic applications: a review.," *J. Lab. Autom.*, vol. 17, no. 5, pp. 330–47, 2012.